Universidad Nacional Autónoma de México

Maestría en Ciencias (Física)
Instituto de Investigaciones en Materiales
Materia Condensada y Nanociencias

Superconductivity in the Amorphous Cu_xZr_{1-x} System. An *Ab Initio* Approach.

Tesis
Que para Optar por el Grado de:
Maestro en Ciencias (Física)

Presenta:
Salvador Villarreal López Rebuelta

Tutor Principal
Dr. Ariel Alberto Valladares Clemente
Instituto de Investigaciones en Materiales

Miembros del Comité Tutor
Dra. Renela María Valladares Mc Nelis
Facultad de Ciencias
Enrique Geffroy Aguilar
Instituto de Investigaciones en Materiales

Ciudad Universitaria, Cd. Mx., Marzo 2023

Abstract

In this work, we calculate the electronic and vibrational properties of amorphous Cu_xZr_{1-x} alloys using *ab initio* Density Functional Theory. The amorphous character of the structures is simulated with a linear heating and cooling techinque known as the *undermelt-quench* approach, and the *partial Pair Distribution Functions* are computed to analyse their structural properties. The electronic and vibrational densities of state are obtained and used to estimate the known superconducting transition temperatures T_c from these parameters only.

We also investigate the case of the crystalline $CuZr_2$ intermetallic compound which, to the extent of the author's knowledge, has not been observed to be superconducting at any temperature above 0.3 K, in contrast to its amorphous counterpart that boasts a T_c of 2.25 K. We report an upper bound for the T_c of the crystalline phase of 47.9 mK, consistent with the lack of experimental results.

Dedication

To my Father, thank you for guiding me into who I have become and giving me an example to follow.

To Melissa, thank you for being by my side, for all of the support, care, and love, you help me be a better version of myself.

To René, I get inspired by your excitement whenever I talk to you about anything related to physics, answering your endless questions.

To Rigoberto, thank you for all of the support, assistance, and advice.

Acknowledgements

The author wishes to express his gratitute towards all the people and institutions that helped him during his graduate studies. This work would not have been possible without them.

I am deeply grateful to my advisors Prof. Ariel Valladares, Prof. Renela Valladares, and Prof. Enrique Geffroy for sharing all of their knowledge and advice. Especially my main advisor Prof. Ariel Valladares, thank you for teaching me so much about physics, in both theory and practice, and thank you for all of the illuminating discussions that have helped me towards understanding a subject as complex as the one in this dissertation. To Isaías Rodríguez and David Hinojosa, thank you for always lending a helping hand whenever something went wrong in the computations.

I would also like to thank Prof. Vicenta Sánchez Morales for reading this document and providing feedback to improve my understanding of the BCS approach and its implementations, as well as Prof. Bernard Delley for his kind and patient explanation of the DSPP and the pseudopotential method.

Thanks to the personnel at the *Instituto de Investigaciones en Materiales* (IIM), especially A. López and A. Pompa for their technical support and maintenance of the computing unit at IIM-UNAM, and the personnel at IIM's library for providing access to the necessary research materials, books, and articles.

I am thankful towards the Computing Center of DGTIC-UNAM where part of the simulations was carried out, as well as the *Dirección General de Bibliotecas* (DGB) and their Digital Library (BiDi-UNAM) that provided access to many of the articles consulted for this work.

I also wish to acknowledge *Consejo Nacional de Ciencia y Tecnología* (CONACyT) for supporting my graduate studies, as well as *Coordinación General de Estudios de Posgrado* (CGEP) and its department of Graduate Scholarships for providing additional financial assistance for the months that were not covered by CONACyT. This project was made possible thanks to the support of DGAPA-UNAM and their *Programa de Apoyo a Proyectos de Investigación e Innovación Tecnológico* (PAPIIT), under the Grant No. IN116520.

Declaration of Authorship

I, Mech. Eng. Salvador Villarreal López Rebuelta, declare that this thesis titled "Superconductivity in the Amorphous Cu_xZr_{1-x} System. An *Ab Initio* Approach" and the work presented herein is my own. I confirm that:

- This work was done wholly during my studies towards an M. Sc. degree in Physics at Universidad Nacional Autónoma de México (UNAM).
- No part of this work has been used previously for any other degree, neither at UNAM nor at any other Institution.
- Where I have consulted the published work of others, this is always clearly attributed.
- Where I have quoted from the work of others, the source is always given. Except for such quotations, this thesis is entirely my work.
- I have acknowledged all the sources of assistance received for the completion of this document.
- Where the thesis uses work done by myself jointly with others, I have specified it.

Salvador Villarreal López Rebuelta

June, 2023.

Contents

Introduction

The crux of condensed matter physics, how the observable properties of the objects around us are determined by their basic constituents, has captivated humanity for millennia. From the purely philosophical musings of Aristotle, who alleged that matter inherited its properties from the balance of elements present in it, to our modern scientific techniques that allow us to detect and ascertain the presence of the true constituents of matter, and measure how they interact with one another. One of the most fascinating phenomena in this field is that of condensation, where the macroscopic state of an object displays quantum properties that would normally be confined only to the microscopic scale where one could observe the individual constituents. The particles that condensate are said to occupy one coherent quantum state. In superconductors, the electrons form one such condensate, but this case is particularly mystifying as the electrons, that conventional wisdom would have them repelling each other, instead bind together and coalesce into a state where they move together without budging. Somehow in the whole mess of interactions, common knowledge is overturned and electrons end up effectively attracting each other as a result of how they interact with the environment in which they move.

The theory of amorphous materials trails behind that of crystals, in a fashion analogous to their belated adoption in human history compared to crystalline ceramics and metals. In the theoretical case, this delay can be attributed to the difficulty in describing the non-repeating structures that retain some degree of order at short range. The prevalence of disorder and defects in these materials pose an intriguing question regarding the existence, and sometimes even superiority of amorphous superconductors over their crystalline counterparts. The phenomenon of Anderson localisation, where the otherwise extended electronic states in crystals get localised around a defect, would appear antithetical to the macroscopically coherent superconducting state, but in an almost paradoxical turn of events, amorphous superconductors do exist and some even persist at temperatures higher than their crystal analogues.

In this work we present some of the basic theory needed to describe amorphous superconductors and the methods used to calculate their properties relevant to superconductivity, and apply them to Cu_xZr_{1-x} alloys, which partake in the apparent paradox described above. In Chapter 1 we introduce the concept of amorphous material along with some techniques used to compute their structural properties. In Chapter 2 we derive the equations of the interactions that give rise to this phase of matter at the microscopic scale,

as well as the groundbreaking theory of Bardeen, Cooper, and Schrieffer. In Chapters 3 and 4 we introduce the basis of the methods employed to solve the quantum mechanical equations of motion of the system. In Chapter 5 we delve into some of the technical details that are essential to make the above solution methods work, as well as the methodology used to evaluate the superconducting properties of the system. In Chapter 6 we present our findings and discuss their implications.

1 Amorphous Materials

In which we introduce the basic concepts and tools that characterize amorphous materials.

Amorphous materials are conventionally introduced for what they are not, doing away with the translational and orientational order that the Bloch framework underlying much of the theory of Solid State Physics requires. Such absence has often led to them being construed as *topologically disordered*[1] crystals [25]. Instead, we emphasise that the premise of long-range order required by Bloch's theorem (see Section 7.1 of H. Ibach and H. Lüth's book [44]) is a pragmatic restriction imposed to facilitate the solution of the Schrödinger equation in crystals, where the atoms are already arranged in such fashion. When the Hamiltonian H commutes with the translation operators $\{T_{\mathbf{a}}\}$, the diagonalisation of H is simplified, as the solutions of the Schrödinger equation are always eigenstates of $T_{\mathbf{a}}$ (*i.e.*, the states $T_{\mathbf{a}} |\mathbf{k}\rangle = e^{i\mathbf{k}\cdot\mathbf{a}} |\mathbf{k}\rangle$). The more general case, where the premise of Bloch's theorem is violated and the corresponding simplifications are invalid, belongs to what can be broadly defined as amorphous materials, which are translationally and orientationally disordered. With this in mind, it is clear that crystals merely represent a subset of all possible structural configurations, which are generally amorphous, and not the other way around.

Bloch's premise of perfect periodicity is far too restrictive for any real-world material to satisfy it. The nuclei in real crystals are displaced by lattice vibrations, while the lattice itself may have a plethora of defects such as vacancies, substitutions, dislocations, etc. Despite these imperfections, the idealised model is a good predictor of the electronic structure of the real crystal. Let us emphasise: At any instant, the real crystal is, *stricto sensu*, topologically disordered, but this does not mean that it is amorphous. The fact that Bloch's theory works so well suggests that the disorder acts as a small perturbation of an otherwise periodic structure. On the other hand, we are interested in materials wherein the absence of order is the (metastable) equilibrium configuration and not merely a perturbation. Therefore, we must unravel the distinction between amorphous and crystalline materials further.

In his seminal paper on the theory of phase transitions [51], Lev D. Landau suggested that the analysis of crystalline phases is made difficult by using an idealised model of a perfect crystal. Instead, he advocates

[1] As Stephen R. Elliott explains [24], topological disorder refers to configurations in which there is no translational periodicity.

modelling the crystal by a probability distribution $\rho(\mathbf{r})$, where $\rho(\mathbf{r})\mathrm{d}^3 r$ determines the probability of finding an atom in the volume element centred at $\mathbf{r}$. In this picture, the perfect crystal would have its distribution given as a sum of Dirac deltas, one for every lattice position, and the thermal motion of the nuclei in the real crystal would manifest in a broadening of these peaks without changing the underlying symmetry of ρ. Furthermore, since the crystal is homogeneous, defects have no reason to present preferentially in some sites more than any others. Thus, these defects can be regarded as a small homogeneous perturbation on the distribution ρ, which does not change the underlying symmetry either. In this sense, we can think of amorphous materials as those that appear disordered even when averaging over the atomic positions and defects: their probability distribution ρ need not have an underlying symmetry.

As with anything pertaining to symmetry, there is a dichotomy between symmetric and non-symmetric objects. Zbigniew H. Stachurski illustrates this distinction in Chapter 1 (Fig. 1.2) of his book [84], where he portrays a clear separation between the two classes of materials. There, he conceptualises a spectrum of materials ranging from the *ideal amorphous solid*[2] to the *ideal crystalline solid*, the in-between states resulting from perturbations of the ideal configurations (and he graphs it along "an undefined, somewhat arbitrary variable"). Although it is clearly not a rigourous notion, this picture is useful in establishing the demarcation between the crystalline and amorphous phases, which we suggest must be the presence or absence of symmetry in the loose way outlined above, inspired by Landau's ideas.

1.1 Short-Range Order

The absence of translational symmetry, outlined above, can be reinterpreted as the atoms not correlating their positions with each other at long distances. That is to say, knowledge of the position of one atom does not aid in the prediction of the location of another if they are distant[3]. At short range, however, matters are quite different.

As Stanford R. Ovshinsky [66] explains, the short-range arrangement of atoms in an amorphous solid is not random, but depends strongly on the chemistry of the elements involved. Of particular importance is the coordination number, namely, the number of atoms in the nearest-neighbour coordination shell[4]. However, unlike their crystalline counterparts, the bond angles and lengths in amorphous materials are not fixed. This variation is expected because atoms at different positions will have varying environments due to the disorder.

[2] Stachurski defines this ideal amorphous solid in Section 1.5 of the same book, with a set of complicated rules of sphere packing.

[3] As we shall see, the precise meaning of "distant" may be observed in the flattening of the PDF curve (*cf.* Section 1.2.1). In our Cu-Zr alloys this happens around the distance to the fourth peak in the PDF, roughly 10 Å.

[4] For covalent and ionic amorphous solids, this number is generally determined by the number of bonds between the elements, which depends on the chemistry of the components. For metals, matters might not be so simple because the electrons don't have specific bonding states to occupy.

The concept of short-range order lends itself to the discussion of the distinction between "amorphous materials" and "glasses". As Ovshinsky [66] and Elliott [25] point out, these materials are structurally equivalent, but they differ in the methods in which they are produced. Simply put, we call glasses those that can be obtained by quenching a melt, the traditional glass-making process that has existed for thousands of years. On the other hand, non-glassy amorphous materials need to be produced by other means, such as gas deposition[5]. Ovshinsky [66] suggests that the main distinction between the two lies in the fact that the liquids that can quench into glasses have atoms with the same coordination as they would in the solid, whereas non-glassy materials have different coordination numbers. Because of the difference in coordination, the non-glassy material is unable to form a low-energy amorphous state and instead crystallises if one tries to quench it from the melt.

1.2 Essentials of the Structural Characterisation of Amorphous Materials

The subject of the structure of non-crystalline materials is a vast topic. We will attempt to convey some of the basic facts in this section, basing our discussion on the work by Yoshio Waseda [93], without intending to be thorough.

As outlined above, despite lacking long-range correlations between the atomic positions, amorphous materials do have a short- and medium-range order that is primarily dependent on the electronic structure (*i.e.*, the chemical properties) of the material. When talking about the structure of these materials we are referring to the details of how other atoms arrange their positions around an atom of interest. When dealing with alloys it is necessary to specify the structure centred around each distinct species of atom, but note that two atoms of the same species are assumed to have on average[6] the same structure around them as they are identical.

Unlike crystals, the structure of amorphous materials cannot be described by simply specifying a lattice and a basis. Despite their added complexity, the same diffraction techniques that are used to determine the structures of a crystals can be adapted to obtain the structural properties of amorphous materials. The

[5] The book by A. M. Glezer and N. A. Shurygina [32] covers in more detail some of the processing methods for amorphous materials, as well as their mechanical properties.

[6] This will only be true on average, because despite being identical, these atoms all have differences in their environments due to the absence of order. This makes them have distinct local electronic densities (*cf.*, Chapter 3 of Adrian P. Sutton's book [86]) and correspondingly different arrangements.

more directly measurable quantity that can be obtained from this sort of experiment is the structure factor $S(\mathbf{Q})$ (see Section 1-2 of [93]), defined as

$$S(\mathbf{Q}) = \frac{1}{N}\left\langle \sum_{j,k} e^{-i\mathbf{Q}\cdot(\mathbf{R}_j - \mathbf{R}_k)} \right\rangle \tag{1.1}$$

where $\mathbf{Q} = \mathbf{q}_{\text{sc}} - \mathbf{q}_{\text{in}}$ represents the difference in wavevector between the scattered and incident beams (these beams are typically, but not necessarily, x-rays). The two sums are each evaluated over the N atomic positions $\mathbf{R}_l$. Finally, the angled brackets $\langle\rangle$ represent a statistical average. As Waseda [93] explains, for amorphous materials, the structure factor thus defined can be determined directly from the diffraction data through (see eq. (1.2.5) of [93])

$$S(Q) = \frac{I^{\text{coh}}(Q)}{Nf^2(Q)} \tag{1.2}$$

where $I^{\text{coh}}(Q)$ is the coherent scattering intensity, and $f(Q)$ is the (average) atomic scattering factor. Note that $Q = |\mathbf{Q}|$ is taken as a scalar because the amorphous materials have no preferential directions, the scattering should therefore be isotropic. Experimentally, one can change the value of Q by modifying either the angle of incidence θ or the wavelength λ of the incident beam, in particular

$$Q = \frac{4\pi}{\lambda}\sin\theta \tag{1.3}$$

Eq. (1.3) follows from elementary diffraction considerations[7]. As Ibach and Lüth [44] point out, there is one final complication in an experimental setting; particularly, one cannot discern a forward scattered particle from one native to the incident beam. As Waseda notes (p. 8 of [93]), we can overcome this complication by removing the forward scattering terms from $S(Q)$. Namely, $S(Q)$ should be replaced with

$$\tilde{S}(Q) = \frac{1}{N}\left\langle \sum_{j,k} e^{-i\mathbf{Q}\cdot(\mathbf{R}_j - \mathbf{R}_k)} \right\rangle - N\delta_{Q,0} \tag{1.4}$$

it is precisely this quantity $\tilde{S}(Q)$ which can be determined unequivocally from diffraction experiments via eqs. (1.2) and (1.3). However, despite the relative ease of measurement, we will not be interested in the structure factor to determine the structure of our amorphous materials, because its direct physical inter-

[7] Note that eq. (1.3) is stated as fact by Waseda (*cf.*, eq. (1.2.1) of [93]). The explicit expression can be inferred, for example, by combining the relation $q_{\text{in}} = 2\pi/\lambda$, of the incident beam, with eqs. (6.10) and (6.11) of N. W. Aschroft's and N. D. Mermin's book [5].

pretation is somewhat convoluted and only appropriate in crystals[8]. Furthermore, as Waseda [93] explains, there is no univocal way to generalise $S(Q)$ in multi-element alloys, existing instead many distinct conventions. Because of these reasons, we will divert our focus to the **pair distribution function** (PDF) $g(r)$, which is related to $\tilde{S}(Q)$ by a Fourier transform

$$\tilde{S}(Q) = 1 + \bar{n} \int \mathrm{d}^3 r \, e^{-i\mathbf{Q}\cdot\mathbf{r}} [g(r) - 1] \tag{1.5}$$

where $\bar{n}$ is the average number density (see, eq. (1.2.14) of [93]). We wish to stress that, as pointed out by Ibach and Lüth [44], the argument of the Fourier transform in eq. (1.5) is $g(r) - 1$ because we are excluding the forward scattering terms from $S(Q)$, but had we included those, the argument would just be $g(r)$. The following section will be devoted to the definition and interpretation of the pair distribution function, which will be our characterisation function of choice for the remainder of this work.

1.2.1 Pair Distribution Function

In essence, the pair distribution function $g(r)$ provides a measure of how likely it is to find an atom inside a spherical shell of radius r and thickness $\mathrm{d}r$ centred on an arbitrary site. If the material is monoelemental (*i.e.*, all the atoms in the material are of the same species), then the nuclear sites can be considered equivalent. In this case, $g(r)$ is taken as the statistical average of the distribution around every atom. The expression of $g(r)$ is given by Waseda (*cf.*, eq. (1.2.7) of [93]) in a slightly different form from ours, which is

$$g(r) = \frac{V}{N^2} \left\langle \sum_{j \neq k} \delta^{(3)} [\mathbf{r} - (\mathbf{R}_j - \mathbf{R}_k)] \right\rangle \tag{1.6}$$

where $\delta^{(3)}$ is a Dirac delta function. An alternative interpretation of g is that it is a dimensionless form of the radial density function $n = \bar{n} g$ that measures the number density inside the spherical shell-shaped volume between r and $r + \mathrm{d}r$. In amorphous materials, the property $g(r) \xrightarrow[r\to\infty]{} 1$ embodies the fact that there is no long-range order, as it represents a lack of correlation between the atomic positions at long distances.

[8] Ashcroft and Mermin [5] define the *geometrical structure factor* as $s_{\mathbf{Q}} = \sum_j e^{i\mathbf{Q}\cdot\mathbf{R}_j}$, which is related to the $S(\mathbf{Q})$ that we are using (we are following the same convention as, *e.g.*, Waseda [93], and Ibach and Lüth [44]) by

$$|s_{\mathbf{Q}}|^2 = S(\mathbf{Q})$$

Ashcroft and Mermin [5] intepret the geometric structure factor as the "attenuation" of the Bragg peak at the reciprocal lattice point $\mathbf{Q}$ due to the interference of the scattered waves (it should be the "amplification" of said peak instead, because its height is proportional to $|s_{\mathbf{Q}}|^2$). This interpretation is unsatisfactory on the account that it requires to be based on a crystalline material, while not giving us any explicit information on the topology of the material.

As mentioned above, the chemistry of the constituents fundamentally determines how the short-range order manifests, which implies that the structures observed around different atomic species may differ. Therefore, in multi-element materials, we require the **partial pair distribution functions** $g_{\alpha\beta}$ to characterise the topology[9]. The indices α and β denote the distinct constituent elements of the material, and $g_{\alpha\beta}$ measures the average distribution of β-type atoms around atoms of α-type. We can specify the atomic positions of α atoms by introducing the index sets $I_\alpha = \{j | \mathbf{R}_j \text{ is the position of an } \alpha\text{-type atom}\}$, which allows us to define the partial pair distribution functions as

$$g_{\alpha\beta}(r) = \frac{V}{N^2} \left\langle \sum_{\substack{j \in I_\alpha,\, k \in I_\beta \\ j \neq k}} \delta^{(3)}[\mathbf{r} - (\mathbf{R}_j - \mathbf{R}_k)] \right\rangle \tag{1.7}$$

Note that our definition of $g_{\alpha\beta}$ differs from the one presented by Waseda by a normalisation factor (*cf.*, eqs. (AL-9)–(AL-11) in p. 10 of Waseda's book [93]). As defined here, the partials in amorphous materials have the limit $g_{\alpha\beta}(r) \xrightarrow[r\to\infty]{} c_\alpha c_\beta \equiv N_\alpha N_\beta / N^2$, where N_α is the total number of atoms of α-type and c_α is their atomic fraction[10]. This choice leads to the desirable property that the complete PDF is equal to the sum of the partials, namely

$$g(r) = \sum_{\alpha,\beta} g_{\alpha\beta}(r) \tag{1.8}$$

An additional property that can be observed in eq. (1.7) is the symmetry of the partials $g_{\alpha\beta} = g_{\beta\alpha}$. They both contribute equally to the complete PDF. For that reason, when we report the structures of our alloys in Chapter 6, combine both contributions as $g_{\text{mixed}} = g_{\text{Cu,Zr}} + g_{\text{Zr,Cu}} = 2g_{\text{Cu,Zr}}$.

[9] See the subsections at the end of Section 1-2 of [93] for a more thorough discussion of this topic.

[10] The normalisation chosen by Waseda [93] is related to ours through $g_{\alpha\beta}^{\text{Waseda}} = (c_\alpha c_\beta)^{-1} g_{\alpha\beta}(r)$, which instead leads to $g_{\alpha\beta}^{\text{Waseda}}(r) \xrightarrow[r\to\infty]{} 1$.

2 Microscopic Theories of Superconductivity

In which we outline the fundamentals of superconductivity at an atomistic scale and how the superconducting state arises as a condensate of Cooper pairs held together by the electron-phonon interaction.

The first successful theoretical description of superconductors at a microscopic scale was developed 46 years after Kamerlingh-Onnes' experimental discovery, by Bardeen, Cooper, and Schrieffer in 1957 [8]. The development of this theory was spurred by the idea, put forward by Leon N. Cooper [15], that a bound state is formed by a single interacting pair in a sea of otherwise free electrons if there is a net attractive interaction of any magnitude between them. The energy of the bound state always lower than the continuous spectrum of the free electrons by an amount Δ, the gap parameter (see eq. (2.50)). This state is known as a **Cooper pair**, and it is one of the fundamental building blocks of the BCS theory.

As we will see in Section 2.2, these Cooper pairs are precisely the ones which condense into a macroscopic wavefunction in BCS theory. In this theory, the coupling that brings about the net electronic attraction required to form a condensate is the electron-phonon interaction. The quantitative description of this interaction used in the BCS theory was first provided by Fröhlich and is known as the **Frölich Hamiltonian** [29]. This Hamiltonian can be recast by means of a similarity transformation which culminates in an effective electron-electron interaction, simultaneously uncoupling them from the phononic dynamics. Physically, the effective attraction between electrons works because a passing electron attracts the nuclei, which creates a net positive charge (after the original electron is gone) that is felt by other electrons in the solid. The mathematical transformation that encapsulates this interaction was also first demonstrated by Frölich in a later article [28]. In the following, we will derive the Fröhlich Hamiltonian and show how the similarity transformation approach is used to obtain an effective electron-electron interaction.

2.1 Preliminaries

2.1.1 The Frölich Hamiltonian

The derivation in this section is partly based on lectures given by Prof. Gerardo García Naumis in his Advanced Solid State course. The lecture notes for this course are currently unavailable, but a similar derivation is performed in Chapter 8 of Ulrich Rössler's book [79].

All the influence that phonons exert on electrons is by means of the periodic distortion they cause in the underlying material's structure. Such a distortion is equivalently described by displacements in the equilibrium positions of the nuclei, which in turn alter the potential felt by the electrons. The difference between the unperturbed and distorted potentials can be interpreted heuristically as the effect of the electron-phonon interaction. Furthermore, the displacements are necessarily small, with a maximum amplitude occurring at the solid-liquid transition and bounded by Fredrick A. Lindemann's melting law [54] to $\Delta r_{\text{rms,max}} \sim 0.1d$, with d the nearest neighbour distance[1]. At lower temperatures the amplitudes are reasonably expected to be significantly smaller, allowing us to treat the distortion as a perturbation of the equilibrium configuration.

For simplicity's sake, we assume that the material's structure is homonuclear (*i.e.*, all the nuclei are of the same element) so that each nucleus[2] produces the same potential w. If we denote the equilibrium position of the nth nucleus by $\mathbf{R}_n$ and its displacement from this position by $\boldsymbol{\delta}_n$, the total potential that the structure exerts on an electron located at $\mathbf{r}$ can be expressed as

$$\mathcal{H}_{e-N} = \sum_n w(\mathbf{r} - \mathbf{R}_n + \boldsymbol{\delta}_n) \tag{2.1}$$

Taking the previous discussion of Lindemann's criterion into consideration, we can expand eq. (2.1) in a Taylor series by noting that $\boldsymbol{\delta}_n$ should be small. That is

$$\mathcal{H}_{e-N} = \underbrace{\sum_n w(\mathbf{r} - \mathbf{R}_n)}_{\mathcal{H}_0} + \underbrace{\sum_n \boldsymbol{\delta}_n \cdot \nabla w(\mathbf{r} - \mathbf{R}_n)}_{\mathcal{H}_{\text{int}}} \tag{2.2}$$

[1] More precisely, Lindemann's melting law relates the melting temperature and the melting volume of a material. The relation between the maximum root-mean-square displacement and the nearest neighbour distance was the premise in Lindemann's argument. The exact relation is $\Delta r_{\text{rms,max}} = \eta_L d$, where $0.05 \lesssim \eta_L \lesssim 0.2$ is a phenomenological coefficient. A derivation of this law using statistical mechanics can be found in [78].

[2] In this context it is common to replace the word 'nucleus' by 'ion', because only the electrons in the valence shell are affected by the change in the nearby charge distribution, while the core electrons at deeper energy levels remain mostly unperturbed. As we shall see in Chapter 4, this is the fundamental picture underlying the pseudopotential approach that greatly reduces the calculations required for heavier elements.

where we have denoted by $\mathcal{H}_0$ the energy generated by the static nuclei, while $\mathcal{H}_{\text{int}}$ gives the interaction energy produced by the nuclear motion. $\mathcal{H}_{\text{int}}$ is in essence, the electron-phonon interaction. We would like to *second-quantise* this interaction to apply it to many-body systems, and we note that in eq. (2.2) $\mathcal{H}_{\text{int}}$ acts as a single-particle operator. As T. Lancaster and S. J. Blundell elucidate in Chapter 4 of their book [50], this kind of operator is second-quantised as

$$H_{\text{int}} = \sum_{n,n',\sigma,\sigma'} c^\dagger_{n,\sigma} \langle n,\sigma \mid \mathcal{H}_{\text{int}} \mid n',\sigma' \rangle c_{n',\sigma'} = \sum_{n,n',\sigma} \langle n \mid \mathcal{H}_{\text{int}} \mid n' \rangle c^\dagger_{n,\sigma} c_{n',\sigma} \tag{2.3}$$

where $|n,\sigma\rangle$ is a basis of the one particle Hilbert space $\mathscr{H}$. To get the second equality, we have used the facts that $\mathcal{H}_{\text{int}}$ does not involve the spins and that the bra-ket is simply a complex number that commutes with the operators. In principle $|n\rangle$ can be any complete basis of the non-spinorial component of $\mathscr{H}$ (*i.e.*, $|n\rangle$ corresponds to a set of wavefunctions $\psi_n(\mathbf{r})$). However, since $\mathcal{H}_{\text{int}}$ depends only on the position of the electron it is convenient to have its matrix elements in the position basis, as they are diagonal. That is

$$H_{\text{int}} = \sum_\sigma \int_V \mathrm{d}^3 r \int_V \mathrm{d}^3 r' \, \langle \mathbf{r} \mid \mathcal{H}_{\text{int}} \mid \mathbf{r}' \rangle \Psi^\dagger_\sigma(\mathbf{r}) \Psi_\sigma(\mathbf{r}') = \sum_\sigma \int \mathrm{d}^3 r \left[\sum_n \boldsymbol{\delta}_n \cdot \boldsymbol{\nabla} w(\mathbf{r} - \mathbf{R}_n) \right] \Psi^\dagger_\sigma(\mathbf{r}) \Psi_\sigma(\mathbf{r}) \tag{2.4}$$

where $\Psi^\dagger_\sigma(\mathbf{r})$ is the field operator, that creates an electron at position $\mathbf{r}$ with spin σ. The second equality is obtained from the fact that $\mathcal{H}_{\text{int}}$ is diagonal in $|\mathbf{r}\rangle$. To find an explicit expression, we note that for a complete set of wavefunctions $\{\psi_\alpha(\mathbf{r})\}$ the field operators can be taken as

$$\Psi_\sigma(\mathbf{r}) = \sum_\alpha \psi_\alpha(\mathbf{r}) c_{\alpha,\sigma} \tag{2.5}$$

substituting this into eq. (2.4) yields

$$H_{\text{int}} = \sum_{n,\alpha,\beta,\sigma} c^\dagger_{\alpha,\sigma} c_{\beta,\sigma} \int_V \mathrm{d}^3 r \, \boldsymbol{\delta}_n \cdot \boldsymbol{\nabla} w(\mathbf{r} - \mathbf{R}_n) \, \psi^*_\alpha(\mathbf{r}) \psi_\beta(\mathbf{r}) \tag{2.6}$$

We can also change the variable onto which the gradient acts by taking a continuum approximation

$$\mathcal{H}_{\text{int}} = \sum_n \boldsymbol{\delta}_n \cdot \boldsymbol{\nabla} w(\mathbf{r} - \mathbf{R}_n) \to \frac{N}{V} \int_V \mathrm{d}^3 R \, \boldsymbol{\delta}(\mathbf{R}) \cdot \boldsymbol{\nabla}_{\mathbf{r}} w(\mathbf{r} - \mathbf{R}) = -\frac{N}{V} \int_V \mathrm{d}^3 R \, \boldsymbol{\delta}(\mathbf{R}) \cdot \boldsymbol{\nabla}_{\mathbf{R}} w(\mathbf{r} - \mathbf{R}) \tag{2.7}$$

Note that in passing from the discrete sum to the continuous integral we have assumed that the material is homogeneous, which allows us to bring N/V outside of the integral as a constant[3]. Recalling that $\boldsymbol{\nabla}_{\mathbf{R}} \cdot (\boldsymbol{\delta} w) = w\boldsymbol{\nabla}_{\mathbf{R}} \cdot \boldsymbol{\delta} + \boldsymbol{\delta} \cdot \boldsymbol{\nabla}_{\mathbf{R}} w$, we obtain

$$\mathcal{H}_{\text{int}} = -\frac{N}{V} \int_{\partial V} \mathrm{d}^3 R \, \boldsymbol{\nabla} \cdot [\boldsymbol{\delta}(\mathbf{R}) w(\mathbf{r} - \mathbf{R})] + \frac{N}{V} \int_V \mathrm{d}^3 R \, w(\mathbf{r} - \mathbf{R}) \boldsymbol{\nabla}_{\mathbf{R}} \cdot \boldsymbol{\delta}(\mathbf{R}) \tag{2.8}$$

We can apply Gauss's theorem to the first term in eq. (2.8) to transform the volume integral into a surface integral, namely

$$\mathcal{H}_{\text{int}} = -\frac{N}{V} \int_{\partial V} \mathrm{d}^2 R_s \, \mathbf{n}_s \cdot \boldsymbol{\delta}(\mathbf{R}) w(\mathbf{r} - \mathbf{R}) + \frac{N}{V} \int_V \mathrm{d}^3 R \, w(\mathbf{r} - \mathbf{R}) \boldsymbol{\nabla}_{\mathbf{R}} \cdot \boldsymbol{\delta}(\mathbf{R}) \tag{2.9}$$

The boundary term vanishes if we choose a surface lying outside the material. We return to expressing $\mathcal{H}_{\text{int}}$ as a sum in order to maintain a clear picture that $w(\mathbf{r} - \mathbf{R}_n)$ represents the potential centred on an nucleus at $\mathbf{R}_n$ and introduce the preceding result in the interaction to find

$$H_{\text{int}} = \sum_{n,\alpha,\beta,\sigma} c^\dagger_{\alpha,\sigma} c_{\beta,\sigma} \int_V \mathrm{d}^3 r \, (\boldsymbol{\nabla}_{\mathbf{R}_n} \cdot \boldsymbol{\delta}_n) w(\mathbf{r} - \mathbf{R}_n) \, \psi^*_\alpha(\mathbf{r}) \psi_\beta(\mathbf{r}) \tag{2.10}$$

Notice that, thus far, we have not needed to introduce any periodicity in the treatment of this problem and we have avoided to frame it in terms of 'lattices' or 'crystals', so that up to this point with eq. (2.10) one may in principle derive an expression for electron-phonon interaction in an amorphous material. Unfortunately, here we will need to introduce a crystalline structure with its corresponding Brillouin zone to express the displacements $\boldsymbol{\delta}_n$ in terms of the phonon spectra in a simple way. From Bloch theory (see, e.g., Chapter 8 of [5]), electrons in a crystal have energy (and translation operator) eigenstates $\psi_{m\mathbf{k}}(\mathbf{r}) = e^{i\mathbf{k}\cdot\mathbf{r}} u_{m\mathbf{k}}(\mathbf{r})$, with m being the band index, $\mathbf{k}$ the crystal–wave vector, and $u_{m\mathbf{k}}$ having the same periodicity as the lattice, we find

$$H_{\text{int}} = \sum_{n,m\mathbf{k},m'\mathbf{k}',\sigma} c^\dagger_{m,\mathbf{k},\sigma} c_{m',\mathbf{k}',\sigma} \int_V \mathrm{d}^3 r \, e^{i(\mathbf{k}'-\mathbf{k})\cdot\mathbf{r}} u^*_{m\mathbf{k}}(\mathbf{r}) u_{m'\mathbf{k}'}(\mathbf{r}) \, w(\mathbf{r} - \mathbf{R}_n) \boldsymbol{\nabla}_{\mathbf{R}_n} \cdot \boldsymbol{\delta}_n \tag{2.11}$$

Now we are finally in a position to properly turn eq. (2.11) into an interaction between particles by quantizing the displacement field $\boldsymbol{\delta}_n$ in terms of phonons, putting the lattice degrees of freedom on the same

[3] In this step we have essentially disregarded the details of the exact nuclear distribution, taking a *coarse-grain* approach to transform the Hamiltonian into a more suitable form.

footing as the electronic ones. As shown by Gerald D. Mahan in Chapter 1 of his book [56], $\boldsymbol{\delta}_n$ can be expressed in terms of the phonon operators $\{a_{\mathbf{q},s}, a^\dagger_{\mathbf{q},s}\}$ as

$$\boldsymbol{\delta}_n = \sum_{\mathbf{q},s} \sqrt{\frac{\hbar}{2MN\Omega_{\mathbf{q},s}}} (a_{\mathbf{q},s} + a^\dagger_{-\mathbf{q},s}) e^{i\mathbf{q}\cdot\mathbf{R}_n}\, \boldsymbol{\epsilon}_s \tag{2.12}$$

where we have omitted the time dependence in the operators because $\boldsymbol{\delta}_n$ is being regarded as a displacement and not an oscillation (*cf.*, eq. (1.85) of [56])[4], this simplification can be done because the nuclei move very slowly compared to the time scales relevant for the electron dynamics[5]. In eq. (2.12) $\mathbf{q}$ is the wave vector, s is the band index (*i.e.*, it refers to whether the phonon band is longitudinal or transverse and acoustic or optical), M is the mass of the nuclei, $\Omega_{\mathbf{q},s}$ is the phonon's frequency, and $\boldsymbol{\epsilon}_s$ is the polarisation vector. The divergence of this displacement is evaluated to yield simply

$$\boldsymbol{\nabla}_{\mathbf{R}_n} \cdot \boldsymbol{\delta}_n = i \sum_{\mathbf{q},s} \sqrt{\frac{\hbar}{2MN\Omega_{\mathbf{q},s}}} (a_{\mathbf{q},s} + a^\dagger_{-\mathbf{q},s}) e^{i\mathbf{q}\cdot\mathbf{R}_n}\, \mathbf{q}\cdot\boldsymbol{\epsilon}_s \tag{2.13}$$

In eq. (2.13), we can see explicitly a fact mentioned in passing by Frölich in his 1950 article [29], that only longitudinal waves interact with the electrons. Since longitudinal waves have a polarisation parallel to the wavevector ($\boldsymbol{\epsilon}_{s,\text{long}} = \mathbf{q}/|\mathbf{q}|$), while in transverse waves, the polarisation is orthogonal to $\mathbf{q}$ ($\boldsymbol{\epsilon}_{s,\text{trans}} \perp \mathbf{q}$), we confirm Frölich's statement by noticing that the integrand of the interaction vanishes for transverse phonons. We can therefore ignore the transverse phonons and focus exclusively on the longitudinal ones.

To reduce the notation somewhat, we will proceed by identifying the indices $(m, \mathbf{k}) \to \mathbf{k}$ and $(s, \mathbf{q})|_{s,\text{long}} \to \mathbf{q}$, taking for granted that index $\mathbf{k}$ implicitly includes an electronic band index, and that $\mathbf{q}$ carries a longitudinal phonon band index. Under these considerations, the interaction Hamiltonian reduces to

$$H_{\text{int}} = i \sum_{n,\mathbf{k},\mathbf{k}',\sigma,\mathbf{q}} q \sqrt{\frac{\hbar}{2MN\Omega_{\mathbf{q}}}} c^\dagger_{\mathbf{k},\sigma} c_{\mathbf{k}',\sigma} (a_{\mathbf{q}} + a^\dagger_{-\mathbf{q}}) \int_V \mathrm{d}^3 r\, e^{i[(\mathbf{k}'-\mathbf{k})\cdot\mathbf{r} + \mathbf{q}\cdot\mathbf{R}_n]} u^*_{\mathbf{k}}(\mathbf{r}) u_{\mathbf{k}'}(\mathbf{r})\, w(\mathbf{r}-\mathbf{R}_n) \tag{2.14}$$

Moreover, we note that the integrand of eq. (2.14) is composed of two parts: the Bloch states times the potential $u^*_{\mathbf{k}} u_{\mathbf{k}'} w$ which has the same period as the lattice, and a modulation by a plane wave that has a

[4] If the reader compares eq. (2.12) with Mahan's [56] eq. (1.85), they would notice some small discrepancies, including a factor of i that we have not kept. This particular edition of Mahan's book seems to have small mistakes in that section (such as missing imaginary units in the exponent), and such factor of i is also incorrect: The phonon displacement plays a role analogous to the position in the harmonic oscillator, and as such it must be proportional to the real part of the annihilation operator. Lancaster and Blundell treat the one-dimensional case in detail in their Chapter 2 of their book [50], and the reader can examine such small details there.

[5] We will discuss this difference in characteristic time scales in more detail when we introduce the Born-Oppenheimer approximation in Chapter 3.

much longer period for all but the phonons with the highest momentum. This allows us to apply the long-wavelength approximation

$$\begin{aligned}\int_V \mathrm{d}^3 r\, e^{i[(\mathbf{k}'-\mathbf{k})\cdot\mathbf{r}+\mathbf{q}\cdot\mathbf{R}_n]} u^*_{\mathbf{k}}(\mathbf{r}) u_{\mathbf{k}'}(\mathbf{r})\, w(\mathbf{r}-\mathbf{R}_n) \\ \approx \int_V \mathrm{d}^3 r\, e^{i[(\mathbf{k}'-\mathbf{k})\cdot\mathbf{r}+\mathbf{q}\cdot\mathbf{R}_n]} \left[\frac{N}{\nu V}\int_{V_{\text{u.c.}}} \mathrm{d}^3 r'\, u^*_{\mathbf{k}}(\mathbf{r}') u_{\mathbf{k}'}(\mathbf{r}')\, V(\mathbf{r}')\right]\end{aligned} \tag{2.15}$$

where we have denoted by $V_{\text{u.c.}}$ the volume of one unit cell of the crystal, ν the number of atoms per unit cell (*i.e.*, N/ν is the total number of unit cells), and $V(\mathbf{r}')$ the (periodic) net potential that the static nuclei arrangement exerts on the electrons (*i.e.*, the sum of the ws). Note that we have to divide the factor in brackets by the total volume to get the units of "energy per unit volume" that is dimensionally correct in an integrand for H_{int}. What eq. (2.15) suggests is that the modulating wave is varying slowly enough that on the scale of a single unit cell it can be treated as a constant[6].

At this juncture we take the continuum approximation for the sum over n again, but now considering the details of the nuclear distribution. That is $\sum_n \to \int_V \mathrm{d}^3 R\, n_{\text{nuc}}$, where the nuclear density must be of the form $n_{\text{nuc}} = \delta^{(3)}(\mathbf{r}-\mathbf{R})$ because $\mathbf{R}$ is a stand-in for the nuclear positions, this expression for the density implies that the nuclei are localised at $\mathbf{R}$. Additionally, upon summation (or here, integration) $\mathcal{H}_{\text{int}}$ must result only in a function only of the electronic position $\mathbf{r}$, which is achieved with the Dirac delta. Combining this with eqs. (2.14), (2.15), we find

$$H_{\text{int}} = i\sum_{\mathbf{k},\mathbf{k}',\sigma,\mathbf{q}} q\sqrt{\frac{\hbar N}{2M\nu^2\Omega_{\mathbf{q}}}} c^\dagger_{\mathbf{k},\sigma} c_{\mathbf{k}',\sigma}(a_{\mathbf{q}} + a^\dagger_{-\mathbf{q}}) \int_V \mathrm{d}^3 r\, \frac{e^{i(\mathbf{k}'-\mathbf{k}+\mathbf{q})\cdot\mathbf{r}}}{V}\left[\int_{V_{\text{u.c.}}} \mathrm{d}^3 r'\, u^*_{\mathbf{k}}(\mathbf{r}') u_{\mathbf{k}'}(\mathbf{r}')\, V(\mathbf{r}')\right] \tag{2.16}$$

It is simple to evaluate the integral $\int_V \mathrm{d}^3 r\, e^{i(\mathbf{k}'-\mathbf{k}+\mathbf{q})\cdot\mathbf{r}} = V\delta_{\mathbf{k}'-\mathbf{k}+\mathbf{q},\mathbf{G}} = V\delta_{\mathbf{k}'+\mathbf{q},\mathbf{k}+\mathbf{G}}$, where we get a Kronecker delta and not a Dirac delta because the integral is taken over a finite volume V and also because $\mathbf{k}$, $\mathbf{k}'$, and $\mathbf{q}$ are discrete. The appearance of the reciprocal lattice vector $\mathbf{G}$ in the Kronecker delta follows from the fact that two $\mathbf{k}$-points are equivalent if they differ by $\mathbf{G}$. If $\mathbf{G}$ is nonzero then the interaction would be describing Umklapp-type scattering, but as Ashcroft and Mermin point out in Chapter 25 of their book [5], this process occurs at higher temperatures comparable with the Debye temperature Θ_D. The temperatures relevant to superconductors described by Frölich's interaction is much lower than Θ_D, allowing us to neglect $\mathbf{G}$. Finally,

$$H_{\text{int}} = i\sum_{\mathbf{k},\mathbf{q},\sigma} D_{\mathbf{k},\mathbf{q}}\, c^\dagger_{\mathbf{k}+\mathbf{q},\sigma} c_{\mathbf{k},\sigma}(a_{\mathbf{q}} + a^\dagger_{-\mathbf{q}}) \tag{2.17}$$

[6] We will see next that $\mathbf{q}$ gets directly incorporated into the same exponent as the $\mathbf{k}$s by taking the continuum approximation, and furthermore that conservation of momentum is given as $\mathbf{k} = \mathbf{k}' + \mathbf{q}$ (in the absence of *Umklapp scattering*). In that situation the modulation does not vary at all, justifying further the long-wavelength approximation.

where we have dropped the unnecessary prime from the $\mathbf{k}'$, and have defined

$$D_{\mathbf{k},\mathbf{q}} = \sqrt{\frac{\hbar N q^2}{2M\nu^2\Omega_{\mathbf{q}}}} \int_{V_{\text{u.c.}}} \mathrm{d}^3 r \, u^*_{\mathbf{k}+\mathbf{q}}(\mathbf{r}) u_{\mathbf{k}}(\mathbf{r}) \, V(\mathbf{r}) \tag{2.18}$$

Eq. (2.17) is **The Fröhlich Hamiltonian** which describes the electron-phonon interaction, forming the foundation of our discussion on the theory of superconductivity. This Hamiltonian was first introduced by Frölich in his 1950 article [29], where he advanced the idea that superconductivity is caused by the electron-phonon interaction[7]. Frölich presented this equation in a slightly more simplified case with free electrons (Fermi liquid quasiparticles in a metal with constant effective mass) and acoustic phonon in the linear dispersion range. It's worth noting that eq. (2.17) can be represented as a set of Feynman diagram vertices, namely

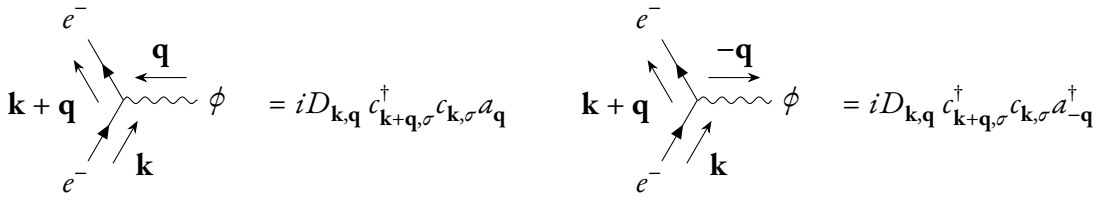

Figure 2.1: Vertices of the electron-phonon interaction given by the Frölich Hamiltonian. The left diagram depicts the absorption of a phonon of momentum $\mathbf{q}$ by an electron of momentum k, while the diagram on the right represents the analogous emission of a phonon of momentum $-\mathbf{q}$.

where we have denoted by the phonons by ϕ. The left diagram represents the interaction in which an electron with initial momentum $\mathbf{k}$ (and spin σ, which was omitted because it is not involved in the interaction) absorbs a phonon of momentum $\mathbf{q}$. Analogously, the diagram on the right represents the emission of a phonon of momentum $-\mathbf{q}$ by the electron. Hence, the total interaction can be interpreted as the sum over all the valid electron and phonon states involved in the interaction[8].

Our subject of study being superconductivity, we are interested in having only the electronic dynamics explicitly, as it is the electronic structure (*i.e.*, the condensation) that gives rise to the vanishing DC resistivity, the Meissner effect, and the thermodynamic properties of the superconductor (*i.e.*, the gap and continuous phase transition). Furthermore, we will see in Section 2.2 that even after we dismiss the phonon states from appearing explicitly in the Hamiltonian, the isotope effect is preserved implicitly in the effective interaction through the appearance of the (renormalised) phonon frequencies $\omega_{\mathbf{q}}$. In the upcoming section, we will see how the Frölich Hamiltonian is transformed into an effective electron-electron interaction.

[7] Remarkably, Frölich submitted this work just one day after the independent results of Maxwell [60] and Reynolds et al. [74] on the isotope effect were published.

[8] The final state of the electron is uniquely determined by its initial spin and momentum and the momentum of the emitted or absorbed phonon.

2.1.2 Effective Phonon-Mediated Electron-Electron Interaction

At this point, it is conducive to reintroduce the non-interacting Hamiltonians, which we will refer to collectively as H_0 in this section. However, note that we will not take the Coulomb interaction into account until we uncouple the electron and phonon dynamics.

$$H = \sum_{\mathbf{k},\sigma} \epsilon_{\mathbf{k}} c^\dagger_{\mathbf{k},\sigma} c_{\mathbf{k},\sigma} + \sum_{\mathbf{q}} \hbar\Omega_{\mathbf{q}} \left(a^\dagger_{\mathbf{q}} a_{\mathbf{q}} + \frac{1}{2} \right) + \sum_{\mathbf{k},\mathbf{q},\sigma} M_{\mathbf{q}}\, c^\dagger_{\mathbf{k}+\mathbf{q},\sigma} c_{\mathbf{k},\sigma} (a_{\mathbf{q}} + a^\dagger_{-\mathbf{q}}) = H_0 + H_1 \tag{2.19}$$

the first two terms are identified as H_0, the Hamiltonian of the free electrons and phonons. The last term is denoted as H_1 which was previously denoted by H_{int} in Section 2.1.1. Note that the coupling factors have been replaced according to $iD_{\mathbf{k},\mathbf{q}} \approx M_{\mathbf{q}}$, which are usually taken to depend only on the phonon momentum. It is customary[9] to transform the Hamiltonian of the free electrons by changing the reference of the energy to the Fermi level ϵ_F (*viz.*, the energy of the highest-energy state occupied at 0 K), namely, $\epsilon_{\mathbf{k}} \to \epsilon'_{\mathbf{k}} = \epsilon_{\mathbf{k}} - \epsilon_F$, as well as transforming the ladder operators per the replacement

$$(c^\dagger_{\mathbf{k},\sigma})' = \theta(\epsilon_{\mathbf{k}} - \epsilon_F) c^\dagger_{\mathbf{k},\sigma} + \theta(\epsilon_F - \epsilon_{\mathbf{k}}) c_{\mathbf{k},\sigma}, \quad (c_{\mathbf{k},\sigma})' = \theta(\epsilon_{\mathbf{k}} - \epsilon_F) c_{\mathbf{k},\sigma} + \theta(\epsilon_F - \epsilon_{\mathbf{k}}) c^\dagger_{\mathbf{k},\sigma} \tag{2.20}$$

where $\theta(x)$ is the Heaviside step function. In other words, the new ladder operators act identically to the original ones when creating or annihilating states above the Fermi level, but their actions transpose for lower energies. Note that the anticommutation relations of these new operators remain unaltered. In terms of these changes, the free electron Hamiltonian is

$$H_{0,\text{el}} = \sum_{\epsilon_{\mathbf{k}} > \epsilon_F,\sigma} \epsilon_{\mathbf{k}} c^\dagger_{\mathbf{k},\sigma} c_{\mathbf{k},\sigma} + \sum_{\epsilon_{\mathbf{k}} < \epsilon_F,\sigma} \epsilon_{\mathbf{k}} c_{\mathbf{k},\sigma} c^\dagger_{\mathbf{k},\sigma} = \sum_{\epsilon_{\mathbf{k}} > \epsilon_F,\sigma} \epsilon_{\mathbf{k}} n_{\mathbf{k},\sigma} + \sum_{\epsilon_{\mathbf{k}} < \epsilon_F,\sigma} |\epsilon_{\mathbf{k}}| (1 - n_{\mathbf{k},\sigma}) \tag{2.21}$$

where we have omitted the primes from the new operators and energies. We have also introduced the number operators $n_{\mathbf{k},\sigma} = c^\dagger_{\mathbf{k},\sigma} c_{\mathbf{k},\sigma}$, and the second term on the right-hand side is obtained by use of the anticommutation relation. To prevent the coming calculations from being cumbersome we will not immediately employ H_0 in the form provided by eq. (2.21). We will instead use the uncluttered form from eq. (2.19), and only apply the replacement supplied by eq. (2.21) at the end of the calculation. Regardless, the reader can rest assured that the result does not depend on this choice because the transformation preserves the commutation relations $[H_0, (c_{\mathbf{k},\sigma})'] = ([H_0, c_{\mathbf{k},\sigma}])'$ and $[H_0, (c^\dagger_{\mathbf{k},\sigma})'] = ([H_0, c^\dagger_{\mathbf{k},\sigma}])'$.

[9] See, for instance, Section 2.2s of Altland's and Simons's book [1]. As discussed there, the Hamiltonian written in terms of these quantities makes more physical sense, as the operators create elementary excitations from the ground state $|\Omega\rangle$ (the "vacuum") where the Fermi sea is full. These excitations are the so-called conduction electrons (which are not electrons but collective excitations of the Fermi liquid that behave analogously) and valence holes (which behave like positive particles). Both types of excitation behave like pointlike particles but arise from an imbalance in the collective local charge distribution (an excess of electrons for "conduction electrons" and a scarcity of them for "valence holes").

To proceed, a similarity transformation through an operator S is performed on the Hamiltonian by means of

$$\begin{aligned} H' &= e^{-S}He^{S} = \left(1 - S + \frac{S^2}{2} + O(S^3)\right)H\left(1 + S + \frac{S^2}{2} + O(S^3)\right) \\ &= H + HS + H\frac{S^2}{2} - SH - SHS + \frac{S^2}{2} + O(S^3) \\ &= H + [H, S] + \frac{1}{2}[[H, S], S] + O(S^3) \end{aligned} \tag{2.22}$$

Note that to be able to truncate the series to second order, as we have done, S must be small. In terms of the free and interaction parts, the transformed Hamiltonian is

$$H' = H_0 + H_1 + [H_0, S] + [H_1, S] + \frac{1}{2}[[H_0, S], S] + \frac{1}{2}[[H_1, S], S] + O(S^3) \tag{2.23}$$

A convenient choice of S that simplifies eq. (2.23) is one such that

$$H_1 + [H_0, S] = 0 \tag{2.24}$$

in which case $S \sim H_1/H_0 \ll 1$, satisfying the requirement to truncate the exponentials. Moreover, $[[H_1, S], S] \sim S^3$ relative to the magnitude of H_0, allowing us to discard that term as well. Then, to order S^2, the transformed Hamiltonian is simply

$$H' = H_0 + \frac{1}{2}[H_1, S] \tag{2.25}$$

One way of proceeding is to guess the form of S, in particular the following ansatz is adequate

$$S = \sum_{\sigma,\mathbf{k},\mathbf{k}',\mathbf{q}} M_{\mathbf{q}}(Aa^{\dagger}_{-\mathbf{q}} + Ba_{\mathbf{q}})c^{\dagger}_{\mathbf{k}\sigma}c_{\mathbf{k}'\sigma} \tag{2.26}$$

And we use the relations

$$[H_0, c_{\mathbf{k}\sigma}] = -\epsilon_{\mathbf{k}}c_{\mathbf{k}\sigma}, \quad [H_0, c^{\dagger}_{\mathbf{k}\sigma}] = \epsilon_{\mathbf{k}}c^{\dagger}_{\mathbf{k}\sigma}, \quad [H_0, a_{\mathbf{q}}] = -\hbar\Omega_{\mathbf{q}}a_{\mathbf{q}}, \quad [H_0, a^{\dagger}_{\mathbf{q}}] = \hbar\Omega_{\mathbf{q}}a^{\dagger}_{\mathbf{q}} \tag{2.27}$$

to evaluate the commutator

$$[H_0, S] = \left[H_0, \sum_{\sigma,\mathbf{k},\mathbf{k}',\mathbf{q}} (Aa^{\dagger}_{-\mathbf{q}} + Ba_{\mathbf{q}})M_{\mathbf{q}}c^{\dagger}_{\mathbf{k}\sigma}c_{\mathbf{k}'\sigma}\right] = \sum_{\sigma,\mathbf{k},\mathbf{k}',\mathbf{q}} M_{\mathbf{q}}[H_0, (Aa^{\dagger}_{-q} + Ba_{q})c^{\dagger}_{\sigma k}c_{\sigma k'}] \tag{2.28}$$

Explicitly,

$$\begin{aligned}
[H_0, S] &= \sum_{\sigma,\mathbf{k},\mathbf{k}',\mathbf{q}} M_{\mathbf{q}} \Big\{ (A a^\dagger_{-\mathbf{q}} + B a_{\mathbf{q}}) [H_0, c^\dagger_{\mathbf{k},\sigma} c_{\mathbf{k}',\sigma}] + [H_0, (A a^\dagger_{-\mathbf{q}} + B a_{\mathbf{q}})] c^\dagger_{\mathbf{k}\sigma} c_{\mathbf{k}'\sigma} \Big\} \\
&= \sum_{\sigma,\mathbf{k},\mathbf{k}',\mathbf{q}} M_{\mathbf{q}} \Big\{ (A a^\dagger_{-\mathbf{q}} + B a_{\mathbf{q}}) (-\epsilon_{\mathbf{k}'} + \epsilon_{\mathbf{k}}) c^\dagger_{\mathbf{k},\sigma} c_{\mathbf{k}',\sigma} + \hbar (A\Omega_{-\mathbf{q}} a^\dagger_{-\mathbf{q}} - B\Omega_{\mathbf{q}} a_{\mathbf{q}}) c^\dagger_{\mathbf{k},\sigma} c_{\mathbf{k}',\sigma} \Big\} \\
&= -\sum_{\sigma,\mathbf{k},\mathbf{k}',\mathbf{q}} M_{\mathbf{q}} \Big\{ A(\epsilon_{\mathbf{k}'} - \epsilon_{\mathbf{k}} - \hbar\Omega_{\mathbf{q}}) a^\dagger_{-\mathbf{q}} c^\dagger_{\mathbf{k},\sigma} c_{\mathbf{k}',\sigma} + B(\epsilon_{k'} - \epsilon_k + \hbar\Omega_{\mathbf{q}}) a_{\mathbf{q}} c^\dagger_{\mathbf{k}+\mathbf{q},\sigma} c_{\mathbf{k}',\sigma} \Big\}
\end{aligned} \tag{2.29}$$

where we used the distributive property of the commutator[10] (*i.e.*, $[a, bcd] = [a, b]cd + b[a, c]d + bc[a, d]$). We also made use of the fact that $\Omega_{-\mathbf{q}} = \Omega_{\mathbf{q}}$. Comparing the right-hand side of eq. (2.29) with the form of H_1 in eq. (2.19), we see that the generator S defined by eq. (2.25) must be

$$S = \sum_{\mathbf{k},\mathbf{q},\sigma} M_{\mathbf{q}} \left(\frac{a^\dagger_{-\mathbf{q}}}{\epsilon_{\mathbf{k}} - \epsilon_{\mathbf{k}+\mathbf{q}} - \hbar\Omega_{\mathbf{q}}} + \frac{a_{\mathbf{q}}}{\epsilon_{\mathbf{k}} - \epsilon_{\mathbf{k}+\mathbf{q}} + \hbar\Omega_{\mathbf{q}}} \right) c^\dagger_{\mathbf{k}+\mathbf{q},\sigma} c_{\mathbf{k},\sigma} \tag{2.30}$$

We omit the explicit calculation of $[H_1, S]$ that appears in H', but note that it is easily (if a bit tediously) performed by applying the distributive property of the commutator and using the canonical commutation/anticommutation relation of the ladder operators. Doing this and simplifying the resulting expression, one finds

$$[H_1, S] = \sum_{\sigma,\sigma',\mathbf{k},\mathbf{k}',\mathbf{q}} M_{\mathbf{q}} M_{-\mathbf{q}} (A_{\mathbf{k}',-\mathbf{q}} - B_{\mathbf{k}',-\mathbf{q}}) c^\dagger_{\mathbf{k}'-\mathbf{q},\sigma'} c_{\mathbf{k}',\sigma'} c^\dagger_{\mathbf{k}+\mathbf{q},\sigma} c_{\mathbf{k},\sigma} + 2H_{e-2ph} \tag{2.31}$$

where we have denoted by $A_{\mathbf{k},\mathbf{q}}$ and $B_{\mathbf{k},\mathbf{q}}$ the coefficients of the phonon operators that appear in the generator S (*cf.*, eqs. (2.26) and (2.30)). The second term in eq. (2.31) represents an interaction of an electron and two phonons at a single vertex, and can be expressed as

$$\begin{aligned}
H_{e-2ph} = \frac{1}{2} \sum_{\sigma,\mathbf{k},\mathbf{q},\mathbf{q}'} M_{\mathbf{q}} M_{\mathbf{q}'} \Big[&(A_{\mathbf{k},\mathbf{q}} + A_{\mathbf{k}+\mathbf{q},\mathbf{q}'}) a^\dagger_{-\mathbf{q}} a^\dagger_{-\mathbf{q}'} + (A_{\mathbf{k},\mathbf{q}} + A_{\mathbf{k}+\mathbf{q}',\mathbf{q}} + B_{\mathbf{k},\mathbf{q}'} + B_{\mathbf{k}+\mathbf{q},\mathbf{q}'}) a^\dagger_{-\mathbf{q}} a_{\mathbf{q}'} \\
&+ (B_{\mathbf{k},\mathbf{q}} + B_{\mathbf{k}+\mathbf{q},\mathbf{q}'}) a_{\mathbf{q}} a_{\mathbf{q}'} \Big] c^\dagger_{\mathbf{k}+\mathbf{q}+\mathbf{q}'} c_{\mathbf{k}}
\end{aligned} \tag{2.32}$$

This two-phonon interaction is not usually taken explicitly, because it involves a single electron whereas we are interested in the effective interaction between two of them. Some authors may discard it outright (*cf.*, Chapter 8 of Rössler's [79] or Chapter 11 of Philip Phillips's book [71]) because for it to contribute to the

[10] More specifically, we used the fact that the set of linear endomorphisms of Fock space $L : \mathcal{F} \to \mathcal{F}$ (*e.g.*, the operators $H_0, a, a^\dagger, c, c^\dagger$, etc.) equipped with addition form a vector space over the field of complex numbers $\mathbb{C}$. If this vector field is further bestowed with a commutator $[.,.]$, it forms an algebra over $\mathbb{C}$. Recall that an algebra is distributive by definition.

electron-electron interaction it requires at least a fourth order term[11] in the coupling parameter $M_{\mathbf{q}}$. It is more accurate, however, to say that this term instead renormalises the phonon dispersion $\Omega_{\mathbf{q}} \to \omega_{\mathbf{q}}$. This was first shown by Frölich in his 1952 article [28], where he showed that in the linear range of the acoustic band the dispersion is renormalised as $\Omega_q = \hbar q s \to \omega_q = \hbar q s'$, where s represents the speed of sound. We will not perform such renormalisation here, but we will make it apparent by changing the notation of the phonon frequency. The electron Hamiltonian is thus reduced to

$$H = \sum_{\sigma,\mathbf{k}} \epsilon_{\mathbf{k}} c^{\dagger}_{\mathbf{k},\sigma} c_{\mathbf{k},\sigma} + \sum_{\sigma,\sigma',\mathbf{k},\mathbf{k}',\mathbf{q}} \frac{|M_{\mathbf{q}}|^2 \hbar\omega_{\mathbf{q}}}{(\epsilon_{\mathbf{k}} - \epsilon_{\mathbf{k}+\mathbf{q}})^2 - \hbar^2\omega_{\mathbf{q}}^2} c^{\dagger}_{\mathbf{k}+\mathbf{q},\sigma} c_{\mathbf{k},\sigma} c^{\dagger}_{\mathbf{k}'-\mathbf{q},\sigma'} c_{\mathbf{k}',\sigma'} + H_C \tag{2.33}$$

where we have relabelled the indices $\mathbf{k} \leftrightarrow \mathbf{k}'$ and $\mathbf{q} \to -\mathbf{q}$ to more closely match the expression presented in the BCS article [8]. We also introduced the Coulomb interaction at this juncture which has been labelled as H_C. Eq. (2.33) represents the total Hamiltonian experienced by the electrons. To arrive at the final form of the electron Hamiltonian we employ the free electron Hamiltonian $H_{0,\mathrm{el}}$ relative to the Fermi level of eq. (2.21), resulting in

$$H = \sum_{\epsilon_{\mathbf{k}}>\epsilon_F,\sigma} \epsilon_{\mathbf{k}} n_{\mathbf{k},\sigma} + \sum_{\epsilon_{\mathbf{k}}<\epsilon_F,\sigma} |\epsilon_{\mathbf{k}}|(1 - n_{\mathbf{k},\sigma}) + \sum_{\sigma,\sigma',\mathbf{k},\mathbf{k}',\mathbf{q}} \left[\frac{|M_{\mathbf{q}}|^2 \hbar\omega_{\mathbf{q}}}{(\epsilon_{\mathbf{k}} - \epsilon_{\mathbf{k}+\mathbf{q}})^2 - \hbar^2\omega_{\mathbf{q}}^2} + V^{\mathrm{C}}_{\mathbf{q}} \right] c^{\dagger}_{\mathbf{k}+\mathbf{q},\sigma} c_{\mathbf{k},\sigma} c^{\dagger}_{\mathbf{k}'-\mathbf{q},\sigma'} c_{\mathbf{k}',\sigma'} \tag{2.34}$$

where $V^{\mathrm{C}}_{\mathbf{q}}$ is $\mathbf{q}$th component of the Fourier transform of the (screened) Coulomb potential. Note that whenever $\Delta\epsilon < \hbar\omega$, the phonon-mediated interaction is attractive. The Hamiltonian expanded in (2.34) will be our starting point to discuss the theory developed by Bardeen, Cooper, and Schrieffer in their seminal article [8].

2.2 The Bardeen-Cooper-Schrieffer Approach

As mentioned above, it was Cooper's insight—that an attractive potential of any magnitude gives rise to a bound state in a pair of electrons—which kickstarted the development of the microscopic theory. We would like to discuss this result in more detail.

[11] This term must be fourth order because each vertex arising from the H_{e-2ph} interaction is quadratic in $M_{\mathbf{q}}$. This just means that every vertex of this interaction involves two phonons (either incoming or outgoing), all the single phonon vertices have been absorbed in the effective interaction term.

2.2.1 Cooper pairs

A reading of Cooper's article reveals that his result follows from considering a single pair of interacting electrons with an individual particle spectrum corresponding to conduction electrons in an isotropic metal with constant effective mass. In other words, the electrons' dispersion is taken as

$$\epsilon_{\mathbf{k}} = \frac{\hbar^2}{2m^*}k^2 \tag{2.35}$$

This simplification is supported by the qualitative similarity in the superconducting transition that occurs in various materials. Then, the energy eigenfunction of the interacting electrons is expanded with respect to the momentum basis

$$\psi(\mathbf{r}_1, \mathbf{r}_2) = \sum_{\mathbf{k}_1,\mathbf{k}_2} a_{\mathbf{k}_1,\mathbf{k}_2}\varphi_{\mathbf{k}_1,\mathbf{k}_2}(\mathbf{r}_1, \mathbf{r}_2) = \frac{1}{V}\sum_{\mathbf{k}_1,\mathbf{k}_2} a_{\mathbf{k}_1,\mathbf{k}_2}e^{i(\mathbf{k}_1\cdot\mathbf{r}_1+\mathbf{k}_2\cdot\mathbf{r}_2)} \tag{2.36}$$

Cooper then proceeds with a change of coordinates to the centre of mass frame (see, *e.g.*, Section 2.4 of Weinberg's book [94] and the equations therein)

$$\mathbf{r} = \mathbf{r}_2 - \mathbf{r}_1, \quad \mathbf{R} = \frac{m_1\mathbf{r}_1 + m_2\mathbf{r}_2}{m_1 + m_2} = \frac{\mathbf{r}_1 + \mathbf{r}_2}{2}, \quad \mathbf{k} = \mu\left(\frac{\mathbf{k}_2}{m_2} - \frac{\mathbf{k}_1}{m_1}\right) = \frac{\mathbf{k}_2 - \mathbf{k}_1}{2}, \quad \mathbf{K} = \mathbf{k}_1 + \mathbf{k}_2 \tag{2.37}$$

where $m_i = m^*$ are the masses of the electrons and $\mu = m_1m_2/(m_1 + m_2) = m^*/2$ is the reduced mass of the two-particle system. With this change of variables, the wavefunction becomes

$$\psi(\mathbf{r}, \mathbf{R}) = \frac{1}{V}\sum_{\mathbf{k},\mathbf{K}} a_{\mathbf{k},\mathbf{K}}e^{i(\mathbf{k}\cdot\mathbf{r}+\mathbf{K}\cdot\mathbf{R})} \tag{2.38}$$

Recall that the interaction between the electrons (*i.e.*, the third term in eq. (2.34)) conserves the total momentum of the system, which is synonymous with saying that the interaction is translationally invariant. Consequently, the energy eigenfunction may also be an eigenfunction of the total momentum[12] $\mathbf{K}$. With this in mind the wavefunction reduces to

$$\psi(\mathbf{r}, \mathbf{R}) = \frac{e^{\mathbf{K}\cdot\mathbf{R}}}{V}\sum_{\mathbf{k}} a_{\mathbf{k}}e^{i\mathbf{k}\cdot\mathbf{r}} \tag{2.39}$$

[12] Recall that for an operator that is not explicitly time-dependent, Heisenberg's equation of motion dictates that $\frac{\mathrm{d}}{\mathrm{d}t}A = \frac{i}{\hbar}[H, A]$. Therefore, the fact that $\mathbf{K}$ is conserved implies that it commutes with the Hamiltonian and that its basis is appropriate to diagonalise H.

The Schrödinger equation then becomes an equation that determines the coefficients of the expansion $a_{\mathbf{k}}$ by projecting it to the momentum basis. Explicitly

$$\int_{V\times V} \mathrm{d}^3r\mathrm{d}^3R\, \varphi^*_{\mathbf{k},\mathbf{K}}(\mathbf{r},\mathbf{R})(H-E)\psi(\mathbf{r},\mathbf{R}) = 0 \tag{2.40}$$

Expanding the ψ according to (2.39), replacing $\varphi^*_{\mathbf{k},\mathbf{K}}$ by its definition, and expanding the Hamiltonian in non-interacting and interacting parts $H = H_0 + H_1$, we find

$$\frac{1}{V^2}\sum_{\mathbf{k}'} a_{\mathbf{k}'} \int_{V\times V} \mathrm{d}^3r\mathrm{d}^3R \left\{(\mathscr{E}_{\mathbf{K}'} + \varepsilon_{\mathbf{k}'} - E)e^{i[(\mathbf{k}'-\mathbf{k})\cdot\mathbf{r}+(\mathbf{K}'-\mathbf{K})\cdot\mathbf{R}]} + e^{i(\mathbf{K}'-\mathbf{K})\cdot\mathbf{R}}\left[e^{-i\mathbf{k}\cdot\mathbf{r}}H_1 e^{i\mathbf{k}'\cdot\mathbf{r}}\right]\right\} = 0 \tag{2.41}$$

where we have evaluated the individual particle Hamiltonian using $H_0\,|\mathbf{k},\mathbf{K}\rangle = (\mathscr{E}_{\mathbf{K}} + \varepsilon_{\mathbf{k}})\,|\mathbf{k},\mathbf{K}\rangle$, with $\mathscr{E}_{\mathbf{K}} = \hbar^2K^2/4m^*$ and $\varepsilon_{\mathbf{k}} = \hbar^2k^2/m^*$ (*i.e.*, the mass associated with the absolute position is the total mass $m_T = 2m^*$, while the one associated with the relative position is the reduced mass $\mu = m^*/2$). Now we use the identity $\int_\Omega \mathrm{d}^n x\, e^{iu\cdot x} = |\Omega|\delta_{u,0}$ to find

$$(\mathscr{E}_{\mathbf{K}} + \varepsilon_{\mathbf{k}} - E)\delta_{\mathbf{K},\mathbf{K}'}a_{\mathbf{k}} + \delta_{\mathbf{K},\mathbf{K}'}\sum_{\mathbf{k}'} a_{\mathbf{k}'}\left[\frac{1}{V}\int_V \mathrm{d}^3r\, e^{-i\mathbf{k}\cdot\mathbf{r}}H_1 e^{i\mathbf{k}'\cdot\mathbf{r}}\right] = 0 \tag{2.42}$$

the term in square brackets represents the matrix elements of the interaction $\langle\mathbf{k}|H_1|\mathbf{k}'\rangle$. Cooper introduces the following expression to approximate this term

$$\langle\mathbf{k}|H_1|\mathbf{k}'\rangle = \begin{cases} -|F|, & \text{if } k,k' \in [k_0,k_m] \\ 0, & \text{otherwise} \end{cases} \tag{2.43}$$

where F is a constant, and the wavevectors k_0 and k_m are introduced as a demarcation of where the phonon mediated interaction of eq. (2.34) is attractive. In particular, if one considers the typical phonon frequency to be commensurate with the Debye frequency $\omega_{\mathbf{q}} \approx \omega_D$, then the range wherein the interaction remains attractive[13] is given by $\Delta\epsilon \lesssim \hbar\omega_D$. The range of momenta is then constrained by

$$\Delta\varepsilon = \frac{\hbar^2}{m^*}(k_m^2 - k_0^2) \approx 2\hbar\omega_D \lesssim 0.4\ \mathrm{eV} \tag{2.44}$$

The upper bound is approximated from the Debye temperature of diamond $\Theta_D^{\text{diamond}} \approx 2240$ K (see, Tohei et al. [88]) which corresponds to an energy of ~ 0.19 eV, but most materials have Debye temperatures that are an order of magnitude smaller than this, including the Cu_xZr_{1-x} alloy. The approximation given by

[13] More accurately, this is the range where the interaction is attractive on average.

eq. (2.43) conceptually amounts to removing all the details of the interaction, accounting for it only in an average sense. As we will see, a similar approximation is performed in the original formulation of BCS theory. With this simplification, the equations for the coefficients become

$$(E - \varepsilon_{\mathbf{k}} - \mathscr{E}_{\mathbf{K}})a_{\mathbf{k}} = -|F| \sum_{\mathbf{k}'} a_{\mathbf{k}'}, \text{ with } k, k' \in [k_0, k_m]; \quad \text{and } \mathbf{K} = \mathbf{K}' \tag{2.45}$$

The last expression in eq. (2.45) is simply the statement of conservation of momentum. In his original article [15], Cooper employs a "trick" that simplifies the coefficients $a_{\mathbf{k}}$ away from the computation, which is demonstrated by Schrieffer in Section 2.2 of his book [81]. It is performed by introducing the constant

$$C = \sum_{k_0 \le k \le k_m} a_{\mathbf{k}} \tag{2.46}$$

with which the equation for the coefficients can be written as

$$a_{\mathbf{k}} = -|F| \frac{C}{E - \varepsilon_{\mathbf{k}} - \mathscr{E}_{\mathbf{K}}} \tag{2.47}$$

this expression for the $a_{\mathbf{k}}$s is substituted back in eq. (2.46). Cancelling the factors of C on both sides of the equation we find

$$1 = -|F| \sum_{k_0 \le k \le k_m} \frac{1}{E - \varepsilon_{\mathbf{k}} - \mathscr{E}_{\mathbf{K}}} = -|F| \int_{\varepsilon_0}^{\varepsilon_m} \mathrm{d}\varepsilon \, \frac{N(\varepsilon, \mathbf{K})}{E - \varepsilon - \mathscr{E}_{\mathbf{K}}} \tag{2.48}$$

where $N(\varepsilon, \mathbf{K})$ is the two-electron density of states[14] with relative energy ε and total momentum $\mathbf{K}$. Here Cooper approximates $N(\varepsilon, \mathbf{K}) \approx N(\varepsilon_0, \mathbf{K})$, allowing us to effortlessly obtain

$$1 = |F| N(\varepsilon_0, \mathbf{K}) \ln\left(\frac{E - \varepsilon_m - \mathscr{E}_{\mathbf{K}}}{E - \varepsilon_0 - \mathscr{E}_{\mathbf{K}}}\right) \tag{2.49}$$

Solving for E and simplifying we find

$$E = \mathscr{E}_{\mathbf{K}} + \varepsilon_0 - \frac{\varepsilon_m - \varepsilon_0}{e^{1/|F|N(\varepsilon_0, \mathbf{K})} - 1} \equiv \mathscr{E}_{\mathbf{K}} + \varepsilon_0 - \Delta \tag{2.50}$$

[14] More concretely, $N(\varepsilon, \mathbf{K})$ is the number of states $|\mathbf{k}, \mathbf{K}\rangle$ in the phase-space volume $\mathrm{d}\Omega(\varepsilon, \mathbf{K}) = \{|\mathbf{k}', \mathbf{K}'\rangle \mid \varepsilon \le \varepsilon_{\mathbf{k}'} \le \varepsilon + \mathrm{d}\varepsilon, \mathbf{K}' = \mathbf{K}\}$ per unit of ε. Namely,

$$N(\varepsilon, \mathbf{K}) \equiv \frac{\mathrm{d}\Omega(\varepsilon, \mathbf{K})}{\mathrm{d}\varepsilon}$$

In this sense $N(\varepsilon, \mathbf{K})$ can be regarded as a "conditional" density of states: $N(\varepsilon|\mathbf{K}) \leftrightarrow$ *the number of two-electron states per unit energy with energy ε, restricted to a fixed total momentum* $\mathbf{K}$. This is roughly analogous to a conditional probability distribution function (see, for instance, Chapter 2 of the book by Mehran Kardar [46]), but without necessarily normalising it to 1.

As Cooper points out [15], this is the lowest energy eigenvalue, and it is a bound state with binding energy Δ. Schrieffer presents a similar but more general treatment of the one-pair problem, and in far more detail, in Chapter 2 of his book [81]. A striking feature observed in eq. (2.50) is that the binding energy is finite for any value of the attractive potential $|F|$, however small.

2.2.2 The BCS Hamiltonian

Now we return to the analysis of the many-electron system described by eq. (2.34). One point that requires further attention is the Coulomb interaction, which has not yet been laid out explicitly. For free electrons, the matrix element is $V_{\mathbf{q}}^{C} = 4\pi e/q^2$, which has an infrared (long-wavelength) divergence at $q = 0$. The worries about this divergence should, however, be assuaged by the fact that the long-wavelength behaviour of the electrons is described primarily by their collective motion as plasma oscillations (plasmons), and the individual particle picture becomes relevant only at wavelengths lower than the corresponding Debye length. This observation was put forth by D. Pines and D. Bohm in their pioneering work on plasmon theory [72]. One of the key propositions of Bardeen, Cooper, and Schrieffer [8] is that, in a manner analogous to the Cooper one-pair problem, a net attractive interaction is sufficient for the electrons to form a bound state, which is, in this case, a condensate. Consequently, they suggest the following criterion for superconductivity

$$-V \equiv \left\langle -\frac{2|M_{\mathbf{q}}|^2}{\hbar\omega_{\mathbf{q}}} + \frac{4\pi e^2}{q^2} \right\rangle < 0 \tag{2.51}$$

where the phonon term of the interaction was simplified from its expression in eq. (2.34) by taking $\Delta\epsilon = \epsilon_{\mathbf{k}} - \epsilon_{\mathbf{k}+\mathbf{q}} \ll \hbar\omega_{\mathbf{q}} \sim \hbar\omega_D$, under the consideration that the states accessible to electrons follow Fermi-Dirac statistics. In particular, the difference in Bloch energies must be commensurate with the corresponding thermal energy, which, in the temperature range relevant to superconductivity, implies that $\Delta\epsilon \sim k_B T_c$. For many superconductors, especially those known in 1957, their critical temperatures are indeed much lower than the Debye temperature $T_c \ll \Theta_D = \hbar\omega_D/k_B$. However, such simplification should not be considered as general today as it was in 1957 when BCS introduced it. Note that the average in eq. (2.51) is taken over the states that are relevant to the superconducting wavefunction (*i.e.*, $\epsilon \lesssim k_B T_c$)

At this juncture, the Hamiltonian is simplified by means of the observation that, due to the fermionic statistics of the electrons, many of the contributions to its matrix elements alternate in sign, cancelling out. Based on this observation, Bardeen, Cooper, and Schrieffer [8] introduce an effective Hamiltonian which accounts only for the interactions between electrons in pairs, namely

$$H_{\text{BCS}} = 2\sum_{\epsilon_{\mathbf{k}}>\epsilon_F} \epsilon_{\mathbf{k}} b_{\mathbf{k}}^{\dagger} b_{\mathbf{k}} + 2\sum_{\epsilon_{\mathbf{k}}<\epsilon_F} |\epsilon_{\mathbf{k}}| b_{\mathbf{k}} b_{\mathbf{k}}^{\dagger} - \sum_{\mathbf{k},\mathbf{k}'} V_{\mathbf{k},\mathbf{k}'} b_{\mathbf{k}'}^{\dagger} b_{\mathbf{k}} \tag{2.52}$$

This is the **BCS Hamiltonian**. The new ladder operators $b_{\mathbf{k}}$ and $b_{\mathbf{k}}^\dagger$ are defined as

$$b_{\mathbf{k}}^\dagger = c_{\mathbf{k}\uparrow}^\dagger c_{-\mathbf{k}\downarrow}^\dagger, \quad b_{\mathbf{k}} = (b_{\mathbf{k}}^\dagger)^\dagger = c_{-\mathbf{k}\downarrow} c_{\mathbf{k}\uparrow} \tag{2.53}$$

which create and annihilate electrons in pairs of net-zero momentum and spin (*i.e.*, Cooper pairs), respectively. The matrix elements $V_{\mathbf{k},\mathbf{k}'}$ comprise the combined effect of the electron-phonon interaction and the screened Coulomb interaction of eq. (2.33) that acts between the pairs and are predominantly positive in the superconductor[15]. In Appendix A of their article [8], BCS show, employing a perturbation theory analysis, that the effective Hamiltonian (2.52) accounts for approximately 99.9% of the ground state energy. These operators can be shown to obey the relations

$$[b_{\mathbf{k}}, b_{\mathbf{k}'}] = 0, \quad [b_{\mathbf{k}}, b_{\mathbf{k}'}^\dagger] = \delta_{\mathbf{k},\mathbf{k}'}(1 - n_{\mathbf{k}\uparrow} - n_{-\mathbf{k}\downarrow}), \quad \{b_{\mathbf{k}}, b_{\mathbf{k}'}\} = 2b_{\mathbf{k}} b_{\mathbf{k}'}(1 - \delta_{\mathbf{k},\mathbf{k}'}) \tag{2.54}$$

2.2.3 Ground State

The BCS ground state is approximated by the variational method using the trial function given by

$$|\Psi\rangle = \prod_{\mathbf{k}} \left[(1 - h_{\mathbf{k}})^{\frac{1}{2}} + h_{\mathbf{k}}^{\frac{1}{2}} b_{\mathbf{k}}^\dagger \right] |\Omega\rangle \tag{2.55}$$

where the $h_{\mathbf{k}} \in \mathbb{R}$ are the variational parameters which, in this case, represent the probability of there being a pair $(\mathbf{k}\uparrow, -\mathbf{k}\downarrow)$. Since each $\mathbf{k}$-pair has a parameter independent of the other wavevectors (*i.e.*, $h_{\mathbf{k}}$ is a function only of k), it is said that $|\Psi\rangle$ defined in this way has the Hartree property[16]. This approximation to the ground state lends itself to an effortless evaluation of the interaction term by means of the orthogonal decomposition

$$|\Psi\rangle = h_{\mathbf{k}}^{\frac{1}{2}} |\varphi_1\rangle + (1 - h_{\mathbf{k}})^{\frac{1}{2}} |\varphi_0\rangle \tag{2.56}$$

where $|\varphi_1\rangle = b_{\mathbf{k}}^\dagger |\varphi_0\rangle$ represents the component in which the pair state $(\mathbf{k}\uparrow, -\mathbf{k}\downarrow)$ is certainly occupied, and $|\varphi_0\rangle = \prod_{\mathbf{k}' \neq \mathbf{k}} \left[(1 - h_{\mathbf{k}})^{\frac{1}{2}} + h_{\mathbf{k}}^{\frac{1}{2}} b_{\mathbf{k}}^\dagger \right] |\Omega\rangle$ represents the component in which the pair state is certainly

[15] We have heavily emphasised the role of the electron-phonon interaction in the current treatment of superconductivity, however, it is fascinating to note that the BCS model is not necessarily affixed to this interaction. Indeed, any physical system with an effective attraction capable of overcoming the Coulomb repulsion may be modelled to some extent by the BCS Hamiltonian.

[16] Recall that the Hartree approximation (*cf.*, Section 4.5 of Weinberg's book [94]) consists in taking the many-particle wavefunction as a product of otherwise independent single-particle wavefunctions $\Psi(\mathbf{r}_1, \mathbf{r}_2, \dots) = \psi_1(\mathbf{r}_1)\psi_2(\mathbf{r}_2)\cdots$. However, a substantial difference with the present case is that the operators $c_\alpha^\dagger$ create adequately antisymmetrised states, unlike the "naïve" Hartree wavefunction, which has no *a priori* symmetry.

unoccupied. We can show their orthogonality explicitly by considering that $\mathbf{k}$ is the mth quantum number labelled in the occupation-number representation and expanding the states in this representation

$$\langle \varphi_1 \mid \varphi_0 \rangle = \sum_{\substack{\{i_\alpha\}_{\alpha\neq m} \\ \{j_\beta\}_{\beta\neq m}}} a^*_{i_1,\ldots,i_{m-1},i_{m+1},\ldots} b_{j_1,\ldots,j_{m-1},j_{m+1},\ldots} \langle i_1,\ldots,i_{m-1},1,i_{m+1},\ldots \mid j_1,\ldots,j_{m-1},0,j_{m+1},\ldots\rangle \equiv 0 \tag{2.57}$$

where $i_\alpha = 0, 1$ (resp. $j_\beta = 0, 1$) is the occupation of the αth (resp. βth) quantum number in the expansion of $|\varphi_1\rangle$ (resp. $|\varphi_0\rangle$) with the expansion coefficient $a_{i_1,\ldots,i_{m-1},i_{m+1},\ldots}$ (resp. $b_{j_1,\ldots,j_{m-1},j_{m+1},\ldots}$). All the inner products inside the sum are zero because the mth quantum number of the two factors is always different. The ground state $|\Psi\rangle$ is then further decomposed in an analogous manner with respect to a different wavevector $\mathbf{k}'$, giving

$$\begin{aligned} |\Psi\rangle &= h_{\mathbf{k}}^{\frac{1}{2}}(h_{\mathbf{k}'}^{\frac{1}{2}} |\varphi_{11}\rangle + (1-h_{\mathbf{k}'})^{\frac{1}{2}} |\varphi_{10}\rangle) + (1-h_{\mathbf{k}})^{\frac{1}{2}}(h_{\mathbf{k}'}^{\frac{1}{2}} |\varphi_{01}\rangle + (1-h_{\mathbf{k}'})^{\frac{1}{2}} |\varphi_{00}\rangle) \\ &= h_{\mathbf{k}}^{\frac{1}{2}} h_{\mathbf{k}'}^{\frac{1}{2}} |\varphi_{11}\rangle + h_{\mathbf{k}}^{\frac{1}{2}}(1-h_{\mathbf{k}'})^{\frac{1}{2}} |\varphi_{10}\rangle + (1-h_{\mathbf{k}})^{\frac{1}{2}} h_{\mathbf{k}'}^{\frac{1}{2}} |\varphi_{01}\rangle + (1-h_{\mathbf{k}})^{\frac{1}{2}}(1-h_{\mathbf{k}'})^{\frac{1}{2}} |\varphi_{00}\rangle \end{aligned} \tag{2.58}$$

where, in a manner analogous to eq. (2.56), the components of the decomposition $|\varphi_{ij}\rangle$ correspond to states where the pair $\mathbf{k}$ (*viz.*, $(\mathbf{k}\uparrow, -\mathbf{k}\downarrow)$) has an occupation of i, and the pair $\mathbf{k}'$ (*viz.*, $(\mathbf{k}'\uparrow, -\mathbf{k}'\downarrow)$) has an occupation of j. These states are all orthogonal, which can be seen by expanding their inner products in the same way as performed in eq. (2.57). We can now evaluate the interaction simply by taking the matrix elements of the third term of eq. (2.52) in terms of the decomposition of eq. (2.58), in particular

$$\langle \Psi \mid b^\dagger_{\mathbf{k}'} b_{\mathbf{k}} \mid \Psi \rangle = \langle \Psi | \, b^\dagger_{\mathbf{k}'} \left[h_{\mathbf{k}}^{\frac{1}{2}} h_{\mathbf{k}'}^{\frac{1}{2}} |\varphi_{01}\rangle + h_{\mathbf{k}}^{\frac{1}{2}}(1-h_{\mathbf{k}'})^{\frac{1}{2}} |\varphi_{00}\rangle \right] = h_{\mathbf{k}}^{\frac{1}{2}}(1-h_{\mathbf{k}'})^{\frac{1}{2}} \langle \Psi \mid \varphi_{01}\rangle \tag{2.59}$$

which, recalling that the hs are assumed to be real variational parameters, yields the following ground state matrix elements

$$\langle \Psi \mid b^\dagger_{\mathbf{k}'} b_{\mathbf{k}} \mid \Psi \rangle = \left[h_{\mathbf{k}} h_{\mathbf{k}'} (1-h_{\mathbf{k}})(1-h_{\mathbf{k}'}) \right]^{\frac{1}{2}} \tag{2.60}$$

The Bloch contribution to the energy is straightforward: The occupation of a $\mathbf{k}$ pair is $h_{\mathbf{k}}$, and the same is individually true for its constituent electrons, so that

$$\langle \Psi \mid b^\dagger_{\mathbf{k}} b_{\mathbf{k}} \mid \Psi \rangle = h_{\mathbf{k}}, \quad \langle \Psi \mid b_{\mathbf{k}} b^\dagger_{\mathbf{k}} \mid \Psi \rangle = \left\langle \Psi \,\middle|\, \left(b^\dagger_{\mathbf{k}} b_{\mathbf{k}} + 1 - n_{\mathbf{k}\uparrow} - n_{-\mathbf{k}\downarrow} \right) \,\middle|\, \Psi \right\rangle = 1 - h_{\mathbf{k}} \tag{2.61}$$

where we have applied the second commutation relation of eq. (2.54). Combining eqs. (2.52), (2.60), and (2.61), we find the ground state's energy

$$E_0 = \langle \Psi \,|\, H_{\mathrm{BCS}} \,|\, \Psi \rangle = 2 \sum_{\epsilon_{\mathbf{k}} > \epsilon_F} \epsilon_{\mathbf{k}} h_{\mathbf{k}} + 2 \sum_{\epsilon_{\mathbf{k}} < \epsilon_F} |\epsilon_{\mathbf{k}}|(1 - h_{\mathbf{k}}) - \sum_{\mathbf{k},\mathbf{k}'} V_{\mathbf{k},\mathbf{k}'} \left[h_{\mathbf{k}} h_{\mathbf{k}'} (1 - h_{\mathbf{k}})(1 - h_{\mathbf{k}'}) \right]^{\frac{1}{2}} \tag{2.62}$$

As we know, thanks to the variational principle[17], the best approximation to the ground state is given by the set of parameters $\{h_{\mathbf{k}}\}$ that minimise E_0. A necessary condition is then

$$\frac{\partial E_0}{\partial h_{\boldsymbol{\kappa}}} = 2\epsilon_{\boldsymbol{\kappa}} \theta(\epsilon_{\boldsymbol{\kappa}} - \epsilon_F) - 2|\epsilon_{\boldsymbol{\kappa}}| \theta(\epsilon_F - \epsilon_{\boldsymbol{\kappa}}) - 2 \left(\frac{-2h_{\boldsymbol{\kappa}} + 1}{2[h_{\boldsymbol{\kappa}}(1 - h_{\boldsymbol{\kappa}})]^{\frac{1}{2}}} \right) \sum_{\mathbf{k}'} V_{\boldsymbol{\kappa},\mathbf{k}'} [h_{\mathbf{k}'}(1 - h_{\mathbf{k}'})]^{\frac{1}{2}} = 0 \tag{2.63}$$

where the last term was obtained by considering the symmetry of the interaction term $V_{\mathbf{k}',\mathbf{k}} = V_{\mathbf{k},\mathbf{k}'}$, resulting in a factor of 2 after reindexing the sum. The Heaviside step functions of eq. (2.63) cover complementary intervals of the Bloch energies, and their coefficients are actually the same because $-|\epsilon_{\mathbf{k}}| = \epsilon_{\mathbf{k}}$ if $\epsilon_{\mathbf{k}} < \epsilon_F$. Therefore, the equation for the coefficients is simplified to

$$\frac{[h_{\mathbf{k}}(1 - h_{\mathbf{k}})]^{\frac{1}{2}}}{1 - 2h_{\mathbf{k}}} = \frac{\sum_{\mathbf{k}'} V_{\mathbf{k},\mathbf{k}'} [h_{\mathbf{k}'}(1 - h_{\mathbf{k}'})]^{\frac{1}{2}}}{2\epsilon_{\mathbf{k}}} \tag{2.64}$$

Here, Bardeen, Cooper, and Schrieffer introduce the average matrix element of the interaction to simplify the calculation of the variational parameters

$$V = \left\langle V_{\mathbf{k},\mathbf{k}'} \right\rangle \Big|_{-\hbar\omega < \epsilon_{\mathbf{k}}, \epsilon_{\mathbf{k}'} < \hbar\omega_D} \tag{2.65}$$

where we have specified that the averaging of the interaction is performed over the states where it is attractive. In phase space (*i.e.*, **k**-space) this corresponds to the volume contained within the surfaces $\epsilon_{\mathbf{k}} = \epsilon_F \pm \hbar\omega_D$ around the Fermi surface. This approximation leads to a potential of the form

$$V_{\mathbf{k},\mathbf{k}'} = \begin{cases} V, & \text{if } |\epsilon_{\mathbf{k}}| < \hbar\omega_D \\ 0, & \text{otherwise} \end{cases} \tag{2.66}$$

[17] See Section 5.5 of Weinberg's book [94] for a brief introduction to the variational method. Alternatively, Chapter 10 of K. Koishi's and G. Paffuti's book [48] provides a more comprehensive survey of the topic.

Note that eq. (2.66) is very similar in spirit to Cooper's approximation to the interaction in the one-pair problem, which was introduced in eq. (2.43). Introducing eq. (2.66) into eq. (2.64) yields

$$\frac{[h_{\mathbf{k}}(1-h_{\mathbf{k}})]^{\frac{1}{2}}}{1-2h_{\mathbf{k}}} = \frac{\epsilon_0}{2\epsilon_{\mathbf{k}}} \tag{2.67}$$

where $\epsilon_0 \equiv V\sum_{\mathbf{k}'}[h_{\mathbf{k}'}(1-h_{\mathbf{k}'})]^{\frac{1}{2}}$ is a new parameter that, as we will see, plays the role of (half of) the energy gap. Eq. (2.67) can be easily transformed into a quadratic equations and solved for $h_{\mathbf{k}}$, resulting in

$$h_{\mathbf{k}} = \frac{1}{2}\left(1 - \frac{\epsilon_{\mathbf{k}}}{\sqrt{\epsilon_{\mathbf{k}}^2+\epsilon_0^2}}\right) \tag{2.68}$$

Note that the second term inside the brackets in eq. (2.68), as is standard in the solution of a quadratic equation, could in principle have either "+" or "−" sign in front of it. However, in the normal state there are no Cooper pairs, and thus all of the $h_{\mathbf{k}}$ must vanish, which makes ϵ_0 zero as well. In eq. (2.68), only the "−" sign is consistent with this requirement, otherwise the $h_{\mathbf{k}}$ would be finite when $\epsilon_0 = 0$. We also write explicitly

$$1 - h_{\mathbf{k}} = \frac{1}{2}\left(1 + \frac{\epsilon_{\mathbf{k}}}{\sqrt{\epsilon_{\mathbf{k}}^2+\epsilon_0^2}}\right) \tag{2.69}$$

which immediately suggests the property $1 - h(-\epsilon) = h(\epsilon)$, an electron-hole symmetry. We can evaluate ϵ_0 using these quantities

$$\epsilon_0 = V\sum_{\mathbf{k}}[h_{\mathbf{k}}(1-h_{\mathbf{k}})]^{\frac{1}{2}} = \frac{V}{2}\sum_{\mathbf{k}}\left(1 - \frac{\epsilon_{\mathbf{k}}^2}{\epsilon_{\mathbf{k}}^2+\epsilon_0^2}\right)^{\frac{1}{2}} = \frac{V\epsilon_0}{2}\sum_{\mathbf{k}}\frac{1}{\sqrt{\epsilon_{\mathbf{k}}^2+\epsilon_0^2}} \tag{2.70}$$

which can be rearranged into

$$\frac{1}{V} = \sum_{\mathbf{k}}\frac{1}{2\sqrt{\epsilon_{\mathbf{k}}^2+\epsilon_0^2}} = \int_{-\hbar\omega_D}^{\hbar\omega_D}\frac{N(\epsilon)\mathrm{d}\epsilon}{2\sqrt{\epsilon^2+\epsilon_0^2}} \tag{2.71}$$

where we have replaced the sum over $\mathbf{k}$ by the an integral over the energies weighted using the density of states $N(\epsilon)$ of a single spin[18]. Noting that $\hbar\omega \sim 10-100$ meV, whereas $\epsilon_F \sim 1-10$ eV (see, for instance,

[18] More specifically, we are not considering that each wavevector $\mathbf{k}$ can accomodate states with either spin. The total electronic density of states considering the duplicity of the spin component is $2N(\epsilon)$.

Table 2.1 of [5]) and assuming that $N(\epsilon)$ is sufficiently smooth, we can replace $N(\epsilon)$ with $N_0 \equiv N(\epsilon_F)$. With this, the integrand becomes symmetric and we have

$$\frac{1}{N_0 V} \approx \int_0^{\hbar\omega_D} \frac{\mathrm{d}\epsilon}{\sqrt{\epsilon^2 + \epsilon_0^2}} = \sinh^{-1}\left(\frac{\hbar\omega_D}{\epsilon_0}\right) \tag{2.72}$$

This tells us that the gap parameter (at 0 K) is

$$\epsilon_0 = \frac{\hbar\omega_D}{\sinh\left(\frac{1}{N_0 V}\right)} \tag{2.73}$$

With the above quantities, we can write the ground state energy E_0 from eq. (2.62) of the superconducting state relative to that of the normal phase as

$$E_0 = 2\int_0^{\hbar\omega_D} N(\epsilon)\mathrm{d}\epsilon\, \epsilon h(\epsilon) + 2\int_{-\hbar\omega_D}^{0} N(\epsilon)\mathrm{d}\epsilon\, |\epsilon|[1 - h(\epsilon)] - \frac{V^2 \sum_{\mathbf{k}}[h_{\mathbf{k}}(1-h_{\mathbf{k}})]^{\frac{1}{2}} \sum_{\mathbf{k}'}[h_{\mathbf{k}'}(1-h_{\mathbf{k}'})]^{\frac{1}{2}}}{V} \tag{2.74}$$

Additionally, we can exploit the electron-hole symmetry of the occupations $h(\epsilon)$ as well as the definition of ϵ_0 to find

$$E_0 \approx 4N_0 \int_0^{\hbar\omega_D} \mathrm{d}\epsilon\, \epsilon h(\epsilon) - \frac{\epsilon_0^2}{V} = 2N_0 \int_0^{\hbar\omega_D} \mathrm{d}\epsilon \left(\epsilon - \frac{\epsilon^2}{\sqrt{\epsilon^2 + \epsilon_0^2}}\right) - \frac{\epsilon_0^2}{V} \tag{2.75}$$

where we have employed eq. (2.68) to arrive to the last expression. Performing the integration (see eq. 202.01 of [23] and the note mentioned beneath) we find

$$\begin{aligned} E_0 &= N_0\left[\epsilon^2 - \epsilon\sqrt{\epsilon^2 + \epsilon_0^2} + \epsilon_0^2 \sinh^{-1}\left(\frac{\epsilon}{\epsilon_0}\right)\right]_0^{\hbar\omega_D} - \frac{\epsilon_0^2}{V} \\ &= N_0\hbar^2\omega_D^2\left(1 - \sqrt{1 + \frac{\epsilon_0^2}{\hbar^2\omega_D^2}}\right) + \epsilon_0^2\left[N_0 \sinh^{-1}\left(\frac{\hbar\omega_D}{\epsilon_0}\right) - \frac{1}{V}\right] \end{aligned} \tag{2.76}$$

Once we evaluate ϵ_0 using eq. (2.73) the terms inside the brackets cancel out, and E_0 simplifies to

$$E_0 = N_0\hbar^2\omega_D^2\left[1 - \sqrt{1 + \frac{1}{\sinh^2\left(\frac{1}{N_0 V}\right)}}\right] = N_0\hbar^2\omega_D^2\left[1 - \coth\left(\frac{1}{N_0 V}\right)\right] = -\frac{2N_0\hbar^2\omega_D^2}{e^{2/N_0 V} - 1} \tag{2.77}$$

2.2.4 Excited States

The next step in the development of this theory is determining the elementary excitations from the ground state and how they generate general excited states. The BCS article [8] contemplates two distinct types of excitation of $|\Psi\rangle$.

The first kind of excited state occurs when a ground state pair is broken and one of the electrons (or holes) transitions from the states $\mathbf{k}' \uparrow, -\mathbf{k}' \downarrow$ that are occupied with a probability $h_{\mathbf{k}}$ to the new states $\mathbf{k}'' \uparrow, -\mathbf{k}' \downarrow$, that are definitely known to be occupied. In the excited configuration, the complementary states $-\mathbf{k}'' \downarrow$, $\mathbf{k}' \uparrow$ are definitely known to be unoccupied. In the language of second quantisation this is expressed as

$$|\Psi^s_{\text{exc}}\rangle = \prod_{\mathbf{k}\neq\mathbf{k}',\mathbf{k}''} \left[(1-h_{\mathbf{k}})^{\frac{1}{2}} + h_{\mathbf{k}}^{\frac{1}{2}} b^\dagger_{\mathbf{k}}\right] c^\dagger_{-\mathbf{k}'\downarrow} c^\dagger_{-\mathbf{k}''\uparrow} |\Omega\rangle \tag{2.78}$$

These states are clearly orthogonal to the ground state $|\Psi\rangle$ since, in the excited states, the wavevectors $\mathbf{k}' \uparrow$ and $-\mathbf{k}' \downarrow$ are unoccupied and occupied, respectively, whereas the latter state can be decomposed (eq. (2.56)) into a component where both wavevectors are occupied and another component where they are both unoccupied. The difference in energy between the ground state and $|\Psi^s_{\text{exc}}\rangle$ can be obtained by substracting the part of the energy in eq. (2.62) associated with the pairs $(\mathbf{k}' \uparrow, -\mathbf{k}' \downarrow)$ and $(\mathbf{k}'' \uparrow, -\mathbf{k}'' \downarrow)$ that do not exist in the excited state from the single-particle energies. Recall that the single-particle energies are $|\epsilon_{\mathbf{k}}|$, namely $+\epsilon_{\mathbf{k}}$ for electrons with $\epsilon_{\mathbf{k}} > \epsilon_F$ and $-\epsilon_{\mathbf{k}}$ for holes with $\epsilon_{\mathbf{k}} < \epsilon_F$. Keeping this in mind, we have

$$\begin{aligned} E^s_{\text{exc}} - E_0 =& |\epsilon_{\mathbf{k}'}| + |\epsilon_{\mathbf{k}''}| - 2|\epsilon_{\mathbf{k}'}|\left[h_{\mathbf{k}'}\theta(\epsilon_{\mathbf{k}'}) - (1-h_{\mathbf{k}'})\theta(-\epsilon_{\mathbf{k}'})\right] - 2|\epsilon_{\mathbf{k}''}|\left[h_{\mathbf{k}''}\theta(\epsilon_{\mathbf{k}''})\right. \\ & \left. -(1-h_{\mathbf{k}''})\theta(-\epsilon_{\mathbf{k}''})\right] + V \sum_{(\mathbf{k}_1,\mathbf{k}_2)\in K} \left[h_{\mathbf{k}_1} h_{\mathbf{k}_2} (1-h_{\mathbf{k}_1})(1-h_{\mathbf{k}_2})\right]^{\frac{1}{2}} \end{aligned} \tag{2.79}$$

where we used the index set $K = \{(\mathbf{k}_1, \mathbf{k}_2) | (\mathbf{k}_1, \mathbf{k}_2 = \mathbf{k}') \vee (\mathbf{k}_1, \mathbf{k}_2 = \mathbf{k}'')\}$ that consists of all the pairs of wavenumbers that include either $\mathbf{k}'$ or $\mathbf{k}''$. A Heaviside step function θ was also used to distinguish the cases of electrons and holes. The terms corresponding to the Bloch energies simplify significantly when we analyse the two cases separately, if $\epsilon > \epsilon_F = 0$ we have $|\epsilon| - 2|\epsilon|h = \epsilon(1-2h)$, whereas if $\epsilon < \epsilon_F$ we get $|\epsilon| - 2|\epsilon|(1-h) = -\epsilon + 2\epsilon(1-h) = \epsilon(1-2h)$, an identical result. This results in an excitation energy of

$$E^s_{\text{exc}} - E_0 = \epsilon_{\mathbf{k}'}(1-2h_{\mathbf{k}'}) + \epsilon_{\mathbf{k}''}(1-2h_{\mathbf{k}''}) + 2V \sum_{\mathbf{k}} \left[h_{\mathbf{k}}(1-h_{\mathbf{k}})\right]^{\frac{1}{2}} \left\{ \left[h_{\mathbf{k}'}(1-h_{\mathbf{k}'})\right]^{\frac{1}{2}} + \left[h_{\mathbf{k}''}(1-h_{\mathbf{k}''})\right]^{\frac{1}{2}} \right\} \tag{2.80}$$

where we have used the symmetry of the double sum to simplify it to a single sum[19]. From eq. (2.68) we see that $1-2h = \epsilon/\sqrt{\epsilon^2+\epsilon_0^2}$, and combining this result with eq. (2.67) we also have $[h(1-h)]^{\frac{1}{2}} = \epsilon_0/2\sqrt{\epsilon^2+\epsilon_0^2}$. These expressions motivate the introduction of a new dispersion for the particle-like excitations given by

$$\mathcal{E}_{\mathbf{k}} = \sqrt{\epsilon_{\mathbf{k}}^2 + \epsilon_0^2} \tag{2.81}$$

in terms of which the excitation energy results

$$E^s_{\text{exc}} - E_0 = \frac{\epsilon^2_{\mathbf{k}'}}{\mathcal{E}_{\mathbf{k}'}} + \frac{\epsilon^2_{\mathbf{k}''}}{\mathcal{E}_{\mathbf{k}''}} + \epsilon_0^2\left(\frac{1}{\mathcal{E}_{\mathbf{k}'}} + \frac{1}{\mathcal{E}_{\mathbf{k}''}}\right) = \mathcal{E}_{\mathbf{k}'} + \mathcal{E}_{\mathbf{k}''} \tag{2.82}$$

In addition to single-particle excitations, Bardeen, Cooper, and Schrieffer also introduce pair excitations. These are derived abstractly, justified by the facts that excited states are always orthogonal to the ground state and by observing that any state $\alpha\,|\psi_1\rangle + \beta\,|\psi_2\rangle$ is orthogonal to $\alpha^*\,|\psi_2\rangle - \beta^*\,|\psi_1\rangle$ whenever $\langle\psi_1|\psi_2\rangle = 0$. A state with a pair excitation is thus written as

$$|\Psi^p_{\text{exc}}\rangle = \prod_{\mathbf{k}\neq\mathbf{k}'}\left[(1-h_{\mathbf{k}})^{\frac{1}{2}} + h_{\mathbf{k}}^{\frac{1}{2}} b^\dagger_{\mathbf{k}}\right]\left[(1-h_{\mathbf{k}'})^{\frac{1}{2}} b^\dagger_{\mathbf{k}'} - h_{\mathbf{k}'}^{\frac{1}{2}}\right]|\Omega\rangle \tag{2.83}$$

We can evaluate the excitation energy in this case by noting that $|\Psi^p_{\text{exc}}\rangle$ can be decomposed orthogonally in the same way as we did with $|\Psi\rangle$ in eqs. (2.56) and (2.58), but this time using the wavevector of the excited pair $\mathbf{k}'$ as one of the components. Specifically

$$\begin{aligned} |\Psi^p_{\text{exc}}\rangle &= (1-h_{\mathbf{k}'})^{\frac{1}{2}}\,|\varphi^p_1\rangle - h_{\mathbf{k}'}^{\frac{1}{2}}\,|\varphi^p_0\rangle \\ &= h_{\mathbf{k}}^{\frac{1}{2}}(1-h_{\mathbf{k}'})^{\frac{1}{2}}\,|\varphi^p_{11}\rangle + (1-h_{\mathbf{k}})^{\frac{1}{2}}(1-h_{\mathbf{k}'})^{\frac{1}{2}}\,|\varphi^p_{01}\rangle - h_{\mathbf{k}}^{\frac{1}{2}}h_{\mathbf{k}'}^{\frac{1}{2}}\,|\varphi^p_{10}\rangle - (1-h_{\mathbf{k}})^{\frac{1}{2}}h_{\mathbf{k}'}^{\frac{1}{2}}\,|\varphi^p_{00}\rangle \end{aligned} \tag{2.84}$$

From these expansions, we see that when $\mathbf{k}'$ denotes the excited pair, and $\mathbf{k}$ is any other wavevector different from $\mathbf{k}'$, the matrix elements of the wavefunction are

$$\begin{aligned} &\left\langle \Psi^p_{\text{exc}} \,\middle|\, b^\dagger_{\mathbf{k}'} b_{\mathbf{k}'} \,\middle|\, \Psi^p_{\text{exc}}\right\rangle = 1 - h_{\mathbf{k}'}, \quad \left\langle \Psi^p_{\text{exc}} \,\middle|\, b_{\mathbf{k}'} b^\dagger_{\mathbf{k}'} \,\middle|\, \Psi^p_{\text{exc}}\right\rangle = h_{\mathbf{k}'}, \quad \text{and} \\ &\left\langle \Psi^p_{\text{exc}} \,\middle|\, b^\dagger_{\mathbf{k}'} b_{\mathbf{k}} \,\middle|\, \Psi^p_{\text{exc}}\right\rangle = \left\langle \Psi^p_{\text{exc}} \,\middle|\, b^\dagger_{\mathbf{k}} b_{\mathbf{k}'} \,\middle|\, \Psi^p_{\text{exc}}\right\rangle = -[h_{\mathbf{k}} h_{\mathbf{k}'}(1-h_{\mathbf{k}})(1-h_{\mathbf{k}'})]^{\frac{1}{2}} \end{aligned} \tag{2.85}$$

And all of the other terms that do not involve the wavevector of the excited pair are identical to the ones in the ground state. Note that the transition amplitude is of equal magnitude as the one in the ground state

[19] We have simplified the sum in eq. (2.79) to match the result presented in the BCS article (eq. (2.48) of [8]). But the reader should note that eqs. (2.79) and (2.80) are not exactly equal, the latter is counting the terms where $\mathbf{k} = \mathbf{k}'$ or $\mathbf{k} = \mathbf{k}''$ twice and formally we would have to substract them. However, this difference of 4 terms can be neglected since the total number of $\mathbf{k}$ states in the sum is very large.

but with opposite sign, therefore if a ground state pair minimises the intearaction energy, an excited pair maximises it. With the expressions in eq. (2.85), the excitation energy becomes

$$E^{p}_{\text{exc}} - E_0 = 2\epsilon_{\mathbf{k}'}(1 - 2h_{\mathbf{k}'}) + 4V \sum_{\mathbf{k}} [h_{\mathbf{k}}(1 - h_{\mathbf{k}})]^{\frac{1}{2}} [h_{\mathbf{k}'}(1 - h_{\mathbf{k}'})]^{\frac{1}{2}} \tag{2.86}$$

where we have again used the fact that the Bloch energies in the cases of electrons and holes have identical expressions, and combined the sum over a symmetric restricted set of indices as a single sum[20]. Using the expressions in the paragraph below eq. (2.80) as well as the new dispersion in eq. (2.81), we find

$$E^{p}_{\text{exc}} - E_0 = 2\frac{\epsilon^2_{\mathbf{k}'}}{\mathcal{E}_{\mathbf{k}'}} + 2\frac{\epsilon^2_0}{\mathcal{E}_{\mathbf{k}'}} = 2\mathcal{E}_{\mathbf{k}'} \tag{2.87}$$

In both types of excitation, the energy difference approaches $2\epsilon_0$ as the Bloch energies approach 0, which verifies our earlier claim that ϵ_0 represents half of the energy gap. We note, as is pointed out in the BCS article [8], that the excitation energy turns out to be independent of whether the particles in question are the two individual particles in eq. (2.82), or two members of an excited pair in eq. (2.87).

Combining these two types of elementary excitation, we arrive at the expression for a general excited states

$$|\Psi_{\text{exc}}\rangle = \prod_{\mathbf{k}\in\mathcal{G}} \left[(1 - h_{\mathbf{k}})^{\frac{1}{2}} + h^{\frac{1}{2}}_{\mathbf{k}} b^{\dagger}_{\mathbf{k}}\right] \prod_{\mathbf{k}'\in\mathcal{P}} \left[(1 - h_{\mathbf{k}'})^{\frac{1}{2}} b^{\dagger}_{\mathbf{k}'} - h^{\frac{1}{2}}_{\mathbf{k}'}\right] \prod_{\mathbf{k}''\in\mathcal{S}} c^{\dagger}_{\text{sign}(\sigma_{\mathbf{k}''})\mathbf{k}'',\sigma_{\mathbf{k}''}} |\Omega\rangle \tag{2.88}$$

where $\mathcal{G}$, $\mathcal{P}$, and $\mathcal{S}$ are sets of wavevectors that contain the ground state pairs, the excited pairs, and the individual particles, respectively. The single-particle excitations are generated by $c^{\dagger}_{\text{sign}(\sigma_{\mathbf{k}''})\mathbf{k}'',\sigma_{\mathbf{k}''}}$ to represent that only one of the states $\mathbf{k}''\uparrow$ or $-\mathbf{k}''\downarrow$ is occupied, but not both. This is a consequence of the fact that the excited pairs are formed by breaking a ground pair, with one of the corresponding $\pm\mathbf{k}, \pm\sigma$ being definitely occupied while the other is definitely unoccupied. The energy of an individual state in the form of eq. (2.88) is simply

$$E_{\text{exc}} = E_0 + 2\sum_{\mathbf{k}'\in\mathcal{P}} \mathcal{E}_{\mathbf{k}'} + \sum_{\mathbf{k}''\in\mathcal{S}} \mathcal{E}_{\mathbf{k}''} \tag{2.89}$$

[20] We are again erroneously double-counting the term $\mathbf{k} = \mathbf{k}'$, but neglecting the small discrepancy this introduces, as we did before (see fn. 19).

2.2.5 BCS Superconductor at Finite Temperature

To simplify the analysis we return to representing the Bloch energies in the Hamiltonian in terms of the single-particle instead of the pair operators, namely

$$H_{\mathrm{BCS}} = \sum_{\epsilon_{\mathbf{k}}>\epsilon_F,\sigma} \epsilon_{\mathbf{k}} n_{\mathbf{k},\sigma} + \sum_{\epsilon_{\mathbf{k}}<\epsilon_F,\sigma} |\epsilon_{\mathbf{k}}|(1-n_{\mathbf{k},\sigma}) - V\sum_{\mathbf{k},\mathbf{k}'} b^{\dagger}_{\mathbf{k}'} b_{\mathbf{k}} \tag{2.90}$$

The states in the form of eq. (2.88) represent the microstates of the system, each of which has an occupation probability given by an ensemble. The equilibrium configuration of the system can be determined by minimising the (Helmholtz) free energy

$$F = E - TS \tag{2.91}$$

with E the ensemble average of the energies in eq. (2.89). We proceed by partitioning the $\mathbf{k}$-space into cells $\Delta^3 k$ small enough that the BCS occupation parameters $h_{\mathbf{k}}$, as well as the thermal occupation probabilities of ground state and excited pairs, and of single-particle excitations can be taken as constant inside each cell. If the total number of available pair states inside the volume $\Delta^3 k$ is $\mathcal{N}_{\mathbf{k}}$, and the numbers of single-particle and pair excitations inside the same volume are $S_{\mathbf{k}}$ and $P_{\mathbf{k}}$, respecitvely. Then, the probability of a wavevector $\mathbf{k}$ inside $\Delta^3 k$ being occupied by a single-particle excitation is $s_{\mathbf{k}} = S_{\mathbf{k}}/\mathcal{N}_{\mathbf{k}}$, by a pair excitation is $p_{\mathbf{k}} = P_{\mathbf{k}}/\mathcal{N}_{\mathbf{k}}$, and the remaining fraction $1-s_{\mathbf{k}}-p_{\mathbf{k}}$ is available to be occupied by ground pairs. Evidently, we are interested in the case where $s_{\mathbf{k}}$ and $p_{\mathbf{k}}$ represent the excitation probabilites given by an ensemble average. In the case outlined above, the expectation value of $n_{\mathbf{k},\sigma}$ that appears in the Bloch energy of the conduction electrons ($\epsilon > \epsilon_F$) is given by

$$\langle n_{\mathbf{k},\sigma}\rangle = \frac{1}{2}s_{\mathbf{k}} + p_{\mathbf{k}}(1-h_{\mathbf{k}}) + (1-s_{\mathbf{k}}-p_{\mathbf{k}})h_{\mathbf{k}} = \frac{1}{2}s_{\mathbf{k}} + p_{\mathbf{k}} + (1-s_{\mathbf{k}}-2p_{\mathbf{k}})h_{\mathbf{k}} \tag{2.92}$$

The factor of ½ in the single excitation comes from the fact that, for a single excitation (eq. (2.88)), only one of the pair states $\mathbf{k}\uparrow$ or $-\mathbf{k}\downarrow$ is definitely occupied, while the other is unoccupied. Since the system has no preference for either spin, the average occupation of either state must be ½. On the other hand, the factors of $1-h_{\mathbf{k}}$ and $h_{\mathbf{k}}$ accompanying the factors of the excited and ground pairs, respectively, are the occupations of each type of pair[21], and had already been obtained in eqs. (2.85) and (2.61). Similarly, for the valence holes ($\epsilon < \epsilon_F$) we find

$$\langle 1-n_{\mathbf{k},\sigma}\rangle = \frac{1}{2}s_{\mathbf{k}} + p_{\mathbf{k}}h_{\mathbf{k}} + (1-s_{\mathbf{k}}-p_{\mathbf{k}})(1-h_{\mathbf{k}}) \tag{2.93}$$

[21] If a ground state pair occupies a given pair state $\mathbf{k}\uparrow, -\mathbf{k}\downarrow$, it does so with an occupancy of $h_{\mathbf{k}}$. Therefore, the occupancy of the constituent electrons (or holes) in either of the single particle states is also $h_{\mathbf{k}}$.

But recall that in Section 2.2.3 we found that the variational parameters $h_{\mathbf{k}}$ have an electron-hole symmetry $1 - h(-\epsilon) = h(\epsilon)$, so that the entire Bloch contribution to the energy may be written as

$$\left\langle \sum_{\epsilon_{\mathbf{k}}>\epsilon_F,\sigma} \epsilon_{\mathbf{k}} n_{\mathbf{k},\sigma} + \sum_{\epsilon_{\mathbf{k}}<\epsilon_F,\sigma} |\epsilon_{\mathbf{k}}|(1 - n_{\mathbf{k},\sigma}) \right\rangle = \sum_{\mathbf{k}} |\epsilon_{\mathbf{k}}| \left[s_{\mathbf{k}} + 2p_{\mathbf{k}} + 2(1 - s_{\mathbf{k}} - 2p_{\mathbf{k}}) h(|\epsilon_{\mathbf{k}}|) \right] \tag{2.94}$$

Now, for the interaction energy we see that each term inside the last sum in eq. (2.90) corresponds to a transition amplitude given by $\langle \Psi_{\text{exc}} \mid b^\dagger_{\mathbf{k}'} b_{\mathbf{k}} \mid \Psi_{\text{exc}} \rangle$ multiplied by the Cooper pairing potential V. We have already evaluated said amplitude between two ground pairs in eq. (2.60), and between excited and ground pairs in eq. (2.85). It only remains to evaluate the amplitude between two excited pairs, which we can do as in the previous cases by performing the orthogonal decomposition of $|\Psi_{\text{exc}}\rangle$ with respect to two excited pair states labelled by $\mathbf{k}$ and $\mathbf{k}'$, this results in

$$|\Psi_{\text{exc}}\rangle = (1 - h_{\mathbf{k}})^{\frac{1}{2}} (1 - h_{\mathbf{k}'})^{\frac{1}{2}} \, |\varphi^{2p}_{11}\rangle - h^{\frac{1}{2}}_{\mathbf{k}} (1 - h_{\mathbf{k}'})^{\frac{1}{2}} \, |\varphi^{2p}_{01}\rangle - (1 - h_{\mathbf{k}})^{\frac{1}{2}} h^{\frac{1}{2}}_{\mathbf{k}'} \, |\varphi^{2p}_{10}\rangle + h^{\frac{1}{2}}_{\mathbf{k}} h^{\frac{1}{2}}_{\mathbf{k}'} \, |\varphi^{2p}_{00}\rangle \tag{2.95}$$

where we have included the superscript $2p$ in the states of the decomposition to emphasise that it is performed between two excited pairs, in contrast to the single p superscript used when we analysed the case of a single excited pair, and no superscript for the case of two ground pairs. As in the previous cases, the transition amplitude is simply the product of the coefficients of the two middle terms in eq. (2.95)

$$\left\langle \Psi_{\text{exc}} \mid b^\dagger_{\mathbf{k}'} b_{\mathbf{k}} \mid \Psi_{\text{exc}} \right\rangle = [h_{\mathbf{k}} h_{\mathbf{k}'} (1 - h_{\mathbf{k}})(1 - h_{\mathbf{k}'})]^{\frac{1}{2}} \tag{2.96}$$

which turns out to be identical to the case of two ground pairs. We notice that the interaction between pairs always has the same magnitude, being attractive if the two pairs are of the same kind and repulsive if they are different[22]. With this, we find the average transition amplitude between two cells $\Delta^3 k$ and $\Delta^3 k'$ as the sum between all four possilbe transitions ($\mathcal{G} \to \mathcal{G}$, $\mathcal{P} \to \mathcal{P}$, $\mathcal{G} \to \mathcal{P}$, and $\mathcal{P} \to \mathcal{G}$), weighted by their probabilities[23]. Consequently,

$$\begin{aligned} \langle b^\dagger_{\mathbf{k}'} b_{\mathbf{k}} \rangle &= [h_{\mathbf{k}} h_{\mathbf{k}'} (1 - h_{\mathbf{k}})(1 - h_{\mathbf{k}'})]^{\frac{1}{2}} [(1 - s_{\mathbf{k}} - p_{\mathbf{k}})(1 - s_{\mathbf{k}'} - p_{\mathbf{k}'}) + p_{\mathbf{k}} p_{\mathbf{k}'} - (1 - s_{\mathbf{k}} - p_{\mathbf{k}}) p_{\mathbf{k}'} \\ &\qquad - p_{\mathbf{k}} (1 - s_{\mathbf{k}'} - p_{\mathbf{k}'})] \\ &= [h_{\mathbf{k}} h_{\mathbf{k}'} (1 - h_{\mathbf{k}})(1 - h_{\mathbf{k}'})]^{\frac{1}{2}} (1 - s_{\mathbf{k}} - 2p_{\mathbf{k}})(1 - s_{\mathbf{k}'} - 2p_{\mathbf{k}'}) \end{aligned} \tag{2.97}$$

[22] In light of this observation one may question *why*, if the pairs have this sort of symmetrical interaction, we can say one type belong to the ground state while relegating the others to the excited states. The answer is, of course, that the occupations of the ground pairs have been established as $h_{\mathbf{k}}$ from the outset when the BCS approximation to the ground state was presented.

[23] We assume that all the states in the starting cell $\Delta^3 k$ and target cell $\Delta^3 k'$ are equally likely to be chosen, and that these choices are independent.

We observe in eqs. (2.94) and (2.97) that the total energy does not depend separately on the probability of single-particle excitations $s_{\mathbf{k}}$ and if pair excitations $p_{\mathbf{k}}$. Instead, we can identify an overall excitation occupancy $f_{\mathbf{k}} = s_{\mathbf{k}}/2 + p_{\mathbf{k}}$ that can be interpreted as the likelihood that an idividual particle state (electron or hole) $\mathbf{k}\uparrow$ is occupied by an excited particle, without distinguishing sinlge-particle from pair excitations, the other half of the pair state $-\mathbf{k}\downarrow$ has the same overall occupancy $f_{\mathbf{k}}$. A single particle excitation can be formed from either of the two possibilities in which $\mathbf{k}\uparrow$ is definitely occupied and $-\mathbf{k}\downarrow$ is unoccupied, or vice-versa. On the other hand, a pair excitation requires both states to be occupied, therefore

$$s_{\mathbf{k}} = 2f_{\mathbf{k}}(1 - f_{\mathbf{k}}), \quad \text{and } p_{\mathbf{k}} = f_{\mathbf{k}}^2 \tag{2.98}$$

where we verify that $f_{\mathbf{k}} = s_{\mathbf{k}}/2 + p_{\mathbf{k}}$, as suggested. Combining eqs. (2.90), (2.94), (2.97), and the overall excitation probabilities $f_{\mathbf{k}}$, we obtain the ensemble average of the energy as

$$E = 2\sum_{\mathbf{k}} |\epsilon_{\mathbf{k}}|\big[f_{\mathbf{k}} + 2(1 - 2f_{\mathbf{k}})h(|\epsilon_{\mathbf{k}}|)\big] - V\sum_{\mathbf{k},\mathbf{k}'}[h_{\mathbf{k}}h_{\mathbf{k}'}(1 - h_{\mathbf{k}})(1 - h_{\mathbf{k}'})]^{\frac{1}{2}}(1 - 2f_{\mathbf{k}})(1 - 2f_{\mathbf{k}'}) \tag{2.99}$$

Finally, to evaluate the entropy of the system we note that our partition of the $\mathbf{k}$-space into cells $\Delta^3 k$ results in the overall excitation occupancies $f_{\mathbf{k}}$ being independent parameters, so that the total entropy is the sum of the individual terms associated to each of the one-particle states, each with its own $f_{\mathbf{k}}$ (these are duplicated due to the spin). Now, we imagine a system made up of a large number of boxes, say N, each of which may contain an excited particle with probability f. We know that the entropy of such system is given by

$$S = k_B \ln(\Omega) \tag{2.100}$$

where Ω in this case represents the number of possible configurations of this system. Since there are a total of fN excited particles then there are $\Omega = \binom{N}{fN}$ different ways to arrange them inside the boxes, giving

$$\begin{aligned} S &= k_B \ln\binom{N}{fN} = k_B \ln\left(\frac{N!}{(fN)!(N - fN)!}\right) \\ &\approx k_B\big\{[N\ln(N) - N] - \big[fN\ln(fN) - fN\big] - \big[(N - fN)\ln(N - fN) - N + fN\big]\big\} \end{aligned} \tag{2.101}$$

where we used the Stirling approximation to obtain the last line. This gives an entropy per box of

$$\frac{s}{k_B} \approx [f + (1 - f)]\ln(N) - f\ln(fN) - (1 - f)\ln(N - fN) = -f\ln(f) - (1 - f)\ln(1 - f) \tag{2.102}$$

Applying this expression for the entropy to each of the one-particle states with overall excitation probabilities of $f = f_{\mathbf{k}}$ we find

$$TS = -k_B T \sum_{\mathbf{k},\sigma} \left[f_{\mathbf{k}} \ln(f_{\mathbf{k}}) + (1 - f_{\mathbf{k}}) \ln(1 - f_{\mathbf{k}}) \right] = -2k_B T \sum_{\mathbf{k}} \left[f_{\mathbf{k}} \ln(f_{\mathbf{k}}) + (1 - f_{\mathbf{k}}) \ln(1 - f_{\mathbf{k}}) \right] \tag{2.103}$$

Which results in a free energy for the BCS superconductor of

$$\begin{aligned} F =& 2 \sum_{\mathbf{k}} |\epsilon_{\mathbf{k}}| \left[f_{\mathbf{k}} + 2(1 - 2f_{\mathbf{k}}) h(|\epsilon_{\mathbf{k}}|) \right] - V \sum_{\mathbf{k},\mathbf{k}'} [h_{\mathbf{k}} h_{\mathbf{k}'} (1 - h_{\mathbf{k}})(1 - h_{\mathbf{k}'})]^{\frac{1}{2}} (1 - 2f_{\mathbf{k}})(1 - 2f_{\mathbf{k}'}) \\ &+ 2k_B T \sum_{\mathbf{k}} \left[f_{\mathbf{k}} \ln(f_{\mathbf{k}}) + (1 - f_{\mathbf{k}}) \ln(1 - f_{\mathbf{k}}) \right] \end{aligned} \tag{2.104}$$

To achieve thermal equilibrium F must be minimised, a necessary condition is that its derivatives with respect to $h_{\mathbf{k}}$ vanish. Note that this is the generalisation to finite temperature of our result in eq. (2.63). We have

$$\frac{\partial F}{\partial h_{\boldsymbol{\kappa}}} = 2\epsilon_{\boldsymbol{\kappa}}(1 - 2f_{\boldsymbol{\kappa}}) - \frac{1 - 2h_{\boldsymbol{\kappa}}}{[h_{\boldsymbol{\kappa}}(1 - h_{\boldsymbol{\kappa}})]^{\frac{1}{2}}} V \sum_{\mathbf{k}'} [h_{\mathbf{k}'}(1 - h_{\mathbf{k}'})]^{\frac{1}{2}} (1 - 2f_{\boldsymbol{\kappa}})(1 - 2f_{\mathbf{k}'}) = 0 \tag{2.105}$$

where we have used the fact that $h(-\epsilon) = 1 - h(\epsilon)$ which implies that $\partial h(|\epsilon_{\mathbf{k}}|)/\partial h_{\mathbf{k}} = \mathrm{sign}(\epsilon_{\mathbf{k}})$, simplifying the first term in eq. (2.105). We can change the labels in eq. (2.105) and simplify it to

$$\frac{[h_{\mathbf{k}}(1 - h_{\mathbf{k}})]^{\frac{1}{2}}}{1 - 2h_{\mathbf{k}}} = \frac{V \sum_{\mathbf{k}'} [h_{\mathbf{k}'}(1 - h_{\mathbf{k}'})]^{\frac{1}{2}} (1 - 2f_{\mathbf{k}'})}{2\epsilon_{\mathbf{k}}} = \frac{\epsilon_0}{2\epsilon_{\mathbf{k}}} \tag{2.106}$$

where we introduced the finite temperature variant of the gap parameter

$$\epsilon_0 = V \sum_{\mathbf{k}} [h_{\mathbf{k}}(1 - h_{\mathbf{k}})]^{\frac{1}{2}} (1 - 2f_{\mathbf{k}}) \tag{2.107}$$

we see that eq. (2.106) is formally identical to the equation for the occupations found for the ground state, eq. (2.67). However, in this case the gap parameter depends on the temperature $\epsilon_0 = \epsilon_0(T)$, since it involves the excitation probability $f_{\mathbf{k}}$. We can also minimise the free energy with respect to $f_{\mathbf{k}}$, which results in

$$\begin{aligned} \frac{\partial F}{\partial f_{\boldsymbol{\kappa}}} =& 2|\epsilon_{\boldsymbol{\kappa}}|[1 - 2h(|\epsilon_{\boldsymbol{\kappa}}|)] + 2\left\{ 2V \sum_{\mathbf{k}'} [h_{\mathbf{k}'}(1 - h_{\mathbf{k}'})]^{\frac{1}{2}} (1 - 2f_{\mathbf{k}'}) [h_{\boldsymbol{\kappa}}(1 - h_{\boldsymbol{\kappa}})]^{\frac{1}{2}} \right\} \\ &+ 2k_B T \left[1 + \ln(f_{\boldsymbol{\kappa}}) - 1 - \ln(1 - f_{\boldsymbol{\kappa}}) \right] = 0 \end{aligned} \tag{2.108}$$

We can rewrite eq. (2.108) in terms of the finite temperature version of the gap parameter ϵ_0, as well as the excitation dispersion $\mathcal{E}_{\mathbf{k}} = \sqrt{\epsilon_{\mathbf{k}}^2 + \epsilon_0^2}$ first introduced in eq. (2.81) (but also using the new ϵ_0). This results in

$$k_B T \ln\left(\frac{1 - f_{\mathbf{k}}}{f_{\mathbf{k}}}\right) = \epsilon_{\mathbf{k}}(1 - 2h_{\mathbf{k}}) + 2\epsilon_0[h_{\mathbf{k}}(1 - h_{\mathbf{k}})]^{\frac{1}{2}} \tag{2.109}$$

where we used the electron hole symmetry $h(-\epsilon) = 1 - h(\epsilon)$ once again to simplify the term associated with the Bloch energy. Since eq. (2.106) is formally identical to eq. (2.67), we can use here all of the expressions obtained for $h_{\mathbf{k}}$ in the case of the ground state without change, specifically eqs. (2.68), (2.69), and the two expressions derived in the paragraph below eq. (2.80). This allows us to simplify eq. (2.109) into

$$\ln\left(\frac{1 - f_{\mathbf{k}}}{f_{\mathbf{k}}}\right) = \frac{1}{k_B T}\left(\frac{\epsilon_{\mathbf{k}}^2}{\mathcal{E}_{\mathbf{k}}} + \frac{\epsilon_0^2}{\mathcal{E}_{\mathbf{k}}}\right) = \frac{\mathcal{E}_{\mathbf{k}}}{k_B T} \tag{2.110}$$

And solving for $f_{\mathbf{k}}$ we find

$$f_{\mathbf{k}} = \frac{1}{e^{\beta \mathcal{E}_{\mathbf{k}}} + 1} \tag{2.111}$$

In eq. (2.111) we appreciate that the $f_{\mathbf{k}}$ behave like a Fermi-Dirac distribution for particle-like excitations with a dispersion $\mathcal{E}_{\mathbf{k}} = \sqrt{\epsilon_{\mathbf{k}}^2 + \epsilon_0^2}$. As Bardeen, Cooper, and Schrieffer elucidate [8], the excitations described by eq. (2.111) represent the electrons and holes of the normal phase.

Finally, we end this section by obtaining an equation for T_c, following the same reasoning done by Bardeen, Cooper, and Schrieffer [8]. We start from eq. (2.107) and substitute the newfound expression (2.111) for $f_{\mathbf{k}}$ as well as the recurring $[h_{\mathbf{k}}(1 - h_{\mathbf{k}})]^{\frac{1}{2}}$ factor, which results in

$$\epsilon_0 = V \sum_{\mathbf{k}} \frac{\epsilon_0}{2\mathcal{E}_{\mathbf{k}}}\left(1 - \frac{2}{e^{\beta \mathcal{E}_{\mathbf{k}}} + 1}\right) = V \sum_{\mathbf{k}} \frac{\epsilon_0}{2\mathcal{E}_{\mathbf{k}}} \frac{e^{\beta \mathcal{E}_{\mathbf{k}}} - 1}{e^{\beta \mathcal{E}_{\mathbf{k}}} + 1} \tag{2.112}$$

Now we divide both sides of eq. (2.112) by ϵ_0, and express the last quotient on the right hand side as a hyperbollic function $(e^x - 1)/(e^x + 1) = (e^{x/2} - e^{-x/2})/(e^{x/2} - e^{-x/2}) = \tanh\left(\frac{x}{2}\right)$, lastly we also convert the sum into an integral, using the same approximation employed in eq. (2.72). All these considerations result in

$$\frac{1}{N_0 V} \approx \int_0^{\hbar\omega_D} \frac{\mathrm{d}\epsilon \, \tanh\left[\frac{\beta}{2}\sqrt{\epsilon^2 + \epsilon_0^2}\right]}{\sqrt{\epsilon^2 + \epsilon_0^2}} \tag{2.113}$$

where we have expressed $\mathcal{E}(\epsilon) = \sqrt{\epsilon^2 + \epsilon_0^2}$. Eq. (2.113) can be regarded as an implicit equation for ϵ_0, but as Bardeen, Cooper, and Schrieffer note [8], the gap $2\epsilon_0$ has to be real and positive for the superconducting

phase to appear, and the threshold where those solutions cease to exist is $\epsilon_0 = 0$. The the temperature that solves eq. (2.113) in that case must be T_c, so we get

$$\frac{1}{N_0 V} = \int_0^{\hbar\omega_D} \frac{\mathrm{d}\epsilon}{\epsilon} \tanh\left[\frac{\epsilon}{2k_B T_c}\right] \tag{2.114}$$

This equation cannot be solved analytically, but for the weak coupling range ($N_0 V < 1$) [8], where $k_B T_c \ll \hbar\omega_D$, it can be shown that it leads to

$$T_c = 1.13\Theta_D \exp\left(-\frac{1}{N_0 V}\right) \tag{2.115}$$

The BCS article [8] later proceeds to evaluate additional thermal and electrodynamic properties arising from this theory, but we will not delve into such details, since we require only to use eq. (2.115).

3 Molecular Dynamics Calculations from the General Hamiltonian

In which we review the equations of motion that govern the behaviour of matter in terms of its constituent particles and introduce some of the simplifications that allow their computational evaluation.

Virtually all the matter encountered in human activities is atomic matter: positive nuclei composed of neutrons and protons, surrounded by electrons. Furthermore, within the scale and energy range of interest in condensed matter, of the four fundamental forces only the electromagnetic interaction is relevant and it does not require Quantum Field Theoretical corrections. The Hamiltonian of this class of systems can be expressed generally as

$$H = -\sum_i \frac{\hbar^2}{2m_e}\nabla^2_{\mathbf{r}_i} - \sum_I \frac{\hbar^2}{2M_I}\nabla^2_{\mathbf{R}_I} + \sum_{j>i} \frac{e^2}{|\mathbf{r}_i - \mathbf{r}_j|} - \sum_{i,I} \frac{e^2 Z_I}{|\mathbf{r}_i - \mathbf{R}_I|} + \sum_{J>I} \frac{Z_I Z_J e^2}{|\mathbf{R}_I - \mathbf{R}_J|} \tag{3.1}$$

where corrections on the order of relativistic effects have been neglected[1]. In eq. (3.1), we use lowercase letters ($i, j, \mathbf{r}$) to denote the electron indices and positions, whereas the nuclear variables are specified by uppercase letters ($I, J, \mathbf{R}, Z$).

[1] The neglected terms are of the same or higher order as relativistic corrections to the kinetic energy, which include the spin-orbit and Darwin terms that appear in the fine structure of hydrogen-like atoms (see Section 21.5 of [48]). Notice, in eq. (3.1), that the electromagnetic interaction is taken simply as a Coulomb potential, without reference to the magnetic fields generated by the moving charges. This is because the divergency from the Coulomb interaction is also a relativistic effect, as illustrated in Section 14.1 of John D. Jackson's book [45], particularly eq. (14.8) for the Liénard-Wiechert potentials

$$\phi(\mathbf{r}, t) = \frac{q}{|\mathbf{r} - \mathbf{r}_q(t_{\text{ret}})| - [\mathbf{r} - \mathbf{r}_q(t_{\text{ret}})] \cdot \frac{\mathbf{v}_q(t_{\text{ret}})}{c}}, \quad \mathbf{A}(\mathbf{r}, t) = \frac{\mathbf{v}_q(t_{\text{ret}})}{c}\phi(\mathbf{r}, t), \quad \text{with } t_{\text{ret}} = t - \frac{|\mathbf{r} - \mathbf{r}_q(t_{\text{ret}})|}{c}$$

where in the non-relativistic limit $t_{\text{ret}} \to t, \phi \to \phi_{\text{Coulomb}}$, and $\mathbf{A} \to \mathbf{0}$. Konishi and Paffuti derive the many-electron Hamiltonian with these corrections for a single nucleus in Section 22.5 of their book [48]. Those terms would apply analogously here, except for the mass correction which we do not require because the nuclear kinetic energy is written explicitly in eq. (3.1).

The atomic matter Hamiltonian H of eq. (3.1) describes the behaviour of the entire system of nuclei and electrons from a quantum mechanical viewpoint. It is worth noting that if we denote by N_e the number of electrons and by N_n the number of nuclei, then H has a total of $N_e + N_n + N_e(N_e - 1)/2 + N_e N_n + N_n(N_n - 1)/2 = (N_e + N_n)(N_e + N_n + 1)/2$ terms. In principle, one could define a wavefunction $\Psi(\mathbf{r}_i, \mathbf{R}_I)$ that contains all the properties of the system and which would satisfy

$$i\hbar \frac{\partial}{\partial t} |\Psi\rangle = H |\Psi\rangle \tag{3.2}$$

However these equations are very complex to solve, and it is conventional to simplify them into a form that is simpler to solve. The first such approximation we will review is the Born-Oppenheimer approximation, which will be outlined hereafter.

3.1 Born-Oppenheimer Approximation

In this section, we introduce an approximation originally introduced by M. Born and J. R. Oppenheimer in their pivotal 1927 article [12] (in German). We will roughly follow some of the derivations presented by D. Marx and J. Hutter in Chapter 2 of their book [58], specifically those leading up to the so-called Born-Oppenheimer Molecular Dynamics, which will be our method of choice to solve the many-body problem. The derivation follows from an ansatz (*cf.* Appendix VIII of the book by Born and K. Huang [11]), where it is suggested that if the stationary solutions to the Schrödinger equation for the system with a fixed nuclear configuration $\{\mathbf{R}_I\}$

$$[H_e - E_n(\mathbf{R}_I)]\phi_n(\mathbf{r}_i; \mathbf{R}_I) = 0, \quad \text{with } H_e = -\sum_i \frac{\hbar^2 \nabla^2_{\mathbf{r}_i}}{2m_e} + \sum_{j>i} \frac{e^2}{r_{i,j}} - \sum_{i,I} \frac{e^2 Z_I}{r_{i,I}} + \sum_{J>I} \frac{Z_I Z_J e^2}{r_{I,J}} \tag{3.3}$$

The set $\{\phi_n\}$ form an (orthonormal) basis of the Hilbert space defined by H_e. The semicolon is used to denote that $\mathbf{R}_I$ are interpreted as parameters of the Hamiltonian rather than variables of the Hilbert space. Then, one may write the solution to the whole problem as an expansion in terms of these simplified solutions:

$$\Psi(\mathbf{r}_i, \mathbf{R}_I, t) = \sum_n \chi_n(\mathbf{R}_I, t)\phi_n(\mathbf{r}_i; \mathbf{R}_I) \tag{3.4}$$

Eqs. (3.3) and (3.4) essentially amount to an adiabatic approximation (see, *e.g.*, Section 12.3 of Konishi's and Paffuti's book [48]): the nuclei move very slowly compared to the electrons so that one may assume them to be fixed when solving for the electronic degrees of freedom. The expansion coefficients χ_n may be interpreted as the nuclear part of the wavefunction (*cf.*, the comments by Marx and Hutter in Section 2.1

of their book [58]) and can be determined from the projections of the Schrödinger equation for Ψ (*i.e.*, eq. (3.2)) onto the electronic components of basis ϕ_n, explicitly

$$i\hbar \int \left(\prod_i \mathrm{d}^3 r_i\right) \phi_k^* \frac{\partial}{\partial t} \sum_n \chi_n \phi_n = \int \left(\prod_i \mathrm{d}^3 r_i\right) \phi_k^* \left(H_e - \sum_I \frac{\hbar^2 \nabla_{\mathbf{R}_I}^2}{2M_I}\right) \sum_n \chi_n \phi_n \tag{3.5}$$

Note that because χ_n does not depend on $\mathbf{r}_i$, it commutes with the Hamiltonian $H_e \chi_n \phi_n = \chi_n H_e \phi_n$. Here we also use the fact that $\{\phi_n\}$ do not depend explicitly on time and substitute eq. (3.3) to find

$$\begin{aligned} 0 &= \sum_n \int \mathrm{d}^{3N_e} r \ \phi_k^* \left(H_e \chi_n - \sum_I \frac{\hbar^2 \nabla_{\mathbf{R}_I}^2}{2M_I} \chi_n - i\hbar \frac{\partial \chi_n}{\partial t}\right) \phi_n \\ &= \sum_n \int \mathrm{d}^{3N_e} r \left[\phi_k^* \phi_n \left(E_n \chi_n - i\hbar \frac{\partial \chi_n}{\partial t}\right) - \phi_k^* \sum_I \left(\phi_n \frac{\hbar^2 \nabla_{\mathbf{R}_I}^2}{2M_I} \chi_n + \chi_n \frac{\hbar^2 \nabla_{\mathbf{R}_I}^2}{2M_I} \phi_n\right)\right] \\ &= \sum_n \delta_{kn} \left(E_n \chi_n - i\hbar \frac{\partial \chi_n}{\partial t} - \sum_I \frac{\hbar^2 \nabla_{\mathbf{R}_I}^2}{2M_I} \chi_n\right) - \sum_n \left[\int \mathrm{d}^{3N_e} r \ \phi_k^* \sum_I \frac{\hbar^2 \nabla_{\mathbf{R}_I}^2}{2M_I} \phi_n\right] \chi_n \end{aligned} \tag{3.6}$$

where we have introduced the notation $\mathrm{d}^{3N_e} r \equiv \left(\prod_i \mathrm{d}^3 r_i\right)$ for brevity. To get to the last equality in eq. (3.6), we have used the orthonormality of $\{\phi_n\}$. We notice that eq. (3.6) can be recast as a Schrödinger equation for the nuclear wavefunctions χ_k, namely

$$i\hbar \frac{\partial \chi_k}{\partial t} = \left[-\sum_I \frac{\hbar^2}{2M_I} \nabla_{\mathbf{R}_I}^2 + E_k(\mathbf{R}_I)\right] \chi_k + \sum_n C_{k,n} \chi_n, \quad \text{with } C_{k,n} = -\int \mathrm{d}^{3N_e} r \ \phi_k^* \sum_I \frac{\hbar^2 \nabla_{\mathbf{R}_I}^2}{2M_I} \phi_n \tag{3.7}$$

In this Schrödinger equation, we recognize that the two terms inside the square brackets represent the total kinetic energy of the nuclei and a potential $E_k(\mathbf{R}_I)$ induced by the electrons[2]. On the other hand, the last term of the first equality of eq. (3.7) can be understood as a kinetic energy correction term: The second equality shows that $C_{k,n}$ are the matrix elements of the nuclear kinetic energy with respect to the wavefunctions where they are static. These elements introduce correlations between the different adiabatic states ϕ_n (except for $C_{k,k}$, which can be regarded as a first-order perturbative correction of E_n). The final step in the Born-Oppenheimer approximation is to discard these factors $C_{k,n} \to 0$, thus making the electronic

[2] As functions of the positions $\mathbf{R}_I$, the E_k give the total energy of the system for that fixed configuration of nuclei. In that sense, the $E_k(\mathbf{R}_I)$ are wholly analogous to the notion of potential used in elementary quantum mechanics, but with the added complexity that they are complicated functions of the electronic degrees of freedom.

wavefunctions ϕ_n truly depend solely on the static nuclear arrangement, without any dependence on their motion. Consequently, the equations of the Born-Oppenheimer approximation may be summarised as

$$\Psi(\mathbf{r}_i, \mathbf{R}_I, t) = \sum_n \chi_n(\mathbf{R}_I, t)\phi_n(\mathbf{r}_i; \mathbf{R}_I), \quad H_e\phi_k = E_k\phi_k, \quad \text{and } i\hbar\frac{\partial\chi_k}{\partial t} = \left(-\sum_I \frac{\hbar^2\nabla^2_{\mathbf{R}_I}}{2M_I} + E_k\right)\chi_k \tag{3.8}$$

3.2 Classical Nuclei Approximation

The next step in this ladder of approximations that are required to arrive at our destination of Born-Oppenheimer Molecular Dynamics is a semiclassical approach. The goal is to simplify the motion of the nuclei from the quantum mechanical description provided by the Scrhödinger equation (*i.e.*, the third relation in eq. (3.8)) and treat them instead as classical point-like particles. This simplification is justified by the fact that, relative to the Bohr radius $r_B \approx 5 \times 10^{-9}$ cm, which embodies the length-scale relevant to atoms, the nuclei can be regarded as localised point-like particles because their radii are much smaller, on the order of $\sim 1 \times 10^{-13}$ cm, depending on the mass number of the nucleus[3].

The procedure that transforms the equation for χ_k into a classical picture is fundamentally a generalisation of Bohm's calculations in his famous pilot-wave interpretation paper [10]. This transformation is performed first by decomposing the wavefunction into a product of an amplitude and a phase, namely

$$\chi_k(\mathbf{R}_I, t) = A_k(\mathbf{R}_I, t)e^{iS_k(\mathbf{R}_I,t)/\hbar} \tag{3.9}$$

where A_k and S_k are real functions. Introducing eq. (3.9) into the Schrödinger equation for χ_k we find

$$i\hbar\frac{\partial A_k}{\partial t} - \frac{\partial S_k}{\partial t}A_k = E_kA_k - \hbar^2\sum_I \frac{\nabla^2_{\mathbf{R}_I}A_k + 2\frac{i}{\hbar}\boldsymbol{\nabla}_{\mathbf{R}_I}A_k\cdot\boldsymbol{\nabla}_{\mathbf{R}_I}S_k + A_k\left(-\frac{1}{\hbar^2}|\boldsymbol{\nabla}_{\mathbf{R}_I}S_k|^2 + \frac{i}{\hbar}\nabla^2_{\mathbf{R}_I}S_k\right)}{2M_I} \tag{3.10}$$

where we have used a few vectorial identities to evaluate the Laplacian on the right-hand side[4]. We have also cancelled out the global phase $e^{iS_k/\hbar}$ from both sides of eq. (3.10). Since this equation is an equality

[3] This value is taken from the formulae (4.3) of Carlos A. Bertulani's book [9], particularly $R_s = (1.128\text{ fm})A^{\frac{1}{3}}$. Note that, just as is the case with atomic sizes and the Bohr radius, R_s is only an approximate length scale, and the radius of a specific nucleus may differ up to an order of magnitude from this value (especially the heavier ones).

[4] In particular, we occupied the generalised Leibniz rule $\nabla^2(AB) = B\nabla^2A + 2\boldsymbol{\nabla}A\cdot\boldsymbol{\nabla}B + A\nabla^2B$, along with the gradient and Laplacian of a composition

$$\boldsymbol{\nabla}f(g(\mathbf{r})) = f'(g(\mathbf{r}))\boldsymbol{\nabla}g(\mathbf{r}), \quad \nabla^2f(g(\mathbf{r})) = \boldsymbol{\nabla}\cdot[f'(g(\mathbf{r}))\boldsymbol{\nabla}g(\mathbf{r})] = f''(g(\mathbf{r}))\boldsymbol{\nabla}g(\mathbf{r})\cdot\boldsymbol{\nabla}g(\mathbf{r}) + f'(g(\mathbf{r}))\nabla^2g(\mathbf{r})$$

between complex numbers, it must be independently satisfied by the real and imaginary parts. Therefore, we have the two real-valued equations

$$\begin{aligned} -A_k \frac{\partial S_k}{\partial t} &= E_k A_k - \sum_I \frac{\hbar^2 \nabla^2_{\mathbf{R}_I} A_k - A_k |\boldsymbol{\nabla}_{\mathbf{R}_I} S_k|^2}{2M_I} \\ \hbar \frac{\partial A_k}{\partial t} &= -\hbar \sum_I \frac{2\boldsymbol{\nabla}_{\mathbf{R}_I} A_k \cdot \boldsymbol{\nabla}_{\mathbf{R}_I} S_k + A_k \nabla^2_{\mathbf{R}_I} S_k}{2M_I} \end{aligned} \tag{3.11}$$

The second equality in eq. (3.11) can be rewritten to let the nuclear probability density $\rho_k = A_k^2 \equiv |\chi_k|^2$ appear by multiplying both sides by $2A_k$ and applying the Leibniz rule for the divergence backwards. In particular

$$\frac{\partial \rho_k}{\partial t} + \sum_I \boldsymbol{\nabla}_{\mathbf{R}_I} \cdot \left(\rho_k \frac{\boldsymbol{\nabla}_{\mathbf{R}_I} S_k}{M_I} \right) = 0 \tag{3.12}$$

This is a continuity equation, which tells us that there is a probability current density $\mathbf{J}_{k,I} = M_I^{-1} \rho_k \boldsymbol{\nabla}_{\mathbf{R}_I} S_k$ associated with the "flow" of the Ith nucleus. As Bohm [10] points out, if the nuclei are interpreted as classical particles described by an ensemble in which $\rho_k(\mathbf{R}_1, \mathbf{R}_2, \dots)$ is the probability of finding nuclei "1" inside the volume element $\mathrm{d}^3 R_1$ centred on $\mathbf{R}_1$, and nuclei "2" inside the volume element $\mathrm{d}^3 R_2$ centred on $\mathbf{R}_2$, and so forth for every index nuclear $1 \leq I \leq N_e$, then $\boldsymbol{\nabla}_{\mathbf{R}_I} S_k$ represents the momentum of the Ith nucleus[5]. Therefore, we must analyse the equation for S_k to determine the effective equation of motion of the "classical" nuclei. The first equality of eq. (3.11) can be simplified and rearranged into

$$\frac{\partial S_k}{\partial t} + \sum_I \frac{|\boldsymbol{\nabla}_{\mathbf{R}_I} S_k|^2}{2M_I} + E_k(\mathbf{R}_I) = \hbar^2 \sum_I \frac{\nabla^2_{\mathbf{R}_I} A_k}{2M_I A_k} \to 0 \tag{3.13}$$

The classical limit is taken symbolically as $\hbar \to 0$, reducing the right-hand side of eq. (3.13) to zero[6]. We have seen that $\boldsymbol{\nabla}_{\mathbf{R}_I} S_k$ may be interpreted as the momentum of nucleus I and the second term in eq. (3.13) has the form of a kinetic energy. Therefore it is easy to recognise the Hamilton-Jacobi equation

[5] A heuristic argument that yields an identical result is that, by analogy to fluid mechanics, the continuity equation is $\dot{\rho} = \boldsymbol{\nabla} \cdot (\rho \mathbf{v})$, with $\mathbf{v}$ the velocity of the fluid (*cf.*, eq. (2.27) presented by J. D. Anderson and J. F. Wendt (Eds.) [4]). Comparing this with eq. (3.12) and noting that the coordinates $\mathbf{R}_I$ correspond to the position of the Ith nucleus, we see that $\boldsymbol{\nabla}_{\mathbf{R}_I} S_k$ must be the particle's momentum since $M_I^{-1} \boldsymbol{\nabla}_{\mathbf{R}_I} S_k$ would be its velocity.

[6] This is equivalent to disregarding the quantum effects entirely. Here we diverge from Bohm's analysis, in which he tries to make sense of the right-hand side of eq. (3.13) in terms of classical mechanics. He calls this term the "quantum-mechanical potential".

(see, *e.g.*, Chapter 10 of Herbert Goldstein's, John L. Safko's, and Charles P. Poole's book [34]) where the Hamiltonian is seen to be

$$H(\mathbf{R}_I, \mathbf{P}_I) = \sum_I \frac{P_I^2}{2M_I} + E_k(\mathbf{R}_I), \quad \text{with } \mathbf{P}_I \equiv \nabla_{\mathbf{R}_I} S_k \tag{3.14}$$

where we readily identify E_k as the potential energy. Eq. (3.14) will be valid for any electronic configuration ϕ_k. Recall that the premise of this approximation was that these configurations are adiabatic: if the electrons start in the eigenstate of energy $E = E_k(\mathbf{R}_I)$, they will remain in that same state throughout the system's evolution. The exact method to determine the electronic configuration differs, but thanks to the variational theorem, the state most readily available to be calculated is the ground state. As such, the Born-Oppenheimer Molecular Dynamics method is regarded as a "ground state method", and one needs to minimise the electronic energy at every step in order to obtain the correct forces on the nuclei. Therefore, if we denote by Ψ_0 the electronic ground state, then the system is described by

$$H_e \Psi_0 = E(\mathbf{R}_I)\Psi_0, \quad \text{and } \frac{\mathrm{d}\mathbf{P}_I}{\mathrm{d}t} = -\nabla_{\mathbf{R}_I} \langle \Psi_0 | H_e | \Psi_0 \rangle \tag{3.15}$$

where H_e has been defined in eq. (3.3). The set of equations in (3.15) prescribes the computational problem we need to solve[7]. However, as we will see shortly, the quantum-mechanical electronic part of eq. (3.15) is impossible to be solved exactly. We will devote the following chapter to presenting the Density Functional Theory method used to obtain an approximate solution to the quantum problem.

[7] Note that a more general version of eq. (3.15) is also given by Marx and Hutter [58], where the Schrödinger equation is time-dependent instead of stationary. It follows from an alternative ansatz that uses a single wavefunction in place of the one used here.

4 Density Functional Theory

In which we provide a cursory introduction to the theory on how the many-electron problem is transformed into a variational problem to facilitate its solution.

In the previous chapter, we have laid out the equations of motion for the electrons and nuclei that comprise what we have termed "atomic matter". The approximations presented there result in a separation of the electronic and nuclear variables, wherein the nuclei act on the electrons as a potential source that determines the state of the latter, a state whose energy, in turn, operates as the potential felt by the former. Thanks to the semiclassical approximation, the equations of motion of the nuclei can be solved easily by using any Ordinary Differential Equation integration method[1], of which the most popular for Molecular Dynamics simulations is the velocity Verlet algorithm, to be presented in Section 5.2. On the other hand, the electrons retain all the complexities of quantum mechanics, and the solution is far more involved. In fact, even representing the wavefunction, let alone performing any calculations, over a modest numerical grid is an impossible feat: N electrons in 3D with a $100\times100\times100$ grid using single-precision floating-point complex numbers would require $32 \times 2^N \times 10^{6N}$ bits (*i.e.*, $4 \times 10^{(6+\log_{10} 2)N} \approx 4 \times 10^{6.3\,N}$ bytes) because Ψ_0 is a function of every possible position and spin of every electron. To put this into perspective, the wavefunction of only the four electrons in a Beryllium atom would require 64 YB (*i.e.*, 6.4×10^{25} bytes), a figure already beyond the global data storage capacity[2]. Density Functional Theory (DFT) provides an alternative viewpoint that directly addresses this problem.

We will present some of the most essential aspects of this theory covering the basics of the Hohenberg-Kohn and Kohn-Sham formulations of DFT, and the exchange-correlation functional. However, for the sake of brevity, many technical details (*e.g.*, v- and N-representability, finite temperature, degeneracy, etc.) will be omitted.

[1] See Chapter 8 of the book by Landau, Páez, and Bordeianu [52] for a general review on such methods.

[2] According to an IDC white paper [73], the global "datasphere" (the aggregation of all data from databases, infrastructure, and personal devices) is estimated to reach 175 ZB (*i.e.*, 1.75×10^{23} bytes) by 2025. This number is more than 360 times less than we would require to store the Beryllium wavefunction.

4.1 Hohenberg-Kohn Theorems

DFT represents a paradigm shift in the solution of the quantum many-body problem. Conceptually, it is justified by the simple yet elegant observation that in a many-body problem with identical quantum particles, we do not need to track the state of every individual particle in the system; instead, the collective particle distribution determines the state of the system. This is thanks to the (anti)symmetry of $|\Psi\rangle$ which dictates that if one of the particles occupies a single-particle state $|\psi_i\rangle$, then every other particle must also occupy it[3] (perhaps in a different term of $|\Psi\rangle$). This intuitive idea was proved rigorously by P. Hohenberg and W. Kohn in their monumental 1964 article [43] for the case in which $|\Psi\rangle$ is the ground state of the system.

In Hohenberg's and Kohn's formulation, the electronic number density becomes the fundamental variable of the problem. In terms of field operators, the density of electrons with spin σ in a many-particle state $|\Phi\rangle$ may be written as

$$n_\sigma(\mathbf{r}) = \left\langle \Phi \,\middle|\, \Psi_\sigma^\dagger(\mathbf{r})\Psi_\sigma(\mathbf{r}) \,\middle|\, \Phi \right\rangle \tag{4.1}$$

where Ψ_σ are the field operators defined in eq. (2.5)[4]. The total (spin-independent) electronic density is naturally written as

$$n(\mathbf{r}) = \sum_\sigma n_\sigma(\mathbf{r}) \xrightarrow{\text{electrons}} n_\uparrow(\mathbf{r}) + n_\downarrow(\mathbf{r}) \tag{4.2}$$

Alternatively, the density may also be expressed in "first quantised" form in terms of the one-particle density matrix

$$n_\sigma(\mathbf{r}) = \rho(\mathbf{r}\sigma, \mathbf{r}\sigma) \tag{4.3}$$

with the density matrix given by

$$\rho(\mathbf{r}\sigma, \mathbf{r}'\sigma') \equiv \sum_{\{\sigma_i\}_{1\le i\le N-1}} \int \left(\prod_{j=1}^{N-1} \mathrm{d}^3 r_j \right) \Phi^*(\mathbf{r}\sigma, \mathbf{r}_1\sigma_1, \dots, \mathbf{r}_{N-1}\sigma_{N-1}) \Phi(\mathbf{r}'\sigma', \mathbf{r}_1\sigma_1, \dots, \mathbf{r}_{N-1}\sigma_{N-1}) \tag{4.4}$$

[3] Recall that the states of many-body quantum systems are described by Fock space (*cf.* Section 4.2 of Lancaster's and Blundell's book [50])

$$\mathcal{F} = \bigoplus_{n\in\mathbb{N}} \mathcal{H}^n, \quad \text{where } \mathcal{H}^n \equiv \underbrace{\mathcal{H} \otimes \cdots \otimes \mathcal{H}}_{n \text{ times}}$$

$\mathcal{H}^n$ is the space consisting of n copies of the single-particle Hilbert space. In non-relativistic quantum mechanics, the number of elementary particles is fixed, and therefore, in an N-electron system, we would limit ourselves to states in the $\mathcal{H}^N$ subspace of Fock space.

[4] Incidentally, these operators satisfy their own set of canonical anticommutation relations:

$$\{\Psi_\sigma(\mathbf{r}), \Psi_{\sigma'}(\mathbf{r}')\} = 0, \quad \text{and } \{\Psi_\sigma(\mathbf{r}), \Psi_{\sigma'}^\dagger(\mathbf{r}')\} = \delta^{(3)}(\mathbf{r}-\mathbf{r}')\delta_{\sigma,\sigma'}$$

where we have chosen the first variable of Φ and Φ^* to remain as the "free indices", but thanks to the (anti)symmetry, swapping them for any of the other positions would yield an identical result. Recalling that the wavefunction is nothing else than a probability amplitude, eq. (4.4) shows that $n_\sigma(\mathbf{r})$ is but the unconditional probability distribution of the first—and by symmetry, every— particle (see, *e.g.*, Chapter 2 of [46]).

The terms of the Hamiltonian acting on the system of particles may be distinguished into three separate contributions: The kinetic energy T, the interaction between the particles U, and the external potential V. These energy operators may be expressed in either first- or second-quantised form, and these two forms can be exchanged at convenience. Firstly, the kinetic energy operator can be expressed in second-quantised form as

$$T = \underbrace{-\sum_i^N \frac{\hbar^2\nabla_i^2}{2m}}_{\text{First-Quantised}} = \underbrace{\sum_{\sigma,\sigma'} \int \mathrm{d}^3r\mathrm{d}^3r'\, \Psi_\sigma^\dagger(\mathbf{r}) \left\langle \mathbf{r}\sigma \left| \frac{p^2}{2m} \right| \mathbf{r}'\sigma' \right\rangle \Psi_{\sigma'}(\mathbf{r}') = -\sum_\sigma \int \mathrm{d}^3r\, \Psi_\sigma^\dagger(\mathbf{r}) \frac{\hbar^2\nabla^2}{2m} \Psi_\sigma(\mathbf{r})}_{\text{Second-Quantised}} \tag{4.5}$$

where we have used the fact that the momentum operator acts as $-i\hbar\boldsymbol{\nabla}$ on the position basis, while not affecting the spin part of the state vector whatsoever. Note that the above second-quantised expression is analogous to eq. (2.3) that we used in the Frölich interaction. The external potential, is also associated to a single particle operator $v_{\text{ext}}(\mathbf{r})$ (*i.e.*, it acts individually on each of the particles). Its expressions are as follows

$$V = \underbrace{\sum_i^N v_{\text{ext}}(\mathbf{r}_i)}_{\text{First-Quantised}} = \underbrace{\sum_{\sigma,\sigma'} \int \mathrm{d}^3r\mathrm{d}^3r'\, \Psi_\sigma^\dagger(\mathbf{r}) \langle \mathbf{r}\sigma \mid v_{\text{ext}}(\mathbf{r}) \mid \mathbf{r}'\sigma' \rangle \Psi_{\sigma'}(\mathbf{r}') = \int \mathrm{d}^3r\, v_{\text{ext}}(\mathbf{r}) \hat{n}(\mathbf{r})}_{\text{Second-Quantised}} \tag{4.6}$$

where we have introduced the density operator $\hat{n}(\mathbf{r}) \equiv \sum_\sigma \Psi_\sigma^\dagger(\mathbf{r})\Psi_\sigma(\mathbf{r})$, with a circumflex to distinguish this operator from the numerical density of eq. (4.2). Finally, the interaction term is associated with a two-particle operator $u_{\text{int}}(\mathbf{r}, \mathbf{r}')$ which is second-quantised with a double integral (*cf.*, eq. (4.52) of Lancaster's and Blundell's book [50])

$$U = \underbrace{\frac{1}{2}\sum_{i\neq j} u_{\text{int}}(\mathbf{r}_i, \mathbf{r}_j)}_{\text{First-Quantised}} = \underbrace{\frac{1}{2}\sum_{\sigma,\sigma'} \int \mathrm{d}^3r\mathrm{d}^3r'\, \Psi_\sigma^\dagger(\mathbf{r})\Psi_{\sigma'}^\dagger(\mathbf{r}')u_{\text{int}}(\mathbf{r}, \mathbf{r}')\Psi_{\sigma'}(\mathbf{r}')\Psi_\sigma(\mathbf{r})}_{\text{Second-Quantised}} \tag{4.7}$$

It is worth noting that although the second-quantised expressions appear more daunting than their first-quantised analogues, they have forgone the problem of needing to keep track of the individual particles, and depend instead only on one or two spatial coordinates. In our system of interest, the electron Hamiltonian

H_e of eq. (3.3), we identify the first term as T, the second term as U, and the last two terms as V, in their first-quantised forms.

The first Hohenberg-Kohn theorem is stated by R. G. Parr and W. Yang [67] as *"The external potential $v_{ext}(\mathbf{r})$ is determined, within a trivial additive constant, by the electron density $n(\mathbf{r})$"*. Although the original formulation of the theorem was constrained to nondegenerate ground states (see Section I of [43]), it can be shown to be valid for degenerate ground states as well, as illustrated by Parr and Yang in Section 3.4 of their book [67][5]. As Hohenberg and Kohn show [43], the proof for the nondegenerate case is performed by *reductio ad absurdum*[6]. In particular, if we have two Hamiltonians, H and H', with ground state energies E and E', such that $v'_{\text{ext}}(\mathbf{r}) \neq v_{\text{ext}}(\mathbf{r}) + k$ for any constant k, then their respective ground states $|\Phi\rangle$ and $|\Phi'\rangle$ are necessarily different because they satisfy disparate Schrödinger equations. However, if we assume that $n'(\mathbf{r}) = n(\mathbf{r})$, then we have that

$$E' < \langle\Phi|H'|\Phi\rangle = E + \langle\Phi|H' - H|\Phi\rangle = E + \langle\Phi|V' - V|\Phi\rangle = E + \int \mathrm{d}^3r[v'_{\text{ext}}(\mathbf{r}) - v_{\text{ext}}(\mathbf{r})]n(\mathbf{r}) \quad (4.8)$$

where, to get the fourth expression, we have used the fact that the kinetic T and interaction U terms of the Hamiltonians remain unchanged (in their second-quantised versions) as they are intrinsic to the particles, and to get the last expression, we have combined eqs. (4.6), (4.1), and (4.2). However, we can switch the primes and repeat the same argument to find

$$E < E' + \int \mathrm{d}^3r[v_{\text{ext}}(\mathbf{r}) - v'_{\text{ext}}(\mathbf{r})]n(\mathbf{r}) \quad (4.9)$$

If we add both inequalities in eqs. (4.8) and (4.9), the integrals cancel out, and we arrive at the contradiction

$$E' + E < E + E' \quad (4.10)$$

which implies that the starting assumption $n' = n$ was false. As Parr and Yang point out [67], the fact that $n(\mathbf{r})$ determines $v_{\text{ext}}(\mathbf{r})$ (as well as the number of electrons N by simple integration of n) means that it also determines the ground state $|\Phi\rangle$ and with it, all the properties of the system. This is perhaps Hohenberg's

[5] This section of their book introduces the Levy constrained-search formulation of DFT, which in principle also resolves the issue of v-representability (*i.e.*, the requirement that the density arises from an antisymmetric ground state of a system realised by some external potential v_{ext}).

[6] More specifically, one employs *reductio ad absurdum* to prove the contrapositive of the theorem instead of performing a direct proof since both statements are logically equivalent: Let $k \in \mathbb{R}$, then $\exists k(n' = n \Rightarrow v'_{\text{ext}} = v_{\text{ext}} + k) \Leftrightarrow \forall k(v'_{\text{ext}} \neq v_{\text{ext}} + k \Rightarrow n' \neq n)$.

and Kohn's most fundamental observation because it allows us to interpret $|\Phi\rangle = |\Phi[n]\rangle$ as a functional of the density. Therefore, the energy of the system may also be expressed in terms of n

$$E[n] = F_{\mathrm{HK}}[n] + \int \mathrm{d}^3 r \, v_{\mathrm{ext}}(\mathbf{r}) n(\mathbf{r}) \tag{4.11}$$

The first term of eq. (4.11) is the **Hohenberg-Kohn universal functional**. F_{HK} must be the same regardless of the number of particles N and the external potential v_{ext}, hence the appellative 'universal': it can easily account for N as this number is just the integral of n, a very simple functional, whereas it is independent of v_{ext} as the only point of entry of the potential is V which is entirely accounted for in the second term of eq. (4.11). Note that, by definition (see eq. (9) of [43]), the universal functional is expressed as

$$F_{\mathrm{HK}}[n] = \langle \Phi | T + U | \Phi \rangle \tag{4.12}$$

This last relation allows us to introduce the second Hohenberg-Kohn theorem. Paraphrasing the statement of the theorem by Parr and Yang [67]: *For any trial density* $\tilde{n}(\mathbf{r})$*, satisfying* $\tilde{n}(\mathbf{r}) \geq 0$ *and* $\int \mathrm{d}^3 r \, \tilde{n}(\mathbf{r}) = N$*, then* $E[n] < E[\tilde{n}]$*, where n is the ground state density*. The proof follows from the fact that, via the first theorem, $\tilde{n}$ determines a trial wavefunction[7] $|\tilde{\Phi}\rangle$ that must differ from the ground state $|\Phi\rangle$. Therefore,

$$\langle \Phi | H | \Phi \rangle < \langle \tilde{\Phi} | H | \tilde{\Phi} \rangle = \langle \tilde{\Phi} | T + U | \tilde{\Phi} \rangle + \langle \tilde{\Phi} | V | \tilde{\Phi} \rangle = F_{\mathrm{HK}}[\tilde{n}] + \int \mathrm{d}^3 r \, v_{\mathrm{ext}}(\mathbf{r}) \tilde{n}(\mathbf{r}) \tag{4.13}$$

where the last expression follows from the definition of F_{HK} in eq. (4.12). We recognize the first and last terms of eq. (4.12) as the energy functionals of the ground state and the trial densities, establishing the theorem.

It is conventional to split the energy functional into its separate contributions:

$$E[n] = T[n] + E_{\mathrm{H}}[n] + E_{\mathrm{ext}} + E_{\mathrm{xc}}^{(\mathrm{HK})} \tag{4.14}$$

where $T[n] = \langle \Phi | T | \Phi \rangle$ is the kinetic energy, $E_{\mathrm{ext}} = \langle \Phi | V | \Phi \rangle$ is the energy coupling the system to the external potential, E_{H} is the classical interaction energy

$$E_{\mathrm{H}}[n] = \frac{1}{2} \int \mathrm{d}^3 r \mathrm{d}^3 r' \, n(\mathbf{r}) u_{\mathrm{int}}(\mathbf{r}, \mathbf{r}') n(\mathbf{r}'), \tag{4.15}$$

[7] Strictly speaking, this is contingent on the v-representability being satisfied, but as mentioned in footnote 5, this issue is solved theoretically by introducing the Levy constrained-search.

also known as the *Hartree term*, and $E_{\text{xc}}^{(HK)}$ is the so-called *exchange-correlation functional*, which absorbs the complicated many-body effects not included in E_{H}. Note that we have written the superindex HK in the exchange-correlation functional $E_{\text{xc}}^{(HK)}[n] \equiv \langle\Phi|U|\Phi\rangle - E_H[n]$ to distinguish it from the Kohn-Sham version of this functional that also includes many-body effects of the kinetic energy (see, *e.g.*, Chapters 2 and 3 of the book by E. Engel and R. M. Dreizler [26])[8].

The second Hohenberg-Kohn theorem ensures that, if we knew the exact expression of F_{HK}, the ground state density and energy could be determined by minimising the functional. Additionally, the first theorem would guarantee that all the properties of the ground state are also determined by such density. Unfortunately, this functional has no simple algebraic expression and can only be approximated in practice[9].

4.2 Kohn-Sham Density Functional Theory

Despite the elegance and simplicity of the Hohenberg-Kohn formulation, the lack of a useful exact expression for F_{HK} limits the method's accuracy. In particular, the traditional models for the kinetic energy functional[10] suffer from low accuracy. On the other hand, if the wavefunction is expressed in the form of a Slater determinant, its kinetic energy is straightforward to compute. Furthermore, if the Hamiltonian of the system does not have an interaction term, then the solution can always be expressed as such a determinant (assuming the particles are Fermions). This fact is used to introduce a hybrid method—developed by Kohn and L. J. Sham in 1965 [47]— where one solves an auxiliary system of noninteracting particles using a Hartree-Fock–like approach.

[8] Note that, as Engel and Dreizler point out in Chapter 4 of their book [26], there is a third definition of the exchange-correlation energy that differs from the ones used in DFT and is used mainly by quantum chemists.

[9] It is worth noting that, in fact, there exist well-known explicit formulas to compute the functional that are exact both in principle and in practice, as P. W. Ayers and Parr point out [6]. However, they are not useful for practical calculations, as they are more computationally expensive than solving the Schrödinger equation using a specified basis [6]. For any practical purpose, we may claim that an exact universal functional does not exist.

[10] The first kinetic energy functional appears in the Thomas-Fermi model, a philosophical predecessor of DFT. The Thomas-Fermi functional can be written as $T_{\text{TF}}[n] = \frac{\hbar^2}{m}\frac{3^{5/3}\pi^{4/3}}{10}\int \mathrm{d}^3 r\, n^{5/3}(\mathbf{r})$, which is a Local Density approximation. Inhomogeneity effects can be introduced by corrections such as the one given by Weizsacker (*cf.* eq. (6.7.1) of [67]) as well as the fourth order gradient correction by Hodge (*cf.* eqs. (6.7.22) and (6.7.23) of [67]). However, as Parr and Yang [67] point out, even up to this order, the approximation is still poor—only describing the average behaviour of the electrons— whereas higher order corrections diverge.

The justification for this method comes from the same Hohenberg-Kohn theorems presented in the preceding Section. Specifically, one considers the auxiliary system with a ground state

$$\Phi_s(\mathbf{r}_1\sigma_1, \mathbf{r}_2\sigma_2, \ldots, , \mathbf{r}_N\sigma_N) = \frac{1}{\sqrt{N!}} \begin{vmatrix} \phi_1(\mathbf{r}_1\sigma_1) & \phi_2(\mathbf{r}_1\sigma_1) & \cdots & \phi_N(\mathbf{r}_1\sigma_1) \\ \phi_1(\mathbf{r}_2\sigma_2) & \phi_2(\mathbf{r}_2\sigma_2) & \cdots & \phi_N(\mathbf{r}_2\sigma_2) \\ \vdots & \vdots & \ddots & \vdots \\ \phi_1(\mathbf{r}_N\sigma_N) & \phi_2(\mathbf{r}_N\sigma_N) & \cdots & \phi_N(\mathbf{r}_N\sigma_N) \end{vmatrix} \tag{4.16}$$

whose density $n_s(\mathbf{r})$ matches that of the ground state of the original interacting system $n(s)$. The first Hohenberg-Kohn theorem ensures that the external potential $v_s(\mathbf{r})$ of the auxiliary system is determined by $n_s = n$. Note, however, that $v_s \neq v_{\text{ext}}$. In particular, we may write (*cf.*, eq. (3.23) of [26])

$$n(\mathbf{r}) \equiv n_s(\mathbf{r}) = \sum_{\sigma,i} \Theta_i |\phi_i(\mathbf{r}\sigma)|^2 \tag{4.17}$$

where Θ_i is the occupation of the orbitals $\phi_i(\mathbf{r}\sigma)$. At 0 K we can write $\Theta_i = \theta(\epsilon_F - \epsilon_i)$ with ϵ_i the energy of the ith orbital (see below) and ϵ_F the Fermi energy (the orbital with the Nth lowest energy). As Engel and Dreizler point out [26], we can generalise these occupations to the finite temperature case by taking $\Theta_i = \{1 + \exp[\beta(\epsilon_i - \mu)]\}^{-1}$. The Hamiltonian of the auxiliary system is then simply

$$H = T + V_s \tag{4.18}$$

where

$$V_s = \int \mathrm{d}^3 r \, v_s(\mathbf{r}) \hat{n}(\mathbf{r}) \tag{4.19}$$

On the other hand, the energy of the interacting system can be decomposed in a form similar to the one in the Hohenberg-Kohn approach

$$E[n] = T_s[n] + E_{\text{ext}}[n] + E_{\text{H}}[n] + E_{\text{xc}}[n] \tag{4.20}$$

this is analogous to the decomposition of eq. (4.14), but the kinetic energy is that of the non-interacting system $T_s[n] = \langle \Phi_s | T | \Phi_s \rangle$. In this case, the exchange-correlation functional can be defined by

$$E_{\text{xc}}[n] \equiv \langle \Phi | T + U | \Phi \rangle - T_s[n] - E_{\text{H}}[n] \tag{4.21}$$

and it includes the many-body effects that arise in the kinetic energy and interaction terms. As noted in [26], $T_s[n] \leq T[n]$, so that $E_{\text{xc}} \geq E_{\text{xc}}^{(\text{HK})}$. Furthermore, E_{xc} is also a universal functional, because it is a function of quantities that are universal functionals (*i.e.*, $|\Phi[n]\rangle$, $T_s[n]$, and $E_{\text{H}}[n]$).

We omit the explicit calculations, which may be consulted in Chapter 3.1 of Engel's and Dreizler's book [26], whereby taking the functional derivative of eq. (4.20) one finds the auxiliary potential to be

$$v_s(\mathbf{r}) = v_{\text{ext}}(\mathbf{r}) + \int \mathrm{d}^3 r'\, u(\mathbf{r}, \mathbf{r}') n(\mathbf{r}') + \frac{\delta E_{\text{xc}}[n]}{\delta n(\mathbf{r})} \equiv v_{\text{ext}}(\mathbf{r}) + v_{\text{H}}(\mathbf{r}) + v_{\text{xc}}(\mathbf{r}) \tag{4.22}$$

This expression requires some knowledge of the exchange-correlation functional E_{xc} which in practice is approximated with one of a variety of expressions, in particular this work will use the PBEsol functional which will be presented in Section 5.1.1. The explicit expression of v_s can be introduced in the Hartree-Fock equations of the noninteracting auxiliary system, which read

$$\left[-\frac{\hbar^2 \nabla^2}{2m} + v_{\text{ext}}(\mathbf{r}) + v_{\text{H}}(\mathbf{r}) + v_{\text{xc}}(\mathbf{r})\right] \phi_i(\mathbf{r}\sigma) = \epsilon_i \phi_i(\mathbf{r}\sigma) \tag{4.23}$$

This are the famous **Kohn-Sham equations**. Note that the equations in (4.23) are different from the conventional Hartree-Fock equations for a system of non-interacting particles because the potentials v_{H} and v_{xc} depend implicitly on the orbitals. Correspondingly, they require a self-consistent field approach to be solved in practice which will be presented in Section 5.1.2. In what follows, we will call the term in brackets on the left-hand side of eq. (4.23) the *Kohn-Sham Hamiltonian*.

Finally, we note that the "energies" ϵ_i that appear in the Kohn-Sham equations are the same ones that appear in the occupations Θ_i of eq. (4.17). However, as Engel and Dreizler point out [26], the orbitals ϕ_i have no physical significance as they are purely mathematical constructs used to reproduce the density.

5 Methodology

In which we lay out the approximations, techniques, and numerical algorithms required to model the dynamics of the system, obtain amorphous structures computationally and optimise them, and evaluate some of their superconducting properties.

The remainder of this Part is dedicated to elaborating, at a high level of abstraction, the procedures required to perform the *ab initio* simulations of the system and the extraction of superconducting properties from those results based on the theoretical framework presented thus far. The topics are presented roughly in a "bottom-up" approach. It should be noted that some of the methods presented here are not unique, having alternatives with varying degrees of success (*i.e.*, accuracy, efficiency, simplicity, etc.). We focus solely on the algorithms we have occupied in our simulations, presenting alternatives only where they are essential to understand our method of choice.

5.1 Solutions to the Kohn-Sham equations

Chapter 4 culminated in the Kohn-Sham equations of DFT, one of the most ubiquitous approaches to solving the quantum problem in nuclear, atomic, molecular, and condensed matter physics. However, the solution of this coupled system of equations still poses some technical difficulties, which we discuss below.

5.1.1 The Perdew-Burke-Ernzerhof Functional Revised for Solids (PBEsol)

Throughout the course of Chapter 4, we have expressed the exchange-correlation functional E_{xc} and its functional derivative $v_{\text{xc}} = \delta E_{\text{xc}}/\delta n$ only symbolically. Furthermore, as mentioned previously, there does not exist any analytic expression for this functional. On the contrary, there is a panoply of approximations to E_{xc} employed in the literature.

The approximations to E_{xc} are classified into several broad categories (an extensive review of which can be found in Chapter 4 of [26]), such as Local Density Approximation (LDA), Generalised Gradient Approximation (GGA), Meta-GGA, LDA+U, Weighted Density Approximation (WDA), etc.

The most basic approximation is LDA, in which the exchange-correlation energy density e_{xc} of the inhomogeneous electrons with density $n(\mathbf{r})$ is approximated to be equal to that of a homogeneous electron gas with a matching density (see Section 4.3 of [26]). That is

$$E_{xc}^{LSDA}[n_\uparrow, n_\downarrow] = \int \mathrm{d}^3 r \, e_{xc}^{hom}(n_\uparrow, n_\downarrow) \tag{5.1}$$

Where we have introduced the slightly more general Local Spin-Density Approximation (LSDA) that allows for a nonzero spin polarisation $\zeta = (n_\uparrow - n_\downarrow)/n$. It is common for this energy to be separated in correlation E_c and exchange E_x terms as they each satisfy different limiting behaviours (at low and high density, polarisation, or in the case of GGA, variation) that are used to adjust the parameters in the approximations.

The LSDA approach can be improved by taking into account the inhomogeneity of n in the energy density e_{xc}. As Engel and Dreizler explain [26], the strategy used in practice is to introduce gradient terms into the energy integrand. In this sense, it can be regarded as a semi-local approximation because the gradient is taken at the same point in space[1]. The first expression of this type is called the *gradient expansion* (GE) and was provided by Hohenberg and Kohn themselves in their seminal article [43]. However, up to second-order corrections (*i.e.*, the so-called GE2), GE does not yield satisfactory results or even an improvement over LSDA [26]. This complication gave rise to GGA methods, which systematically generalise GE without suffering the same drawbacks. We will use precisely one of these functionals, in particular the one developed by Perdew, Burke, and Ernzerhof in 1996 [68], whose parameters were later revised for Solids by Perdew *et al.* in 2008 [69], which is better known under the acronym PBEsol.

Both the PBE and PBEsol functionals have the same form. They are parametrised in terms of a handful of constants and, more importantly, two "free" parameters μ and β, that can be chosen to satisfy relevant constraints. The functionals are expressed by Perdew, Burke, and Ernzerhof [68] as

$$E_c^{PBE(sol)} = \int \mathrm{d}^3 r \, [\epsilon_c^{hom}(r_s, \zeta) + H(r_s, \zeta, t)]n, \quad E_x^{PBE(sol)} = \int \mathrm{d}^3 r \, \epsilon_x^{hom}(n) F_x(s) n \tag{5.2}$$

Note that the energy densities of the homogeneous parts in eq. (5.2) are given per particle, hence the additional factor of n in both integrals. Before discussing the gradient corrections, we will first clarify the

[1] On the other hand, the competing method of *complete linear response* accounts for the inhomogeneity in a fully non-local manner. However, it suffers from technical problems for having an ill-defined density in the integrand's kernel, and it is not used in practice [26].

notation and the expressions of the LSDA terms that are also non-trivial. The variables used by Perdew, Burke, and Ernzerhof [68, 69] to parametrise these functionals are all functions of the density and its gradient that have been chosen for convenience or physical clarity: *(i)* $r_s(n)$ is the local Seitz radius which also determines the local Fermi wavevector of the free electron model $k_F(n)$ according to $n = 3/4\pi r_s^3 \equiv k_F^3/3\pi^2$, *(ii)* the spin polarisation ζ was introduced above, and *(iii)* the two dimensionless density gradients t and s are given by

$$t = \frac{|\boldsymbol{\nabla} n|}{2\phi k_s n}, \quad s = \frac{|\boldsymbol{\nabla} n|}{2k_F n}; \quad \text{with } \phi \equiv \frac{(1+\zeta)^{2/3} + (1-\zeta)^{2/3}}{2}, \quad \text{and } k_s \equiv \sqrt{\frac{4k_F}{\pi a_0}} \tag{5.3}$$

The two new variables ϕ and k_s appearing in the dimensionless density gradient t are, respectively, a spin-scaling factor[2] and the Thomas-Fermi screening wavevector. In the definition of the latter, a_0 is the Bohr radius given by $a_0 = \hbar^2/2m_e e^2$. The exchange energy density per particle of the homogeneous gas $\epsilon_{\mathrm{x}}^{\mathrm{hom}}$ has a simple expression given in [68] as

$$\epsilon_{\mathrm{x}}^{\mathrm{hom}}(n) = -\frac{3e^2 k_F}{4\pi} \equiv \frac{3^{4/3} e^2 n^{1/3}}{4\pi^{1/3}} \tag{5.4}$$

However, the correlation energy density of the homogeneous gas is more complicated. The PBE article [68] cites an earlier paper by Perdew and Y. Wang [70] for the expression for $\epsilon_{\mathrm{c}}^{\mathrm{hom}}$ (the PW, or sometimes PWC, functional), which they express using an alternative parametrisation of a spin-interpolation formula that was introduced earlier by Vosko, Wilk, and Nusair [92] in 1980 for the development of the eponymous VWN functional[3]. This formula is

$$\begin{aligned} \epsilon_{\mathrm{c}}^{\mathrm{hom}}(r_s,\zeta) =& \epsilon_{\mathrm{c}}^{\mathrm{hom}}(r_s,0) + \alpha_{\mathrm{c}}(r_s)\frac{f(\zeta)}{f''(0)}(1-\zeta^4) + [\epsilon_{\mathrm{c}}^{\mathrm{hom}}(r_s,1) - \epsilon_{\mathrm{c}}^{\mathrm{hom}}(r_s,0)]f(\zeta)\zeta^4, \\ & \text{with } f \equiv \frac{(1+\zeta)^{4/3} + (1-\zeta)^{4/3} - 2}{2^{4/3} - 2} \end{aligned} \tag{5.5}$$

The distinction between the PW and VWN functionals is in how they parametrise the three functions of r_s, which are the correlation energy densities in the unpolarised $\epsilon_{\mathrm{c}}^{\mathrm{hom}}(r_s, 0)$ and the totally polarised $\epsilon_{\mathrm{c}}^{\mathrm{hom}}(r_s, 1)$

[2] Note that the spin-scaling factor ϕ can also be written in terms of the density as $\phi = (n_\uparrow^{2/3} + n_\downarrow^{2/3})/2^{1/3} n^{2/3}$

[3] Note that other parametrisations of LSDA yield equally good results, including VWN. Perdew and Wang acknowledge this point but propose a different parametrisation to "avoid some minor problems" of alternative expressions [70]. We adhere to the PW functional, but different parametrisations should pose no problem as they yield remarkably similar results (see, *e.g.*, Figs. 4.2 and 4.3 of [26] comparing several LDAs, including PW and VWN).

cases, and the correlation contribution to the spin stiffness[4] α_c. Perdew and Wang use the same analytic expression to represent these three functions, namely

$$G(r_s; A, \alpha_1, \beta_1, \beta_2, \beta_3, \beta_4, p) = -2A(1+\alpha_1 r_s)\ln\left[1+\frac{1}{2A(\beta_1 r_s^{1/2}+\beta_2 r_s+\beta_3 r_s^{3/2}+\beta_4 r_s^{p})}\right] \tag{5.6}$$

The numerical values of these parameters for each of the three functions are given in Table I of Perdew's and Wang's article [70] (the ones relevant to our discussion correspond to the last three columns). We can finally discuss the gradient corrections, which in the PBE(sol) functional [68] are given by

$$H(r_s,\zeta,t) = \frac{e^2\gamma\phi^3}{a_0}\ln\left[1+\frac{\beta}{\gamma}\left(\frac{1+\alpha t^2}{1+\alpha t^2+\alpha^2 t^4}\right)\right], \quad \text{with } \alpha = \frac{\beta}{\gamma}\left[\exp\left(-a_0\epsilon_c^{\text{hom}}/e^2\gamma\phi^3\right)-1\right]^{-1} \tag{5.7}$$

where $\gamma \approx (1-\ln 2)/\pi^2$ is a weak function of the spin polarisation that is approximated as a constant. On the other hand, the exchange correction is [68]

$$F_x(s) = 1+\kappa-\frac{\kappa^2}{\kappa+\mu s^2} \tag{5.8}$$

where $\kappa = 0.804$ is an empirical coefficient. In the original formulation of PBE [68], the values of β and μ are determined to match two targets in the slowly-varying limit ($t, s \to 0$): β is taken to match the gradient expansion (GE2) of the correlation energy ($\beta^{\text{PBE}} = \beta^{GE}$), while μ was selected so that the second order gradient correction to the exchange energy cancels out with the correlation correction ($\mu^{\text{PBE}} = \pi^2\beta^{\text{PBE}}/3 \approx 2\mu^{GE}$). This choice was based on the observation that LSDA yields better results in this limit than the PW91-GGA functional[5]. On the other hand, the PBEsol functional [69] sacrifices some accuracy in the description of free neutral atoms, as well as the exact cancellation of the gradients in the slow-varying limit in order to restore the GE2 exchange ($\mu^{\text{PBEsol}} = \mu^{GE}$) and improve the energy calculations of surfaces[6]. These choices ultimately result in systematically better results in solids modelled with PBEsol when compared with PBE[7] [69].

[4] Vosko, Wilk, and Nusair [92] define the spin stiffness as $\alpha_c = \partial^2\epsilon_c^{\text{hom}}/\partial\zeta^2\big|_{\zeta=0}$. This relation is readily verified by explicitly evaluating the derivative of eq. (5.5).

[5] For more context, the PBE functional was designed as an improvement over PW91 by having a simpler expression (in practice, this helps in the construction of pseudopotentials) and better results in the slowly varying limit [68].

[6] Perdew *et al.* [69] do this by fitting β to get better results of jellium cluster surface energies (according to the TPSS meta-GGA functional which is taken as a possible lower bound for the surface energy).

[7] Perdew *et al.* also show a systematic improvement against TPSS, as well as massive improvements against LSDA in every type of solid except semiconductors [69].

5.1.2 Self-Consistent Field Solution of the Kohn-Sham Equations

With the introduction of an explicit expression for the exchange-correlation functional, we can readily calculate the Kohn-Sham Hamiltonian operator that appears in eqs. (4.23). However, how exactly these equations are solved remains to be seen, as they are a set of N nonlinear, coupled integro-differential equations. Undoubtedly, the most popular approach is the Self-Consistent Field (SCF) method, which is started by introducing a set of trial orbitals $[\phi_i(\mathbf{r}\sigma)]^0$ as the generators of v_{H} and v_{xc}. Following their evaluation, the potentials are fixed at their calculated values for the remainder of the iteration. Solving the resulting Kohn-Sham equations that yield a new set of orbitals $[\phi_i(\mathbf{r}\sigma)]^1$. This approach is an iterative method that can be summarised with the following equation

$$\left\{-\frac{\hbar^2\nabla^2}{2m} + v_{\mathrm{ext}}(\mathbf{r}) + \left[v_{\mathrm{H}}(\mathbf{r}) + v_{\mathrm{xc}}(\mathbf{r})\right]_{\phi_i=[\phi_i]^n}\right\}[\phi_i(\mathbf{r}\sigma)]^{n+1} \equiv H_{\mathrm{KS}}^n[\phi_i(\mathbf{r}\sigma)]^{n+1} = \epsilon_i^{n+1}[\phi_i(\mathbf{r}\sigma)]^{n+1} \tag{5.9}$$

where we have introduced the notation H_{KS}^n to denote the Kohn-Sham Hamiltonian evaluated at the orbtials of the n-th step. In general, the new orbitals $[\phi_i]^{n+1}$ will differ from the ones obtained in the previous step $[\phi_i]^n$. Only when the correct orbitals are inserted into the interaction potentials will both sets of orbitals coincide, and the Kohn-Sham equation can be assumed to be solved, which is why the method is called *self-consistent*. In practice, the two sets of orbitals are not expected to match exactly but are only expected to be approximately equal within some margin of error. A reasonable stopping criterion is when the new step yields a "negligible" change in the density and the total energy simultaneously.

The SCF method is assumed to minimise the energy because the Kohn-Sham equations are equivalent to the Euler-Lagrange equations of the Hohenberg-Kohn energy but represented in terms of the auxiliary system. This means that once the orbitals are self-consistent, they become a valid representation of the ground state density according to eq. (4.17).

Roothaan-Hall Equations for a Specified Basis

A particularly convenient and efficient approach to solving eq. (5.9) is to expand the wavefunctions of the auxiliary system in some basis, which turns the SCF recursive formula into a matrix eigenvalue equation. Such a decomposition can be written in the following general form

$$|\phi_i\rangle = \sum_\alpha a_\alpha |\alpha\rangle \tag{5.10}$$

The set of states $\{|\alpha\rangle\}$ in which we expand the orbitals is called a **basis set**. Some popular choices for $\{|\alpha\rangle\}$ are plane waves, localised orbitals (atomic or Gaussian), and generalised Wannier functions[8]. We will focus on the case of an atomic-orbital basis set occupied by the DMol^3 code that we will use. In such case, the expansion

$$\phi_i(\mathbf{r}\sigma) = \sum_{\mathbf{R}_I,n,l,m} C_{n,l,m}\, \psi^m_{nl}(\mathbf{r} - \mathbf{R}_I)\chi_\sigma \tag{5.11}$$

is called a Linear Combination of Atomic Orbitals, or LCAO for short. Note that the sum is also taken over the nuclear positions $\mathbf{R}_I$, around which the atomic orbitals are assumed to be centred[9]. If we were to represent an arbitrary wavefunction, we would need a basis set that spans the entirety of the Hilbert space (which is, of course, impossible since it is infinite-dimensional). However, because we want to obtain the ground state configuration of the system, then the energy of the individual basis states cannot be too large. As a general guideline, since the kinetic energy operator is proportional to the Laplacian, states with more "wiggles" are more energetic. Thus, one need only include them up to some appropriate cutoff[10].

Once the issue of a basis set has been settled, the Kohn-Sham equations can be recast in terms of the matrix elements of the Kohn-Sham Hamiltonian. This procedure of expanding the orbitals in a fixed basis to retrieve a matrix equation was derived independently by Clemens C. J. Roothaan [77] and George G. Hall [36] in 1951 for the solution of the Hartree-Fock equations, predating the advent of DFT. Since, as we have pointed out in Section 4.2, the Kohn-Sham equations share the structure of the Hartree-Fock ones, the equations derived by Roothaan and Hall can be applied identically to solve the Kohn-Sham auxiliary system. The Roothaan-Hall equations for the SCF method in this case are:

$$\sum_\beta F_{\alpha\beta}(c^n_{i,\mu})c^{n+1}_{i,\beta} = \epsilon^{n+1}_i \sum_\beta S_{\alpha\beta}c^{n+1}_{i,\beta} \tag{5.12}$$

where

$$c^n_{i,\mu} \equiv \langle\mu|[\phi_i]^n\rangle\,, \quad F_{\alpha\beta}(\{c^n_{i,\mu}\}) \equiv \langle\alpha|H^n_{\mathrm{KS}}|\beta\rangle\,, \quad \text{and } S_{\alpha\beta} \equiv \langle\alpha|\beta\rangle \tag{5.13}$$

[8] For example, CASTEP and Quantum Expresso use plane waves, DMol^3 uses atomic orbitals, Gaussian orbitals are used in the eponymous Gaussian code, and ONETEP uses generalised Wannier functions.

[9] With this sum over $\mathbf{R}_I$, we are over-specifying the one-particle Hilbert space $\mathscr{H}$. The orbitals of a single atom at an arbitrary $\mathbf{R}$ are enough to form a basis of $\mathscr{H}$, but to represent states far away from $\mathbf{R}$ we would require orbitals of very high energy, which is not desirable.

[10] The "energy" of a basis state is used only as a benchmark of when one may reasonably truncate the expansion, but in a general case, it will not match the actual energy of the KS orbitals. In the case of plane waves, this "energy" is naturally $\hbar^2k^2/2m$, and for LCAO, the energy of the isolated atomic states may be used.

The factor $S_{\alpha\beta}$ is called the *overlap matrix*, and it accounts for the fact that the basis set may not be orthonormal. If one uses an orthonormal basis set, $\mathbf{S}$ would be just the identity matrix. A more compact way to express eq. (5.12) is to write it as a matrix equation

$$\mathbf{S}^{-1} \cdot \mathbf{F}(\mathbf{c}^n) \cdot \mathbf{c}_i^{n+1} = \epsilon_i^{n+1} \mathbf{c}_i^{n+1}, \quad \text{with } \mathbf{c} \equiv \prod_i \mathbf{c}_i \tag{5.14}$$

Note that the overlap matrix $\mathbf{S}$ need only be computed once at the beginning of the SCF procedure, and it just needs to be stored to be referenced in the following steps. Afterwards, the solution is reduced to computing $\mathbf{F}$ and obtaining the N lowest eigenvalues and eigenvectors of $\mathbf{S}^{-1}\mathbf{F}$ at every step until the new orbitals match the old ones within an acceptable margin.

The only remaining point to address is how these calculations are performed with high computational efficiency. A thorough discussion of this point is beyond the scope of this work, but in the following subsection, we discuss one of the most crucial methods used for this purpose, the pseudopotential technique.

5.1.3 Pseudopotential Approach to the Core Electrons

A substantial simplification can be performed by relying upon the well-known fact that electrons involved in the bonding and interactions between atoms are only the more mobile ones on higher energy levels, the so-called valence shell. In contrast, the electrons in lower energy levels remain nearly unperturbed even if the surroundings of the atom change significantly. This approach affords us twofold benefits that greatly reduce the computation time of the Kohn-Sham DFT calculation: *(i)* this calculation scales as $\sim N^3$, with N the number of electrons, or more precisely, N is the number of orbitals in the basis set[11]. By bundling the electrons in the lower energy levels—denominated as *core electrons*— with the nuclei into an *ion*, we directly reduce the number of electrons in the computation. *(ii)*, as Richard M. Martin points out [57], the pseudopotentials are smoother and weaker than the original nuclear potential, resulting in smoother *pseudofunctions* ("pseudised" wavefunctions, see below) that require smaller basis sets to be represented[12].

From a practical standpoint, we may regard the pseudopotential approach as a computational tool that reduces the number of electrons needed to be explicitly taken into account by transforming the nuclear potential V_{ext} into an effective potential that also encapsulates the effects of the implicit core electrons.

[11] S. Goedecker and G. E. Scuseria [33] explain how this $O(N^3)$ scaling comes to be in KS-DFT and compare it with other popular methods in this respect.

[12] This issue is predominant in plane wave basis sets because the original potential becomes very strong approaching the nucleus, giving rise to short wavelength oscillations. Volker Heine [38] illustrates this point by noting that, for aluminium, a plane wave calculation of the secular energy equation would require $\sim 10^6$ modes to converge, in contrast to ~ 20 if one uses pseudopotential methods.

In this picture, the single-particle wavefunctions of the electrons can be separated into valence and core states, with the distinction demarcating the energy below which the electrons can be considered as unperturbed by a change in the atomic environment. Following the notation of Martin [57], we write the valence and core states as $|\psi_i^{\mathrm{v}}\rangle$ and $|\psi_i^{\mathrm{c}}\rangle$, respectively. In particular, the valence wavefunctions satisfy the Schrödinger equation

$$H\,|\psi_i^{\mathrm{v}}\rangle = \left(\frac{P^2}{2m} + v\right)|\psi_i^{\mathrm{v}}\rangle = \epsilon_i^{\mathrm{v}}\,|\psi_i^{\mathrm{v}}\rangle \tag{5.15}$$

With this, we can introduce the pseudopotential $\tilde{v}$ formally as a transformation of the strong[13] potential[14] v that simultaneously transforms the wavefunctions into smoother functions $\tilde{\psi}_i^{\mathrm{v}}$—called **pseudofunctions**— while preserving the spectrum of the original valence wavefunctions ϵ_i^{v}. This new operator $\tilde{v}$ is usually non-local[15], in contrast to the original potential which is local. Eq. (5.15) is thus formally converted into

$$\tilde{H}\,|\tilde{\psi}_i^{\mathrm{v}}\rangle = \left(\frac{P^2}{2m} + \tilde{v}\right)|\tilde{\psi}_i^{\mathrm{v}}\rangle = \epsilon_i^{\mathrm{v}}\,|\tilde{\psi}_i^{\mathrm{v}}\rangle \tag{5.16}$$

which has a structure identical to the original Schrödinger equation but replaces the potential and wavefunctions with their pseudised counterparts[16]. One of the universal concepts in pseudopotential theory is the **core radius** R_{c}: it is only inside the sphere of radius R_{c} that the pseudopotential and pseudofunctions differ from their original counterparts but outside of it, they match the quantities of the original Schrödinger equation (5.15). Explicitly:

$$\tilde{v}(r > R_{\mathrm{c}}) = v(r), \quad \text{and } \tilde{\psi}_i^{\mathrm{v}}(r > R_{\mathrm{c}}, \theta, \phi) = \psi_i^{\mathrm{v}}(r, \theta, \phi) \tag{5.17}$$

The underlying reason why the pseudofunctions are smoother than the original wavefunctions $\tilde{\psi}_i^{\mathrm{v}}$, is that the pseudopotential is weaker than v, but this only happens when the orbital angular momentum quantum number l of the valence state has already been occupied by core states [14]. This fact follows from the so-called *"cancellation theorem"*, which was stated by M. L. Cohen and Heine [14] as the fact that, if there are any core states for a given l (*viz.*, $\exists i$ such that $L^2\,|\psi_i^{\mathrm{c}}\rangle = \hbar^2 l(l+1)\,|\psi_i^{\mathrm{c}}\rangle$), then $\tilde{v}(r < R_{\mathrm{c}})$ is almost zero[17].

[13] As Heine [38] points out, the most useful definition of a "strong" potential is one that has at least one bound state.

[14] Note that we are using a lowercase v in these single-particle potentials to distinguish them from the total V_{ext} that acts on all of the electrons.

[15] A non-local operator O can be written as $O = \sum_{i,j} |i\rangle\, O_{ij}\, \langle j|$.

[16] The simplest pseudopotential corresponds to the Orthogonalised Plane Wave (OPW) model of Conyers Herring [39], whose expression in the form of eq. (5.16) can be found in Section 11.2 of Martin's book [57]. Alternatively, in Section III of [38], Heine introduces the matrix elements of $\tilde{v}$ in a plane wave basis for both the OPW model and Slater's [82] earlier but more complicated Augmented Plane Wave (APW) model. OPW and APW may be regarded as the precursors of modern pseudpotential methods.

[17] It should be noted that this "cancellation theorem" is not a theorem in the mathematical sense. As Cohen and Heine [14] clarify, it is a conclusion derived from empirical evidence and theoretical arguments.

A fundamental aspect of these pseudopotentials is that they may be described equivalently in terms of their scattering properties[18] as they are in terms of the spectrum ϵ_i^{v} that they need to match [14]. This gives ample freedom in the choice of pseudopotential functions, which are by no means uniquely determined by these conditions. Consequently, there exist multiple families of pseudopotentials that may appear as $\tilde{v}$ in eq. (5.16) that give rise to the same energy spectrum approximately or exactly and they can be chosen to have properties that are convenient to us. In particular, we are interested in Bernard Delley's **density functional semicore pseudopotential** (DSPP) [21] that was implemented in the DMol^3 software, which we have used in all of our DFT calculations.

Delley's DSPP is a semilocal pseudopotential that aims at satisfying (or closely approaching) the norm-conserving condition in multiple configurations by means of an optimisation[19] procedure [21]. The *semilocal* class of pseudopotentials consists of operators whose non-locality depends only on the angular variables of the wavefunction. They can be expressed generically (*cf.*, eq. (11.15) of [57]) as

$$\tilde{v} = v_{\mathrm{loc}} + v_{\mathrm{SL}} = v_{\mathrm{loc}}(r) + \sum_{l,m} |lm\rangle \left[v_l(r) - v_{\mathrm{loc}}(r)\right] \langle lm| \tag{5.18}$$

where v_{loc} is the local part of the potential and the second term comprises the semilocal terms. Note that eq. (5.18) implies that valence electrons with different orbital angular momentum wavenumbers experience different effective potentials. Additionally, as Martin points out [57], we can express v_{loc} and v_l as functions only of the scalar r thanks to the fact that the ion is assumed to have a spherically symmetric potential, which also makes it possible to deal with every component of the angular momentum individually[20].

The action of a semilocal potential on a wavefunction expressed in the position basis is evaluated as

$$v_{\mathrm{SL}}\, \varphi(r, \Omega) = \sum_{l,m} Y_l^m(\Omega)[v_l(r) - v_{\mathrm{loc}}(r)] \int \mathrm{d}\Omega'\, Y_l^m(\Omega')\varphi(r, \Omega') \tag{5.19}$$

where Ω is the solid angle.

[18] In particular, as Cohen and Heine [14] point out, the pseudopotential must match $v(\mathbf{r})$ identically in the interstitial region (*i.e.*, outside the core spheres of radius R_{c}), and the wavefunctions $\psi(\mathbf{r}) = R_l(r; E)Y_l^m(\theta, \phi)$ must have the same logarithmic derivatives at R_{c}, namely

$$\frac{1}{\tilde{R}_l(R_{\mathrm{c}}; E)} \frac{\mathrm{d}\tilde{R}_l}{\mathrm{d}r}(R_{\mathrm{c}}; E) = \frac{1}{R_l(R_{\mathrm{c}}; E)} \frac{\mathrm{d}R_l}{\mathrm{d}r}(R_{\mathrm{c}}; E)$$

[19] The optimisation is made by minimising the sum root-mean-squared errors in both the valence eigenvalues and the norm-conservation, with their magnitudes weighed by expressing them in atomic units, along with some penalties to give the pseudopotential the desired shape [21].

[20] This is because eigenfunctions of H in a central potential can simultaneously be eigenfunctions of L^2 and one component of $\mathbf{L}$ [94].

The primary target of DSPP, the **norm-conservation**, means that the pseudopotential is *ab initio*: its parameters are not determined experimentally. Instead, they are fitted to match DFT results from all-electron calculations [57]. In addition to the aforementioned general properties stated above (*i.e.*, matching spectrum, equivalence to non-pseudised wavefunction in the interstitial region, and agreement of logarithmic derivatives), this family of pseudpotentials also satisfies the norm conservation condition:

$$\int_0^{R_c} r^2 \mathrm{d}r \, |\tilde{R}_l(r)|^2 = \int_0^{R_c} r^2 \mathrm{d}r \, |R_l(r)|^2 \tag{5.20}$$

which means that the charge held inside the core sphere in the pseudofunction matches the one in the original wavefunction. A particularly convenient consequence of this condition is that the pseudofunctions satisfy the usual orthonormality conditions (see Section 11.4 of [57])

$$\left\langle \tilde{\psi}^{\mathrm{v}}_{i,\sigma} \,\middle|\, \tilde{\psi}^{\mathrm{v}}_{j,\sigma'} \right\rangle = \delta_{ij}\delta_{\sigma\sigma'} \tag{5.21}$$

a relation which makes the Kohn-Sham equations (4.23) preserve their form even after the pseudopotential transformation is performed [57].

In the particular case of DSPP, Delley [21] has chosen to fit the pseudopotential to the PBE and PW functionals simultaneously[21]. Delley also decides to include the semicore states[22] in addition to the valence states to increase the accuracy and portability of the method [21]. This addition is suited for local orbital and not plane wave basis sets, as Delley explains [21]. One final technicality to be addressed is that when one performs the DFT calculation to fit the free parameters in the pseudopotential, one does not find the effective potential of just the "bare" ion. The calculation also includes the screening effects caused by the other valence electrons [57], including Hartree-like and exchange-correlation contributions. It is necessary to unscreen these effects to obtain the bare-ion pseudopotential (see Section 11.6 of [57]). A problem that arises in this procedure is that the pseudopotential approach aims to eliminate all the electronic degrees of freedom of the core, but these electrons also appear in the exchange-correlation energy in an explicitly nonlinear fashion [55], and if one were to unscreen the pseudopotential considering only the valence density the final product would depend on the valence configuration, instead of just on the orbital angular momentum l. Louie, Froyen, and Cohen [55] address this issue by including the core density $n_{\mathrm{c}}(\mathbf{r})$ as part of the energy needed to unscreen, namely (*cf.*, eq. (11.36) of [57] and eq. (9) of [55])

$$v_l(r) = v_{l,\mathrm{total}}(\mathbf{r}) - v_{\mathrm{H}}[\tilde{n}_{\mathrm{v}}](\mathbf{r}) - v_{\mathrm{xc}}[\tilde{n}_{\mathrm{v}} + n_{\mathrm{c}}](\mathbf{r}) \tag{5.22}$$

[21] He notes that the errors are kept "roughly at the same low level" as when fitting for a single functional [21].

[22] We may regard the semicore states as those with lower energies than the valence states: low enough not to have much electron mobility or to get involved directly in bonding, but not so low that they are unaffected by perturbations in the immediate neighbourhood of the atom.

where $\tilde{n}_\mathrm{v}$ is the density calculated from the pseudised states. The nonlinear effect of the core density in the exchange-correlation energy of the valence electrons is only relevant when $\tilde{n}_\mathrm{v}$ and n_c are of similar magnitude and does not matter near the nucleus, where most of the charge is concentrated [55]. This situation allows one to represent the core density inside a sphere of radius r_d (note that $r_\mathrm{d} < R_\mathrm{c}$) in a smoother, more convenient form (similar to the general trend with pseudopotentials), only requiring an exact representation for $r > r_\mathrm{d}$ [55]. Delley [21] applies this method by introducing

$$\ln[n_\mathrm{c}(r)] = \sum_{i=1}^{n} c_i \left(\frac{r}{r_\mathrm{d}}\right)^{2-i}, \quad r > r_\mathrm{d} \tag{5.23}$$

where the expansion coefficients c_i are determined by fitting them to the all-electron calculation. And the density in the "unimportant" region $r < r_\mathrm{d}$ is taken as an even polynomial

$$n_\mathrm{c}(r) = \sum_{i=0}^{m} b_i r^{2i}, \quad r < r_\mathrm{d} \tag{5.24}$$

with the coefficients b_i determined by matching $n_\mathrm{c}(r_\mathrm{d})$ as calculated by eq. (5.23) up to the third derivative (and also maintaining the total core charge) [21]. Finally, the DSPP expression for the potentials V_l is given as a sum of Legendre polynomials

$$v_l(r) = \sum_{i=0}^{k} a_{i,l} P_{2i}\left(\frac{r}{r_{\mathrm{c},l}}\right), \quad r < r_{\mathrm{c},l} \tag{5.25}$$

The current version of DSPP uses nine terms of the sum in eq. (5.25), the last four coefficients $\{a_{i,l}\}_{i=5,\ldots,8}$ are determined by matching the original bare-ion potential $v(r > r_{\mathrm{c},l}) = -z_\mathrm{ion}/r$ up to the third derivative[23], signifying that there are five free coefficients $\{a_{i,l}\}_{i=0,\ldots,4}$ for every partial wave used to fit the all-electron calculation [21][24]. Additionally, every partial wave has its own core radius $r_{\mathrm{c},l}$, which is also treated as a free parameter to be optimised. The global core radius may be taken as $R_\mathrm{c} = \max(r_{\mathrm{c},l})$. Finally, note that the local part of the potential introduced in eq. (5.18) is taken as $v_\mathrm{loc} = v_{l_\mathrm{max}}$, the potential associated with the highest partial wave under consideration (*e.g.*, $l_\mathrm{max} = 3$ in both Cu and Zr). We have calculated[†] the DSPPs of Cu and Zr in the version currently used by DMol^3 and they are plotted in Fig. 5.1.

[23] The ionic charge z_ion (also written as z^*) is the sum of the nucleus's and the core electron's charge. The potential being $\propto 1/r$ matches the fact that the charge distribution is taken as spherically symmetric, so that only the total charge appears in the multipole expansion (see Section 4.1 of [45]).

[24] Or rather, the optimisation yields all nine coefficients, but the DSPP files report only the first five of them, since the others would be redundant as they may be determined using the constraints.

[†] I wish to express my gratitude to Prof. Bernard Delley for helping me understand the DSPP files as well as the pseudopotential method in general.

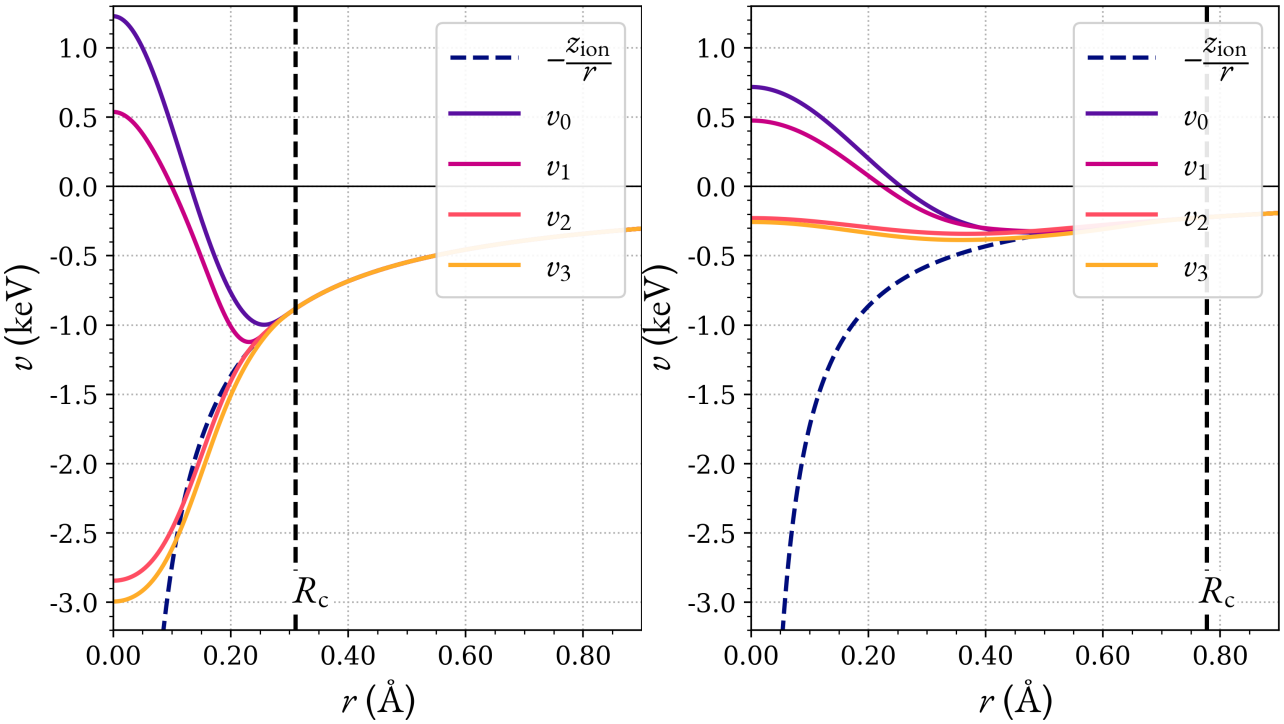

Figure 5.1: Pseudopotentials for Cu (left) and Zr (right) computed using eq. (5.25), with the data from version `s_01d21` of DSPP retrieved from the DMol^3 installation directory.

In Fig. 5.1 we observe that Cu has a notably smaller core radius R_c. This reflects the fact that the DSPP for Cu has only 10 electrons in the ion, with the remaining 19 having to be treated explicitly, resulting in a small core. In contrast, the Zr pseudopotential has 28 electrons in the ion, leaving 12 to be treated explicitly, this results in a higher degree of screening which we observe in the shallower potentials as well as a larger core radius. Physically, this difference demonstrates the fact that the electronic structure of Cu is more susceptible to changes in its immediate environment. We also observe the aforementioned "cancellation theorem" of Cohen and Heine [14] to some extent, where in Cu v_0 and v_1 are close(er) to zero because those angular momenta are occupied by electrons (of the s and p shells) in the core. In Zr we also see that v_0, v_1, and v_2 are close to zero as we would expect from the non-theorem, however it is interesting that even the local term $v_3 = v_{\text{loc}}$ appears to follow this pattern.

5.2 Classical Nuclear Dynamics

As we saw in Chapter 3, the nuclei may be treated within a good approximation as classical, with their motion given by an electron-generated potential resulting from the energy expectation value of the electronic state (*viz.*, their energy eigenvalue, since we are considering the ground state)

$$V_N(\mathbf{R}_I) = \langle \Psi_0 | H_e | \Psi_0 \rangle \tag{5.26}$$

with which the nuclear equations of motion are nothing but Newton's second law applied to this potential, namely, the second equality in eq. (3.15). We can recast that equation in terms of just the position, that is

$$\frac{\mathrm{d}^2 \mathbf{R}_I}{\mathrm{d}t^2} = -\frac{\nabla_{\mathbf{R}_I} V_N}{M_I} \equiv \mathbf{A}_I \tag{5.27}$$

where we have introduced the Ith nucleus's acceleration $\mathbf{A}_I = \ddot{\mathbf{R}}_I$. Our method of choice, which has been implemented in the DMol^3 software, is the **velocity Verlet** algorithm. As Landau, Páez, and Bordeianu [52] note, this method is performed by updating both the position $\mathbf{R}_I$ and velocity $\mathbf{V}_I = \dot{\mathbf{R}}$ of the particles from a reference time t to their new state at time $t + \Delta t$ according to

$$\begin{aligned} \mathbf{R}_I(t + \Delta t) &= \mathbf{R}_I(t) + \Delta t \mathbf{V}_I(t) + \frac{1}{2}\Delta t^2 \mathbf{A}_I(t) \\ \mathbf{V}_I(t + \Delta t) &= \mathbf{V}_I(t) + \Delta t \bar{\mathbf{A}}_I, \quad \text{with } \bar{\mathbf{A}}_I = \frac{\mathbf{A}_I(t + \Delta t) + \mathbf{A}_I(t)}{2} \end{aligned} \tag{5.28}$$

This method is a *Symplectic integrator* which makes it preserve the energy[25] of the system with a bounded error even over long times [22]. Eqs. (5.28) can be solved using a fully explicit scheme by:

1. Specifying the initial positions[26] $\mathbf{R}_I^0$ and velocities $\mathbf{V}_I^0$
2. Calculating the initial accelerations $\mathbf{A}_I^0$ according to eq. (5.27)
3. Udating the positions $\mathbf{R}_I^{n+1}$ using the previously obtained $\mathbf{R}_I^n$, $\mathbf{V}_I^n$, and $\mathbf{A}_I^n$.
4. Calculating the updated accelerations $\mathbf{A}_I^{n+1}$ at the new positions $\mathbf{R}_I^{n+1}$.
5. Updating the velocities $\mathbf{V}_I^{n+1}$ using the previously obtained $\mathbf{V}_I^n$, $\mathbf{A}_I^n$, and $\mathbf{A}_I^{n+1}$.
6. Repeating steps 3–5 as needed.

[25] This is a consequence of the more general fact that these methods preserve the symplectic structure (*i.e.*, the Poisson Bracket $\{\cdot,\cdot\}$) of phase space [22]. This property is expected, as these methods were designed for Hamiltonian systems (see [19, 80]).

[26] For brevity, we are using the reduced notation $X^n \equiv X(t_0 + n\Delta t)$, where t_0 is the initial time of the simulation and $n \in \mathbb{N}$.

The crux of the problem in Molecular Dynamics simulations is the calculation of the nuclear forces and accelerations that are performed in steps 2 and 4, above. In particular, we need to calculate the gradient

$$\nabla_{\mathbf{R}_I} \langle \Psi_0 | H_e | \Psi_0 \rangle \tag{5.29}$$

to obtain the nuclear forces. This can be performed using the **Hellmann-Feynman theorem** (see Section 3.1.4 of [48] or Section 5.6 of [94]), which may be stated as

$$\frac{\partial E_n}{\partial g} = \frac{\partial \langle \psi_n | H | \psi_n \rangle}{\partial g} = \left\langle \psi_n \left| \frac{\partial H}{\partial g} \right| \psi_n \right\rangle \tag{5.30}$$

for a system with a Hamiltonian H whose potential V depends parametrically[27] on some variable g, namely $H = p^2/2m + V(\mathbf{r}; g)$. This theorem can be applied directly in our case to obtain the nuclear forces required in steps 2 and 4, above. Namely,

$$\mathbf{A}_I^n = \left\langle \Psi_0 \left| \nabla_{\mathbf{R}_I} H_e(\mathbf{R}_I^n) \right| \Psi_0 \right\rangle \tag{5.31}$$

One should note that corrections due to an incomplete basis set and an imperfect self-consistency may apply as well in eq. (5.31), as Marx and Hutter elaborate [58]. However, such details are beyond the scope of this dissertation.

5.3 Geometry Optimisations: Broyden-Fletcher-Goldfarb-Shanno Algorithm

In addition to describing the nuclear motion, we often also require to obtain an equilibrium structure of the material. This can be performed by minimising the nuclear potential $V_N(\mathbf{R}_I)$ with respect to the nuclei's positions $\mathbf{R}_I$.

Recall that for functions of a single variable $f = f(x)$, the Newton-Raphson method is one of the most popular minimisation algorithms thanks to the fact that it converges exponentially to the correct extremum when the starting point is close to it[28]. Its simple expression for obtaining minima is

$$x^{k+1} = x^k - \frac{f'\left(x^k\right)}{f''\left(x^k\right)} \tag{5.32}$$

[27] Compare our own eq. (5.30) with eq. (3.6) of Konishi's and Pafutti's book [48]. They take the derivate only of the potential V, but since the kinetic energy is independent of g, we can exchange it with all of H.

[28] More precisely, it is a *second-order* iterative method, which means that the error in the approximate value of the true minimum at the $(k+1)$th step scales as $\varepsilon^{k+1} \sim (\varepsilon^k)^2$. See Section 10.11 of [40] for more details.

Eq. (5.32) can be readily generalised to the case of multiple variables $f = f(\mathbf{x})$, as Roger Fletcher presents in Section 3.1 of his book [27], by writing

$$\mathbf{x}^{k+1} = \mathbf{x}^k - \mathbf{H}_f^{-1}(\mathbf{x}^k) \cdot \boldsymbol{\nabla} f(\mathbf{x}^k) \tag{5.33}$$

where $\mathbf{H}_f$ is the Hessian matrix of function f. However, as Fletcher points out (see Section 3.2 of [27]), a problem with eq. (5.33) is that it requires knowledge of the analytical expression of $\mathbf{H}_f$, which may not be available or may be impractical to compute. In particular, as we saw in Section 5.2, the gradient $\boldsymbol{\nabla} V_N$ is already complicated to compute and requires the usage of the Hellmann-Feynman theorem, whereas no such convenient expression is known for $\mathbf{H}_{V_N}$. To circumvent these issues, the class of *quasi-Newton* methods may be used, one of which is the **Broyden-Fletcher-Goldfarb-Shanno** (BFGS) algorithm that we are interested in. As Fletcher points out (p. 56 of [27]), BFGS is possibly the best quasi-Newton method.

In the quasi-Newton methods, the inverse of the Hessian matrix is approximated in the initial step and then corrected during every iteration [27]. We write[29] this approximation as $\mathbf{S}^k \approx \mathbf{H}_f^{-1}(\mathbf{x}^k)$. The BFGS formula for this quantity is

$$\mathbf{S}^{k+1} = \mathbf{S}^k + \left(1 + \frac{\boldsymbol{\gamma}^k \cdot \mathbf{S}^k \cdot \boldsymbol{\gamma}^k}{\boldsymbol{\delta}^k \cdot \boldsymbol{\gamma}^k}\right) \frac{\boldsymbol{\delta}^k \boldsymbol{\delta}^k}{\boldsymbol{\delta}^k \cdot \boldsymbol{\gamma}^k} - \frac{\boldsymbol{\delta}^k \boldsymbol{\gamma}^k \cdot \mathbf{S}^k + \mathbf{S}^k \cdot \boldsymbol{\gamma}^k \boldsymbol{\delta}^k}{\boldsymbol{\delta}^k \cdot \boldsymbol{\gamma}^k} \tag{5.34}$$

where $\boldsymbol{\delta}^k = \mathbf{x}^{k+1} - \mathbf{x}^k$ is the change in coordinates and $\boldsymbol{\gamma}^k = \boldsymbol{\nabla} f(\mathbf{x}^{k+1}) - \boldsymbol{\nabla} f(\mathbf{x}^k)$ is the change in the gradient, both evaluated from step k to $k+1$. A notable point of this method is that, as Fletcher notes [27], the initial matrix $\mathbf{S}^0$ can be any positive definite matrix. Therefore, we do not need to calculate $\mathbf{H}_f$ exactly or approximately at any point in the implementation. When applied to our atomic structures, we only need to calculate $\boldsymbol{\nabla} V_N$ using the Hellmann-Feynman theorem[30] presented in Section 5.2.

5.4 Undermelt-Quench Approach to Amorphisation

As mentioned in Chapter 1, amorphous materials are characterised by short-range order that depends on the atoms' chemistry. Data given by the PDFs $g_{\alpha\beta}(r)$, BADs, or the structure factor only account for the average structural properties and are insufficient to determine a unique structure. Furthermore, an arbitrary random distribution of atoms will not reproduce the correct structural properties. To address this problem,

[29] Fletcher [27] uses a different notation from ours. He denotes the Hessian by $\mathbf{G}^{(k)}$ and its approximate inverse by $\mathbf{H}^{(k)}$. Instead, we reserve the letter H for the Hessian matrix since that is its standard notation.

[30] Note that here we mean the gradient with respect to all the nuclear coordinates $\boldsymbol{\nabla} = \boldsymbol{\nabla}_{\mathbf{R}_1} + \boldsymbol{\nabla}_{\mathbf{R}_2} + \cdots$.

Ariel A. Valladares, our group's principal investigator, developed a first-principles technique to accurately produce the structures encountered in amorphous solids [90], the **undermelt-quench** method.

This procedure begins by generating of a cell with the correct material composition and density, typically with a few hundred atoms, that is arranged in a structure known to be unstable for that given material[31]. A Molecular Dynamics (MD) simulation (see Section 5.2) is performed on the initial structure, whereby it is heated with a constant temperature slope up to just below its melting (solidus) temperature T_{m} and is then cooled down at the same rate until its temperature approaches 0 K. In this method, one neither reaches T_{m} nor 0 K exactly because the Nosé-Hoover thermostat does not produce a consistent temperature slope at every step. Instead, a buffer of $\sim$ 10 K is used at both extremes to prevent the material from melting or reaching an unphysical negative temperature. This process is similar to the quenching used to harden steel, and we reach temperatures just below the melting point, hence the name *undermelt-quench*. A visual representation of this part of the process is shown in Fig. 5.2.

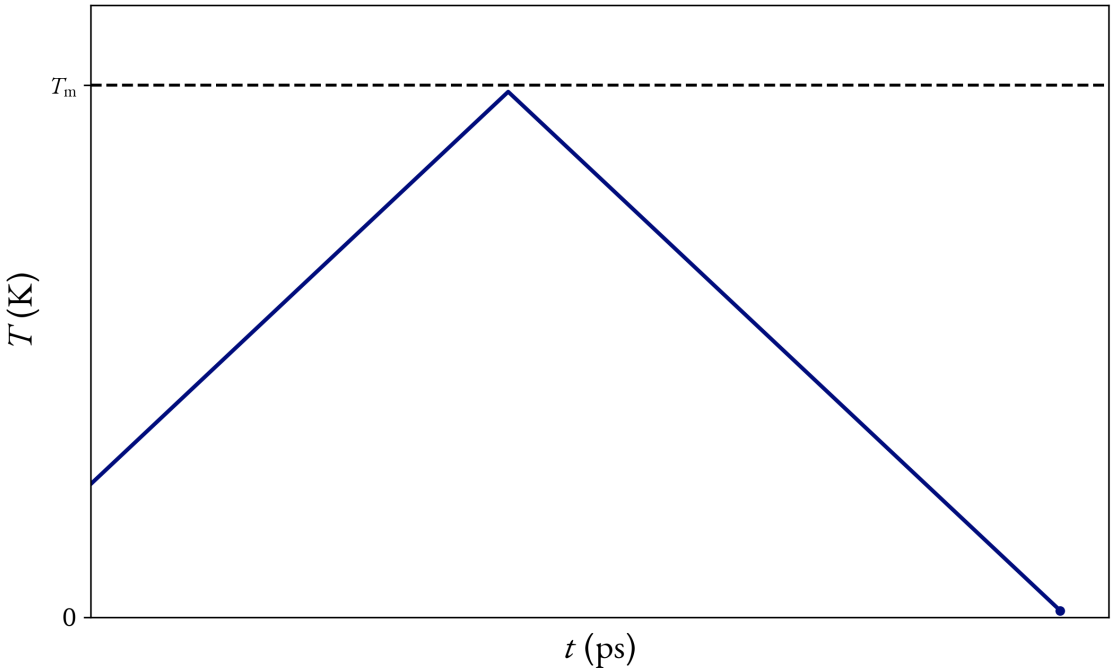

Figure 5.2: Generic schematic representing the MD process of Valladares's [90] undermelt-quench method. We have included the units of ps in the time axis as a reference to the typical order of magnitude that the process takes[32]. Note that after the MD process finishes, indicated by the dot in the figure, a Geometry Optimisation is still required to reach a stable structure.

[31] For instance, in the $\mathrm{Cu}_x\mathrm{Zr}_{1-x}$ system, the intermetallic compound CuZr_2 is a tetragonal crystal with a C11b structure. When we perform the undermelt-quench approach, it is necessary to use a sufficiently different structure so that no domain of our sample crystallises during the process.

[32] The entire MD process usually takes a time roughly on the order of $\sim$ 1 ps. There are usually a few hundred steps, and depending on the elements in question (lighter atoms require shorter time-steps to capture their motion), each may occur in about 1–20 fs.

The underlying idea behind this process is that, by starting with a structure far removed from the equilibrium crystal, the atoms are unable to rearrange into such a crystal. Instead, the resulting structure approaches a local minimum, which is likely amorphous since the starting point does not have the symmetry of the crystal. Unlike the quenching process performed on steels, where microcrystals are formed whose structure is a perturbation of the equilibrium configuration[33], here we expect amorphous structures because the cooling rates are much higher than what is achievable experimentally, and there is no time for a crystal to form.

Since 0 K is not achieved in the MD process, we do not expect the resulting structure to match the (metastable) equilibrium structure of the amorphous material. Therefore, in the undermelt-quench method, a geometry optimisation process (see Section 5.3) is performed on the final MD structure to reach the actual equilibrium configuration.

5.5 Vibrational Density of States

The last type of calculation that we need to perform with DFT is the phonon spectrum of the classical nuclei, or more specifically, the vibrational density of states (vDoS). The background of this topic may be reviewed in Chapter 4 of Ibach's and Lüth's book [44]. As introduced there, phonons appear in the Taylor expansion of the nuclear potential V_N around the equilibrium configuration as the harmonic term. Namely,

$$V_N(R_{I,i} + u_{I,i}) = V_N(R_{I,i}) + \frac{1}{2} \sum_{J,K,j,k} \frac{\partial^2 V_N}{\partial R_{J,j} \partial R_{K,k}} u_{J,j} u_{K,k} + O(u^3) \tag{5.35}$$

where $R_{I,i}$ denotes the ith cartesian component of the position $\mathbf{R}_I$ of the Ith nucleus, and $u_{I,i}$ denotes its respective displacement from the equilibrium position. With this equation, Ibach and Lüth [44] proceed to show that the equations of motion for the nuclei may be written as

$$M_I \ddot{u}_{J,j} + \sum_{K,k} \left(\frac{\partial^2 V_N}{\partial R_{J,j} \partial R_{K,k}} \right) u_{K,k} = 0 \tag{5.36}$$

which is the equation for a harmonic oscillator in $3N_{\text{nuc}} = N_{ph}$ dimensions, with N_{nuc} the number of nuclei under consideration. The conventional way to solve this is introducing the ansatz of a plane wave solution (*cf.*, eq. (4.5) of [44])

$$u_{J,j} = \frac{1}{\sqrt{M_J}} \tilde{u}_{J,j}(\mathbf{q}) e^{i(\mathbf{q}\cdot\mathbf{R}_J - \omega_{\mathbf{q}} t)} \tag{5.37}$$

[33] The martensite formed when quenching steel has a body-centred tetragonal structure instead of the body-centred cubic structure of ferrite, which globally minimises the energy. In the words of Verdeja González, Fernández-González, and Verdeja González [91], *"[The structure of martensite] is like a ferrite cell deformed preferentially [along] the c axis."*

which transforms the equations of motion into

$$-\omega_{\mathbf{q}}^2 \tilde{u}_{J,j}(\mathbf{q}) + \sum_{K,k} \underbrace{\frac{1}{\sqrt{M_J M_K}} \left(\frac{\partial^2 V_N}{\partial R_{J,j} \partial R_{K,k}} \right) e^{i\mathbf{q}\cdot(\mathbf{R}_K - \mathbf{R}_J)}}_{D_{Jj,Kk}} \tilde{u}_{K,k}(\mathbf{q}) = 0 \tag{5.38}$$

where we have identified the **dynamical matrix** $D_{Jj,Kk}$ inside the summation in the right-hand side. In this classical picture, the phonons are regarded as the normal modes of the oscillator, the eigenvectors of $D_{Jj,Kk}$. We can see from eq. (5.38) that the eigenvalues are precisely the $\omega_{\mathbf{q}}^2$. This equation has $3N_{\text{nuc}}$ solutions for every value of $\mathbf{q}$. Note that we did not need to specify if the atoms were arranged in a crystal or an amorphous solid.

The difficulty in performing the vDoS calculation is that in this case, we need to explicitly obtain the Hessian matrix

$$(\mathbf{H}_{V_N}) = \frac{\partial^2 V_N}{\partial R_{J,j} \partial R_{K,k}} \tag{5.39}$$

which we were able to bypass previously when performing the geometry optimisation thanks to a clever approximation. More specifically, we can calculate $\boldsymbol{\nabla} V_N$ for every configuration with the Hellmann-Feynman theorem, and we need to take the second derivative of each of the components of this vector to obtain $\mathbf{H}_{V_N}$. One of the ways to perform this calculation, which is the one used in the DMol^3 code, is the **finite displacement** method, where the derivative is evaluated explicitly by changing every atomic coordinate by a small but finite amount ε. Mathematically,

$$\frac{\partial^2 V_N}{\partial R_{J,j} \partial R_{K,k}} = \frac{\frac{\partial V_N}{\partial R_{K,k}}(\mathbf{R}_1, \mathbf{R}_2, \dots, \mathbf{R}_J + \varepsilon \hat{\mathbf{e}}_j, \dots) - \frac{\partial V_N}{\partial R_{K,k}}(\mathbf{R}_1, \mathbf{R}_2, \dots, \mathbf{R}_J, \dots)}{\varepsilon} \tag{5.40}$$

where $\hat{\mathbf{e}}_j$ is the jth cartesian basis vector. The derivatives in the numerator on the right-hand side of eq. (5.40) are, as mentioned before, evaluated with the Hellmann-Feynman theorem, but this calculation needs to be performed at the equilibrium configuration and at each of the N_{ph} perturbed configurations. Therefore, this method requires $N_{ph} + 1$ or $3N_{\text{nuc}} + 1$ DFT cycles in total.

The solutions of eq. (5.38), *i.e.*, the set of eigenvalues and eigenvectors, comprise the phonon spectrum. The vDoS encapsulates this spectrum as a function of the phonon frequency ω. We can express it formally as

$$F(\omega) = \frac{V}{(2\pi)^3 N_{\text{nuc}}} \sum_{\omega_{\mathbf{q}}} \int_V \mathrm{d}^3 q \, \delta(\omega - \omega_{\mathbf{q}}) \tag{5.41}$$

This expression is provided by Göran Grimvall in Chapter 6 of his book [35] (eq. (6.5)), and it is normalised to yield the conventional value of 3. With the vDoS we are able to calculate the Debye frequency ω_D that appears (in the form of $\Theta_D = \hbar\omega_D/k_B$) in the formula for T_c. As Grimvall shows (*cf.* eqs. (6.22) and (6.34) of [35]), ω_D is given by

$$\omega_D = \exp\left[\frac{1}{3} + \frac{\int_0^{\omega_{\max}} \mathrm{d}\omega\ \ln(\omega)F(\omega)}{\int_0^{\omega_{\max}} \mathrm{d}\omega\, F(\omega)}\right] \tag{5.42}$$

where $\omega_{\max}$ is the maximum frequency of the vDoS.

5.6 Mata-Valladares Approach to the T_c Calculation

As we have seen in Chapter 2, the BCS theory of superconductivity is based on the electron-phonon interaction. This means that to compute either the Cooper pairing potential V, we need knowledge of the electronic properties close to the Fermi surface, the phonon spectrum, and information about the electron-phonon interaction itself. *Ab initio* computations of the electron-phonon interaction may in principle be performed within the DFT framework to obtain the function $\alpha^2(\omega)$ which is an average of the electron-phonon interaction appearing in the more generalized theory of superconductivity of Gerasim M. Eliashberg [61]. One can combine $\alpha^2(\omega)$ with the vDoS $F(\omega)$ to obtain a dimensionless coupling constant λ (see eq. (5) of [61]) that gives a measure of the strength of the electron–phonon interaction. The difference of λ and the Morel–Anderson pseudopotential μ^*, which is a dimensionless measure of the Coulomb interaction strength, plays the role of the N_0V of BCS theory in the weak coupling range [61] (*i.e.*, $\lambda - \mu^* \xrightarrow{\lambda \ll 1} N_0V$).

The most efficient approach for the calculation of λ is the linear response method[34], the implementation of which can be found in Rolf Heid's notes [37]. Unfortunately, as it can be seen in Heid's notes (*cf.* eqs. (104) and (105) of [37]), this calculation requires obtaining the phonon spectrum, and then calculating a matrix element for every one of the N_{ph} phonons and N_e electronic states. Since the phonon spectrum in DMol^3 is calculated using the finite displacement method, one DFT calculation is required for each of the N_{ph} modes. If we denote the number of electrons by N, with $N_e \sim N_{ph} \sim N$ scaling proportionally as more atoms (with a fixed composition) are added, then the calculation of DFT energy scales as $O(N^3)$, the phonon spectrum as $O(N^4)$, and the electron-phonon interaction as presented by Heid [37] scales as $O(N^5)$. Because of this high computational complexity, it is impossible to directly calculate the electron-phonon interaction in amorphous materials, where one inherently requires large cells with many atoms to portray the disorder.

[34] An alternative method uses finite differences, it has the advantage of being more versatile (it can use any electronic structure method, not only DFT), and can obtain higher-order terms in the electron phonon interaction (anharmonic terms), as Bartomeu Monserrat explains [62]. These advantages, however, come with a higher computational cost [62].

To circumvent this problem, Mata-Pinzón *et al.* [59], members of our group, have put forward another method that can be applied to amorphous materials, unlike the explicit calculation introduced above. In essence, one assumes that the Cooper pairing potential V is not affected drastically if the material's structure changes [76], this allows us to approximate V as invariant, and in turn, if T_c is known in one of the material's structure, we can extrapolate its value to a different structure. This method has been employed successfully by our group in an number of previous publications [41, 42, 59, 76, 89], and we will outline this method in what follows.

Recall that BCS theory predicts a critical temperature of the superconducting transition T_c given by

$$T_c = 1.13\Theta_D \exp\left(-\frac{1}{N_0 V}\right)$$

where Θ_D is the Debye temperature, N_0 is the electronic density of states at the Fermi level, and V is the Cooper pairing potential, we derived this result as eq. (2.115) in Section 2.2.5. We can introduce a superscript to label the quantities according to which structure they correspond to, in particular, we use "k" and "u" to label the phases where T_c is known and unknown, respectively. Then, as outlined by Rodríguez *et al.* [76], the BCS equation may be transformed into

$$\left(T_c^{(k)}\right)^{N_0^{(k)}/N_0^{(u)}} = \left(1.13\Theta_D^k\right)^{N_0^{(k)}/N_0^{(u)}} \exp\left(-\frac{1}{N_0^{(u)} V}\right) \tag{5.43}$$

where, in the right-hand side, we have matched the exponential to what should appear in the equation for $T_c^{(u)}$. If the quotient of densities at the Fermi level is denoted by $\eta \equiv N_0^{(u)}/N_0^{(k)}$, then the equation for $T_c^{(u)}$ can be expressed as

$$T_c^{(u)} = 1.13\Theta_D^{(u)}\left(T_c^{(k)}\right)^{1/\eta}\left(1.13\Theta_D^{(k)}\right)^{-1/\eta} \tag{5.44}$$

In eq. (5.44) we see that the explicit dependence on the Cooper pairing potential has disappeared, and the only quantities involved are the Debye temperatures and the densities at the Fermi level, forgoing the necessity of an electron-phonon calculation. Eq. (5.44) can be simplified a bit further by introducing the quotient of Debye temperatures $\delta \equiv \Theta_D^{(u)}/\Theta_D^{(k)}$, in summary

$$T_c^{(u)} = \delta\left(T_c^{(k)}\right)^{1/\eta}\left(1.13\Theta_D^{(k)}\right)^{(\eta-1)/\eta}, \quad \text{where } \eta = \frac{N_0^{(u)}}{N_0^{(k)}}, \delta = \frac{\Theta_D^{(u)}}{\Theta_D^{(k)}} \tag{5.45}$$

which depends only on the electronic and vibrational properties of the "known" structure, and the quotients η, δ.

In practice, to apply this approach to the T_c calculation we need to:

1. Prepare the computational amorphous samples that will represent "k" and "u". This is typically done using the undermelt-quench approach[35] outlined in Section 5.4.
2. A DFT calculation is performed on each of the amorphous samples to obtain the eDoS at the Fermi level, N_0.
3. The Debye Temperature, Θ_D, of every sample is obtained following the method outlined in Section 5.5.
4. The T_c of one of the samples ("u") is estimated with eq. (5.45) using the data calculated in the previous steps as well as the known T_c of the other sample ("k").

5.7 Software

All of the DFT calculations were performed with the DMol^3 code [20] within the User Interface provided by the Materials Studio suite from Dassault Systèmes Biovia Corp. [18]. This includes the electronic (eDoS) and vibrational (vDoS) densities of state.

All of the structural properties of the amorphous cells were computed using the Correlation software by Rodriguez *et al.* [75]. The graphical displays of the materials' structures were generated using the Discovery Studio Visualizer from Dassault Systèmes Biovia Corp. [17].

All of the plots in this work have been generated using standalone programs developed by the author in Python 3.10.6. To graph discrete data in continuous plots, a (Gaussian) kernel smoothing has been performed where required. A representative selection of these programs is shown in Appendix A.

[35] Note that the Mata-Valladares approach to the T_c calculation is not restricted in terms of which method is used to generate an amorphous sample. One could feasibly apply it to samples generated with, e.g., the sphere packing methods presented by Stachurski [84]. However, we use the undermelt-quench amorphisation because it yields true *first principles* results, from the intitial structure to the properties of the system.

6 Results

Where we showcase and discuss the findings obtained from our simulations.

We have obtained amorphous samples of six distinct alloys in the Cu_xZr_{1-x} system using the Undermelt quench approach (see Section 5.4), namely, for $x = 0.25$, 0.33, 0.45, 0.5, 0.55, and 0.6. Their cell sizes have been chosen to match the experimental densities presented by Z. Altounian and J.O. Strom-Olsen [3], which complement those of their earlier work together with Guo-hua [2] as well as the more recent results by Li *et al.* [53] for the concentration $x = 0.5$ that is missing in the former articles[1]. In the amorphisation procedure we have used the solidus temperatures provided in the phase diagram by Hiroaki Okamoto [65], reproduced here in Fig. 6.1.

The values relevant to our alloys are summarised in Tab. 6.1.

Table 6.1: Mass densities and solidus temperatures of the amorphous Cu_xZr_{1-x} alloys that have been used in this work. Retrieved from the data in [2, 3, 16, 53] and Fig. 1 of [65].

	$Cu_{0.25}Zr_{0.75}$	$Cu_{0.33}Zr_{0.67}$	$Cu_{0.45}Zr_{0.55}$	$Cu_{0.5}Zr_{0.5}$	$Cu_{0.55}Zr_{0.45}$	$Cu_{0.6}Zr_{0.4}$
$\rho\left(\frac{\mathrm{g}}{\mathrm{cm}^3}\right)$	6.85	6.95	7.14	7.30	7.34	7.37
T_m (K)	1268	1275	1195	1208	1193	1206

We have obtained the eDoS of all these structures, but the vDoS have been computed only for $x = 0.25$, 0.33, and 0.5 due to computational constraints. We will present our results in the upcoming sections.

[1] Article [3] does include a value of ρ for $x = 0.5$, but it is only interpolated. Also, note that Li *et al.* [53] do not directly report the numerical value of the density and instead use a plot. We use the value retrieved from said plot by Cui *et al.* [16].

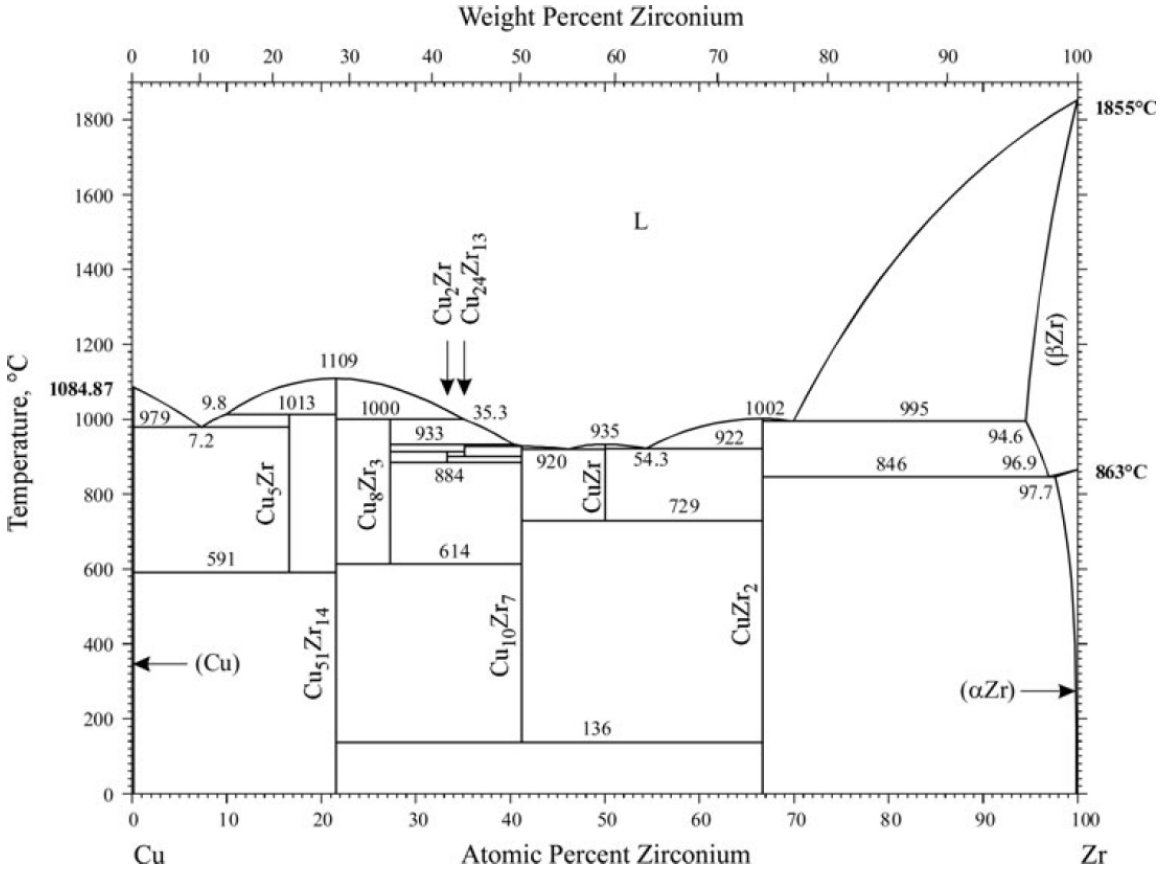

Figure 6.1: Phase diagram of the Cu-Zr system. Reproduced from Okamoto's work [65].

6.1 Amorphous Structures

We have successfully generated the amorphous structures of the six alloys using the undermelt-quench approach described in Section 5.4. The molecular dynamics process was performed using a time step of 10.70 fs, which was determined using the following rule of thumb

$$t_s = \alpha\sqrt{M_{\text{min}}}, \quad \text{with } \alpha = \frac{3}{\sqrt{5}}\,\text{fs}\cdot\text{Da}^{-1/2} \tag{6.1}$$

where t_s is the time step and M_{min} is the lesser of the atomic masses in the simulation. All of the amorphous cells were obtained using an initial 216-atom diamond supercell with random substitution to match the appropriate concentration, and whose size was chosen to match the mass densities in Tab. 6.1. Note that the diamond structure with a coordination number of 4 is very suitable as an unstable configuration in Cu_xZr_{1-x} alloys, since the structure of pure Cu and Zr are FCC and HCP, respectively, both with a coordination number of 12. Furthermore, the only stable intermetallic crystal in the range analysed is $CuZr_2$ (see the low temperature range in Fig. 6.1), which has a C11b structure (see [13]) where both elements have

a coordination of 8 (the nearest neighbours of any Cu atom are 8 Zr atoms, and the converse is also true). The temperatures of our samples are plotted in Fig. 6.2.

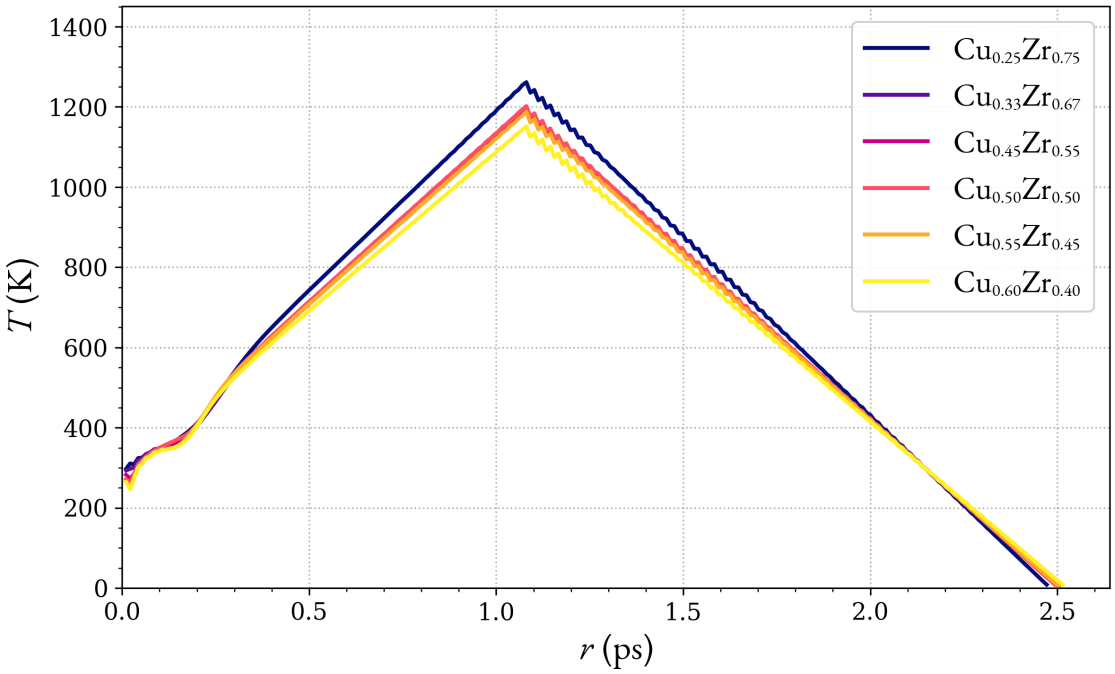

Figure 6.2: Temperatures during the Molecular Dynamics process of the Undermelt-quench amorphisation procedure for the six selected alloys. Note that the heating and cooling rates are close to $\sim 10^{15}$ K/s. The heating is performed from ambient temperature ($\approx$ 300 K) in 100 steps, and the cooling is performed at an equal rate until a temperature below 10 K is achieved.

If we compare the schematic presented in Fig. 5.2 with our results here in Fig. 6.2, we can see that the latter does not follow the shape of the ramp exactly; instead, a small dip at the start of the up-ramp and some oscillations in the down-ramp are observed. This difference may be attributed to the fact that the temperature is regulated using a Nosé-Hoover NVT thermostat (see, *e.g.*, [95]), which couples the atoms to additional heat bath variables. The variations represent the thermostat "attempting" to equilibrate the current atomic temperature with the target temperature.

After the dynamics had finished, the resulting structures were examined, showing they did not present undesirable crystallisation. These structures were subsequently optimised using the method described in Section 5.3. The final configuration of each alloy is displayed in Fig. 6.3. Note that throughout this document, all Cu atoms are displayed in orange while the Zr atoms are coloured teal.

At a glance, we can see in Fig. 6.3 that the structures are amorphous, however, we need an objective property to quantify the structural properties. Namely, the Pair Distribution Functions (PDFs). These are plotted in Fig. 6.4. Note that in Fig. 6.4 we have denoted the combined contribution of mixed partial PDFs as $g_{\mathrm{Cu,\,Zr}}$,

although if we were to be consistent with the notation in Chapter 1, we would need to write $g_{\mathrm{Cu,\,Zr}} + g_{\mathrm{Zr,\,Cu}}$.

An interesting detail to note is that Figs. 6.4 (a) and (b), corresponding to the concentrations in the $\mathrm{Cu}_x\mathrm{Zr}_{1-x}$ system that are not within the glass forming range, there is a fourth peak apparent in the $g(r)$, whereas in the other four alloys that are inside the range, this feature is a lot less prominent, and may be closer to a fluctuation around the limit value of 1. This appears to suggest that in the absence of a fourth peak, the amorphous phase is more likely to appear. To support this claim, we may argue that pronounced peaks at longer distance are evidence that the nuclear positions are correlated more strongly, making it harder to form an energetically disadvantageous amorphous phase. However, a more extensive study is necessary to determine whether this is either an artefact of our limited number of samples, a phenomenon exhibited only in the $\mathrm{Cu}_x\mathrm{Zr}_{1-x}$ system, or a general characteristic of bulk metallic glasses.

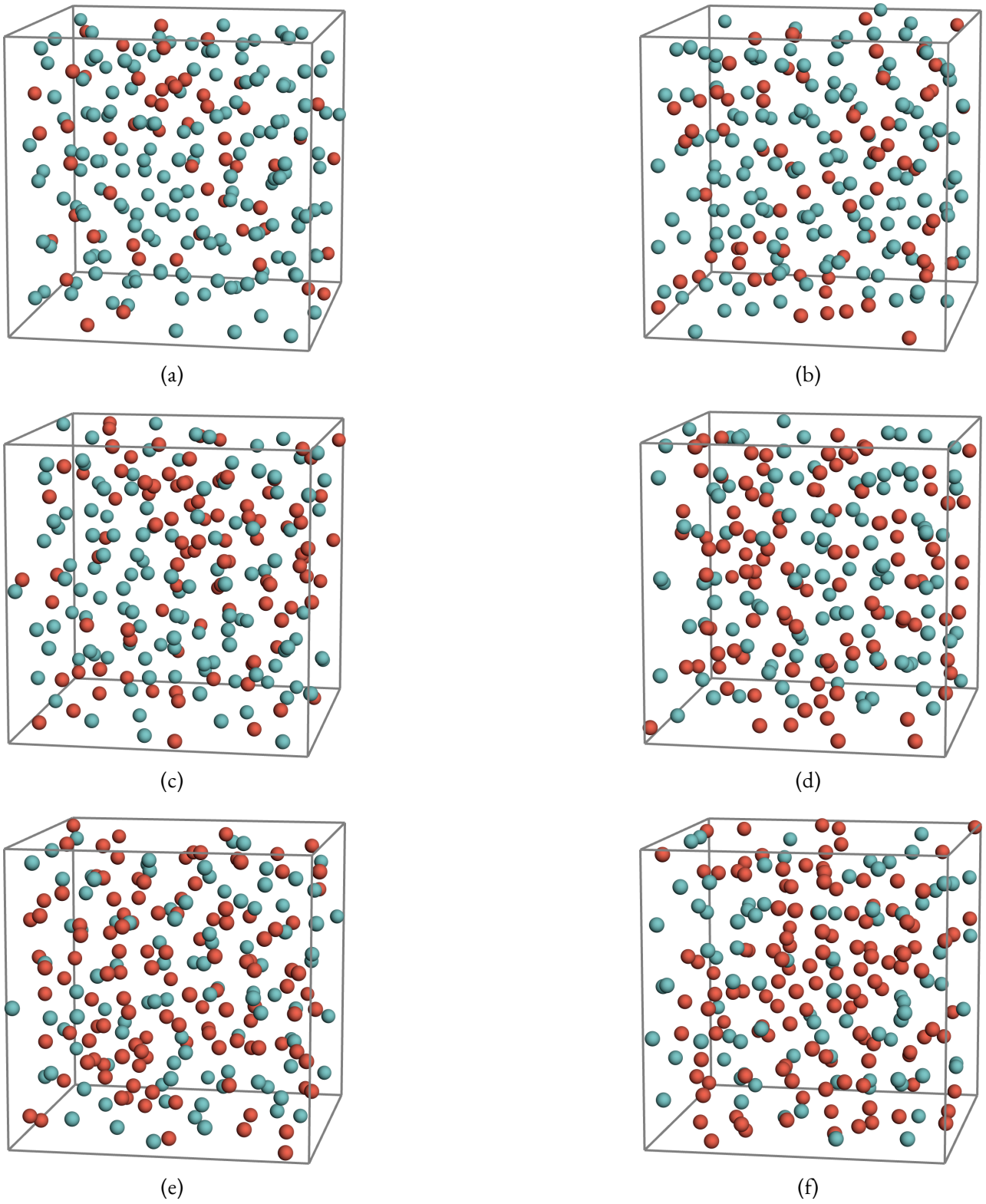

Figure 6.3: Optimised structures of the amorphous alloys in the Cu_xZr_{1-x}, with (a) $x = 0.25$, (b) $x = 0.33$, (c) $x = 0.45$, (d) $x = 0.5$, (e) $x = 0.55$, and (f) $x = 0.6$.

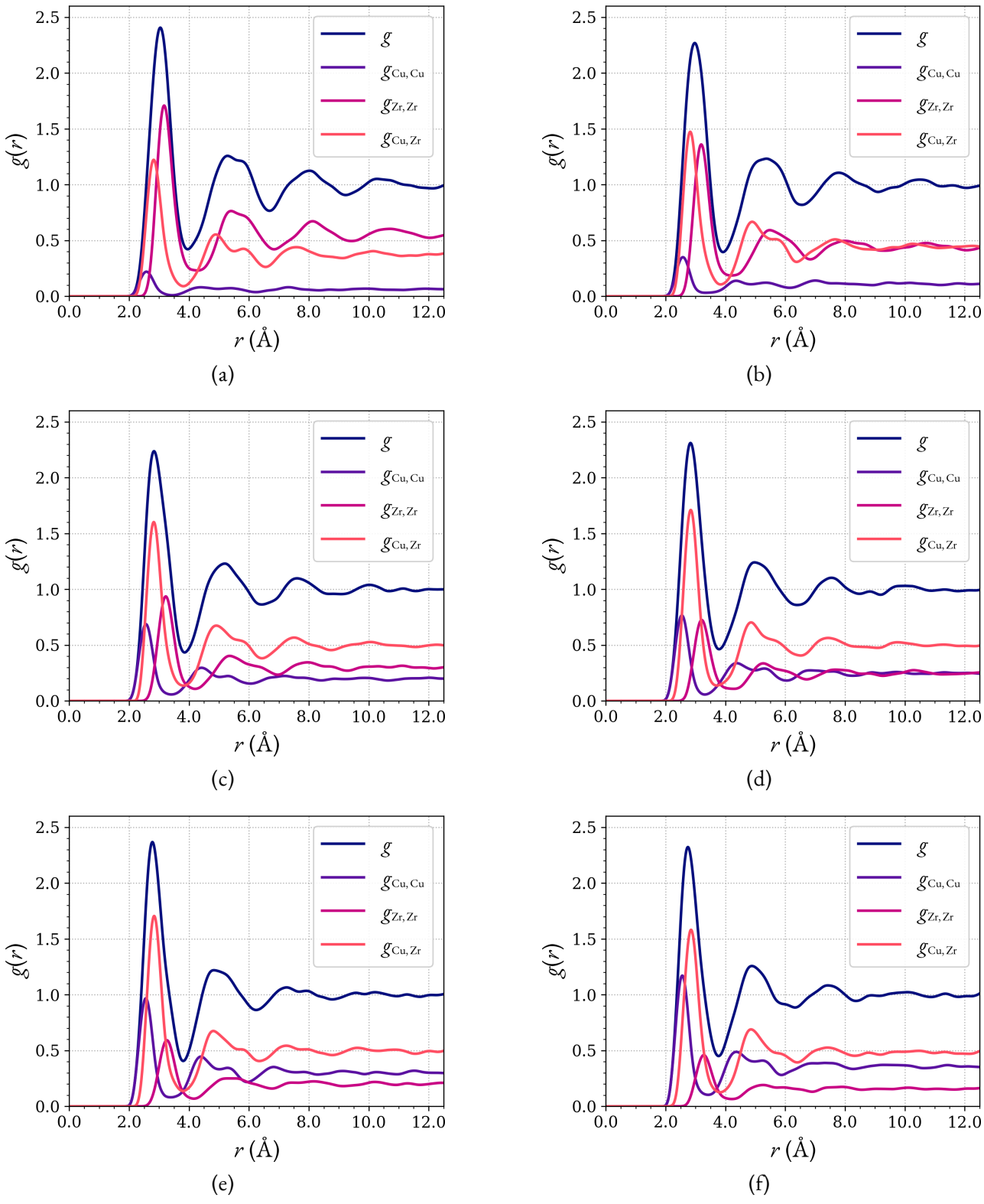

Figure 6.4: Partial and total PDFs of the Cu_xZr_{1-x} cells displayed in Fig. 6.3. (a) $x = 0.25$, (b) $x = 0.33$, (c) $x = 0.45$, (d) $x = 0.5$, (e) $x = 0.55$, and (f) $x = 0.6$.

6.2 Electronic Properties

After having determined the equilibrium amorphous structure of every alloy of interest in Section 6.1, we obtained the electronic density of states (eDoS) for each of the cells shown. The partial (for each band) and total eDoS calculated for the cells in Fig. 6.3 are displayed in Fig.

We see in Fig. 6.5 that the most prominent contribution is the d band, with its first peak around −3 eV becoming wider and higher as the concentration of Cu increases. On the other hand, the plateau on this same band around ε_F becomes shorter as x increases. This tells us that the main contributor to the first peak is Cu, and that the effect of adding Zr is to increase the eDoS at the Fermi level. This last point is of utmost importance to us, because the superconducting T_c depends strongly on $N_0 = N(\varepsilon_F)$, as we saw in Section 2.2. The values of N_0 are shown in Tab. 6.2.

Table 6.2: Densities of states at the Fermi level N_0, obtained from the eDoS in Fig. 6.5. We see a systematic decrease in N_0 as the copper content increases.

	$Cu_{0.25}Zr_{0.75}$	$Cu_{0.33}Zr_{0.67}$	$Cu_{0.45}Zr_{0.55}$	$Cu_{0.5}Zr_{0.5}$	$Cu_{0.55}Zr_{0.45}$	$Cu_{0.6}Zr_{0.4}$
$N_0\ \left(\frac{\text{st}}{\text{eV}\cdot\text{at}}\right)$	1.131	1.065	0.953	0.922	0.887	0.853

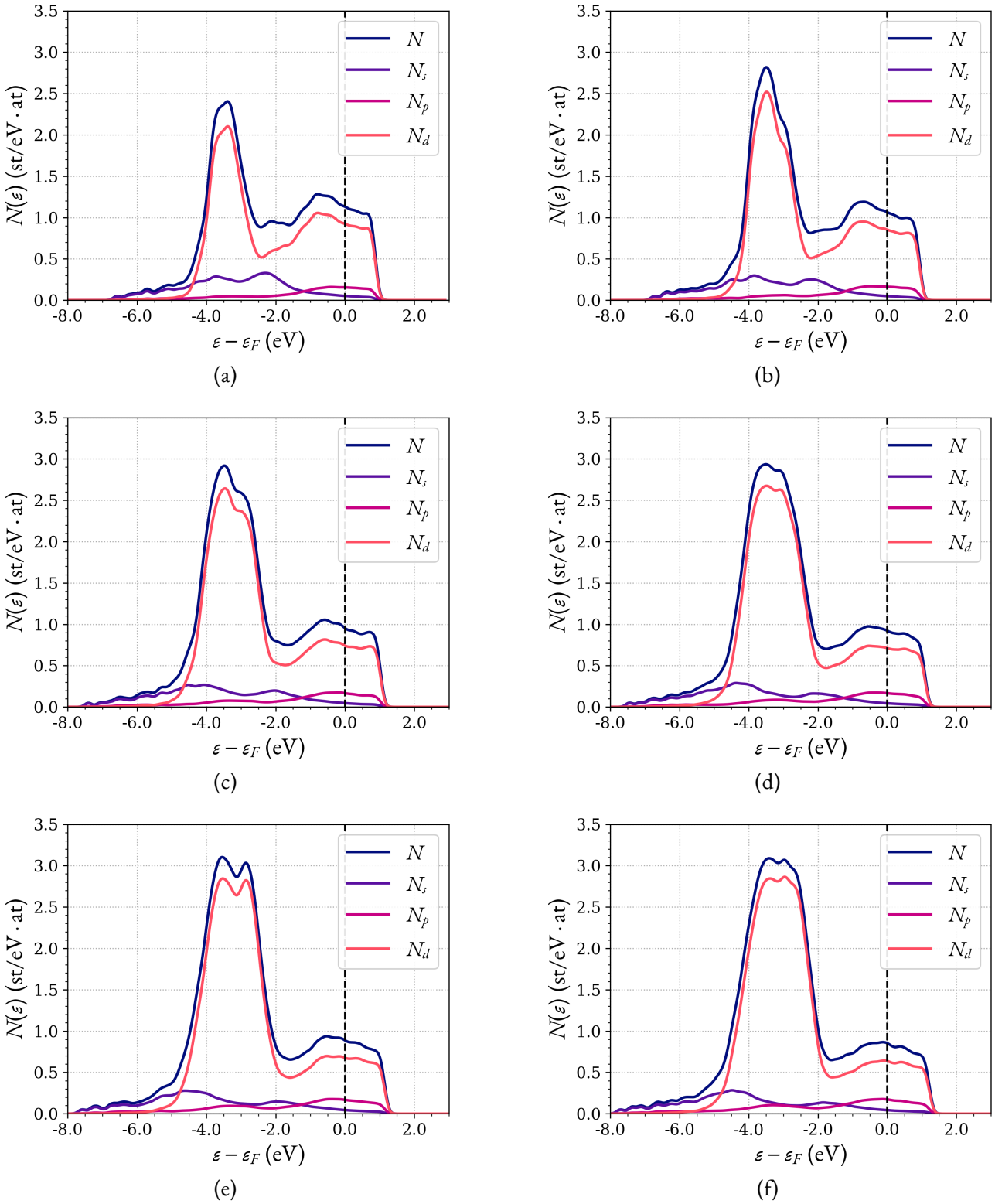

Figure 6.5: Partial and total eDoS of our amorphous Cu_xZr_{1-x} cells. (a) $x = 0.25$, (b) $x = 0.33$, (c) $x = 0.45$, (d) $x = 0.5$, (e) $x = 0.55$, and (f) $x = 0.6$. The dotted vertical line represents the Fermi level ε_F.

6.3 Vibrational Properties

We have computed the vibrational densities of state (vDoS) for three concentrations of our alloys, namely, for $x = 0.25$, 0.33, and 0.5. Due to computational constraints, it was not possible to calculate the vDoS of the other three alloys. These spectra are shown in Fig. 6.6.

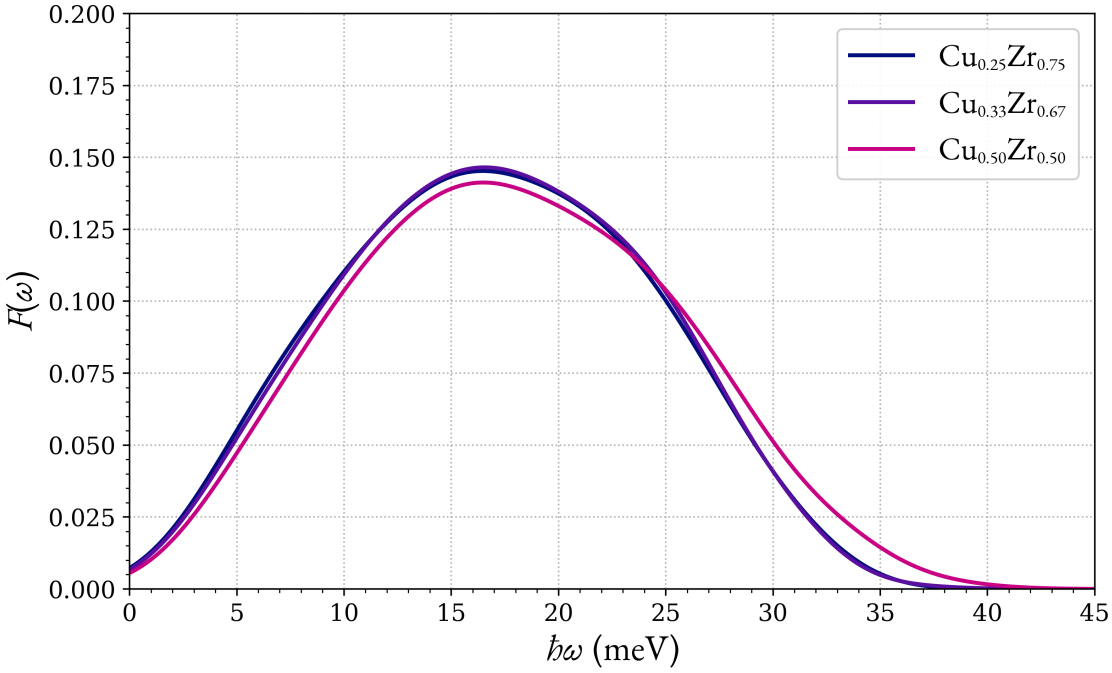

Figure 6.6: Vibrational densities of state of the amorphous Cu_xZr_{1-x} alloys corresponding to $x = 0.25$, 0.33, and 0.5.

With the data in Fig. 6.6 we have computed the Debye frequencies ω_D of the three alloys using Grimvall's [35] expression, eq. (5.42) presented in Section 5.5. The resulting values of ω_D and the corresponding Debye temperatures Θ_D are displayed in Tab. 6.3.

Table 6.3: Debye frequencies and temperatures of our amorphous alloys, obtained from the vDoS in Fig. 6.6.

	$Cu_{0.25}Zr_{0.75}$	$Cu_{0.33}Zr_{0.67}$	$Cu_{0.5}Zr_{0.5}$
$\hbar\omega_D$ (meV)	20.98	21.19	22.14
Θ_D (K)	243.5	245.9	256.9

An important note regarding the plots and data in Fig. 6.6 and Tab. 6.3 is that they were obtained using a Gaussian Kernel Smoothing method. The bandwidth was chosen using the Sheather–Jones criterion (see, *e.g.*, Section 10.2 of [31]). The Debye frequencies $\hbar\omega$ as functions of the Gaussian bandwidth b used for the smoothing are displayed Fig. 6.7

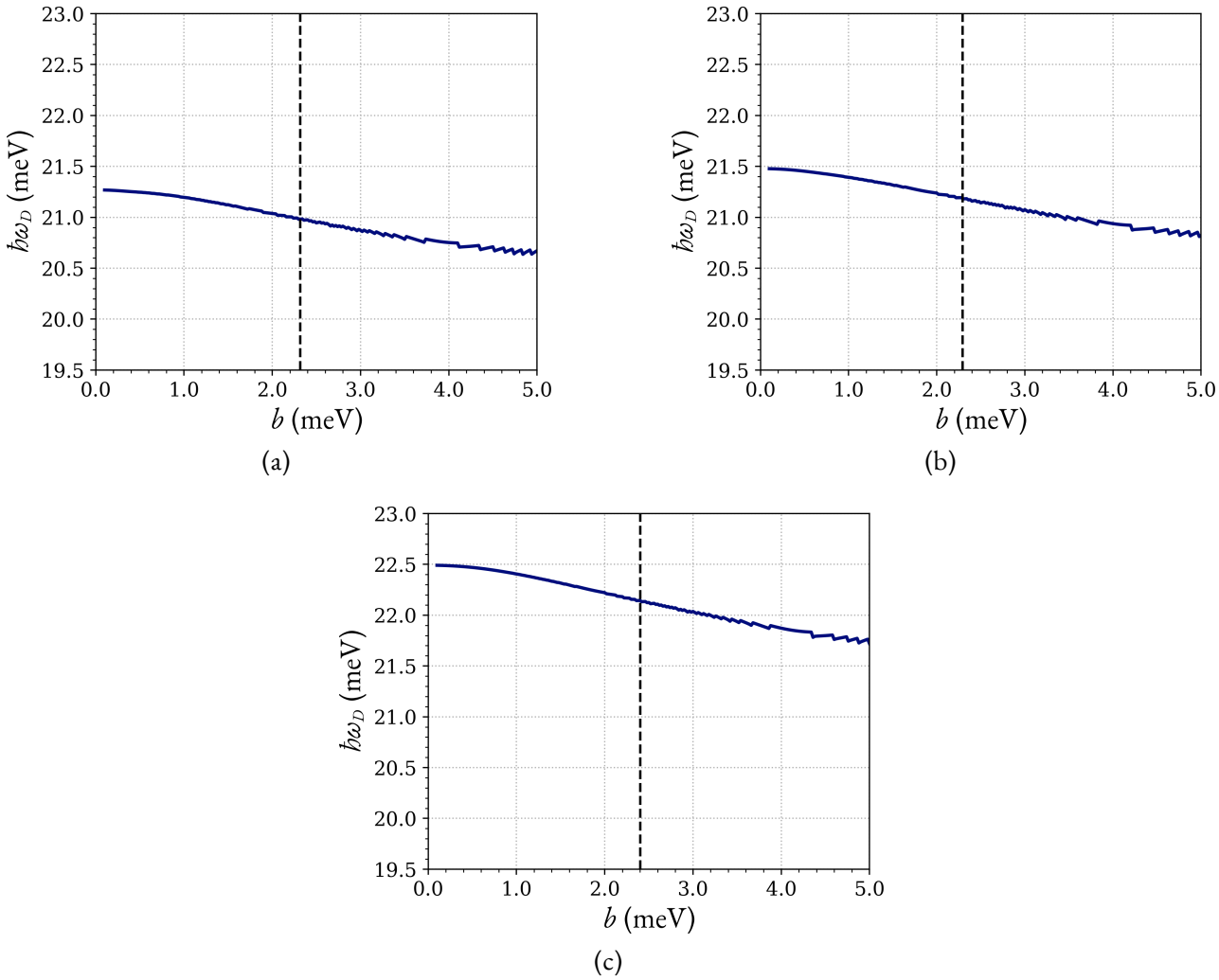

Figure 6.7: The variation of the Debye frequencies $\hbar\omega$ with the change in smoothing bandwidth b for a Gaussian kernel $K(z;b) = (2\pi b^2)^{-1/2} e^{-z^2/2b^2}$. The final bandwidth was chosen to satisfy the Sheather–Jones criterion (see eq. (10.28) of [31]), and is indicated with the dotted vertical line. (a) $x = 0.25$ with $b_{\mathrm{SJ}} = 2.318$ meV, (b) $x = 0.33$ with $b_{\mathrm{SJ}} = 2.293$ meV, (c) $x = 0.5$ with $b_{\mathrm{SJ}} = 2.403$ meV.

Note that the domain of $(0, 5]$ meV for b was chosen arbitrarily. Within this domain, the variation of $\hbar\omega_D$ with the smoothing is less than 3.5% of the final value for all three sets of data.

6.4 Estimation of T_c

With the data presented in Sections 6.2 and 6.3 we can apply the Mata-Valladares approach to the T_c calculation, particularly eq. (5.45). Recall that in Section 5.6, we considered two similar but distinct materials where one of the values of T_c is known, whereas the other one is not. We found that, assuming that the Cooper pairing potential V is equal in both samples, we can estimate the critical temperature of a sample $T_c^{(u)}$ ("u" for *unknown*) using the known value $T_c^{(k)}$ ("k" for *known*) of the other. Our T_c calculations are summarised in Fig. 6.8, where we use the notation $x^{(k)}$ to denote the Cu concentration of the "k" alloy. We only report two values of $T_c^{(u)}$ for each $x^{(k)}$ because when both samples are the same, eq. (5.45) reduces trivially to $T_c^{(u)} = T_c^{(k)}$ since in that case $\eta = \delta = 1$.

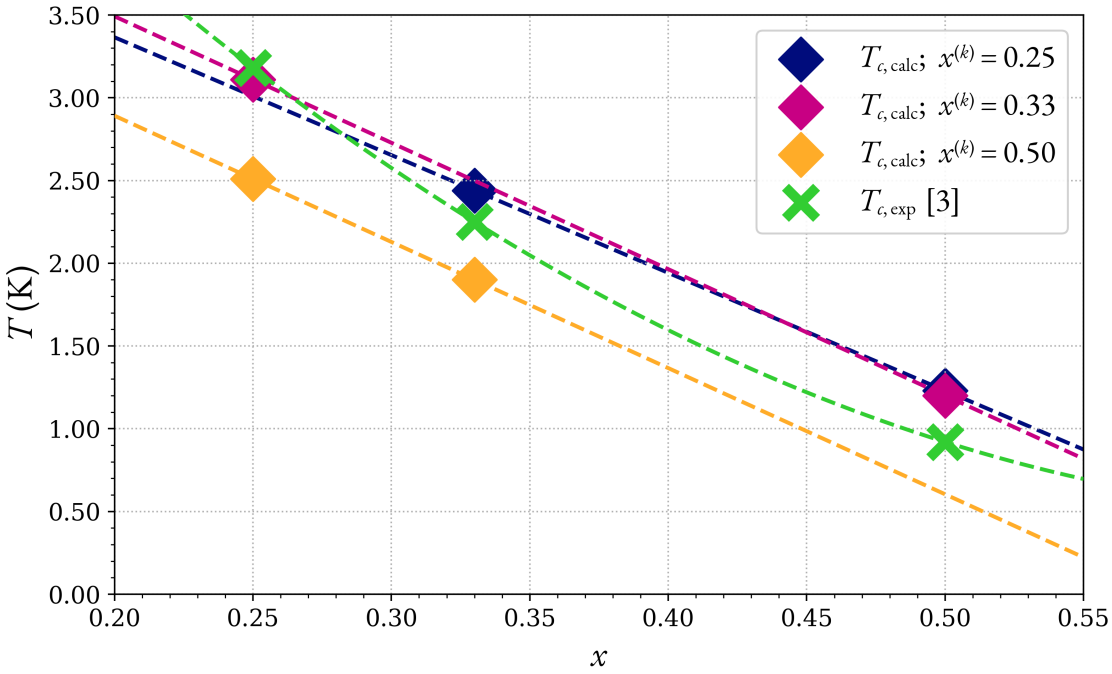

Figure 6.8: T_c calculations obtained from the Mata-Valladares approach. The experimental values of T_c, employed as $T_c^{(k)}$ in eq. (5.45), were obtained by Altounian and Strom-Olsen [3] and are indicated in green. We have included a line of best fit for each set of estimated or experimental T_c.

Additionally, we can solve for the Cooper pairing potential in the BCS equation for T_c in each of the concentrations, namely $V = [N_0 \ln(1.13\Theta_D/T_c)]^{-1}$, the results of which are summarised in Tab. 6.4

Table 6.4: Cooper pairing potentials for the amorphous alloys. Computed from the data in Tabs. 6.2, 6.3, and the experimental results in [3].

	$Cu_{0.25}Zr_{0.75}$	$Cu_{0.33}Zr_{0.67}$	$Cu_{0.5}Zr_{0.5}$
$V\left(\frac{\mathrm{eV\cdot at}}{\mathrm{st}}\right)$	0.198	0.197	0.188

6.5 The Crystalline $CuZr_2$ Intermetallic Compound

In addition to the amorphous alloys mentioned in the preceding section, we also analysed the $CuZr_2$ crystal, which is the only stable crystalline phase occurring in the range of concentrations ($x \in [0.25, 0.6]$) considered in this work, as is clearly seen in Fig. 6.1.

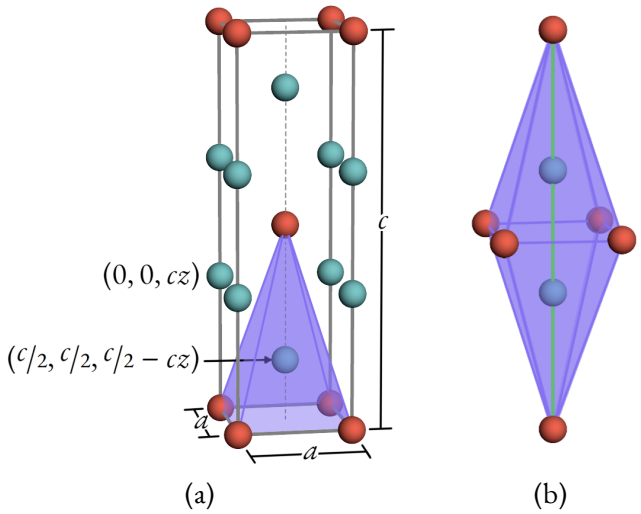

Figure 6.9: C11b crystalline structure of the $CuZr_2$ intermetallic compound. According to the results of Chebotnikov and Molokanov [13], $a = 3.218$ Å, $c = 11.18$ Å, and $z = 0.3468$. In (a) the standard tetragonal cell is displayed with its structural parameters indicated and in (b) we show the octahedral unit cell.

The $CuZr_2$ crystal has a tetragonal C11b (Si_2Mo-type) structure, described by M. V. Nevitt and J. W. Downey [63]. More recent structural parameters are provided by V. N. Chebotnikov and V. V. Molokanov [13]. The corresponding structure, including the numerical values of the parameters, is shown in Fig. 6.9.

All of the atoms in the structure in Fig. 6.9 lie on parallel vertical lines (*viz.*, in the [001] direction) that pass through the vertical edges and the centerline. In this type of structure, the cell is symmetric under reflections about the plane that bisects the vertical axis perpendicularly (*viz.*, the (002) plane). However, the position of the Zr atoms along the vertical axes is not uniquely determined, instead depending on the parameter z which differs between compounds (see [63]). Note that the Cu atoms make a body centered tetragonal cell, where the central site is equivalent to any of the corners. The four atoms at the base together with the central one form a square pyramid whose base edges are of length a and with height $c/2$. A Zr atom is located inside the pyramid along the vertical axis at a distance zc from the apex. More generally, every Zr atom is located inside a pyramid of identical proportions that is formed from four Cu atoms in one of the horizontal planes together with a single Cu in an adjacent plane. In Fig. 6.9 (b) we show how one of these pyramids may be joined with its mirror image with respect to the (001) plane to form an octahedron that has Cu atoms as vertices and two Zr atoms along its major diagonal (*i.e.*, the green line in Fig. 6.9 (b)).

Starting from the structure described above, we generated a 216-atom supercell (4×3×3 of the one depicted in Fig. 6.9 (a)), which was later passed through an undermelt-quench procedure before calculating its eDoS and vDoS. The reasons for this specific procedure are twofold: to yield results that are as comparable to

the amorphous sample as possible, and to eliminate the presence of negative phonon energies from the spectrum[2]. The PDFs before and after the undermelt-quench process are shown in Fig. 6.10

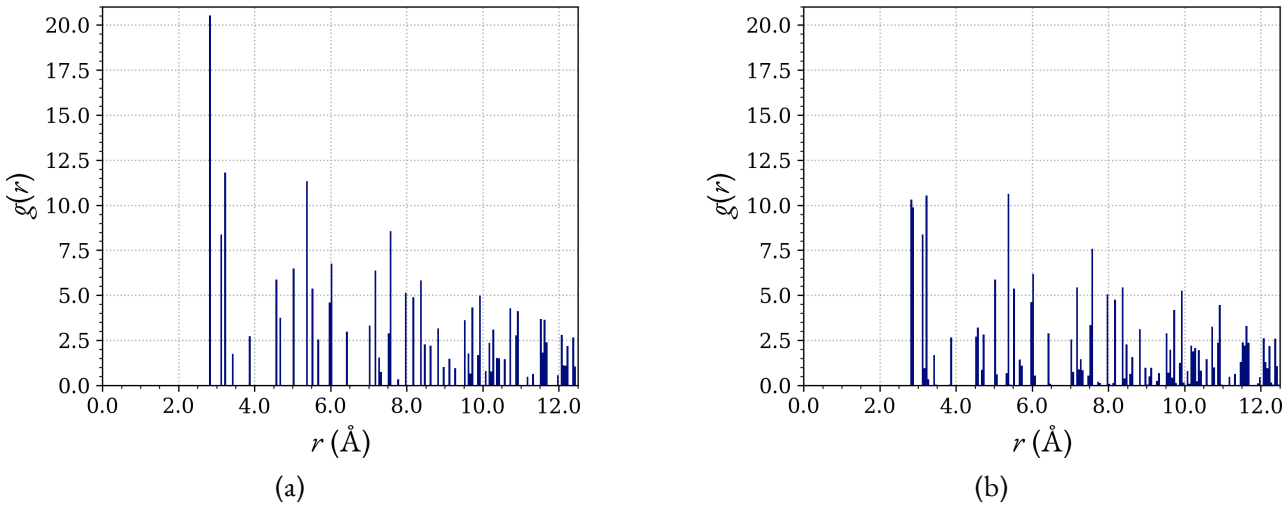

Figure 6.10: Pair distribution functions $g(r)$ of the of the $CuZr_2$ crystalline intermetallic compound. (a) The original structure reported by Chebotnikov and Molokanov [13], (b) The structure obtained with the undermelt-quench method. Note the vertical scale here, which differs from the one in Section 6.1 by a factor of ~ 8.

A clearer picture of the distinction between the structures is seen by taking the difference between their PDFs, as shown in Fig. 6.11.

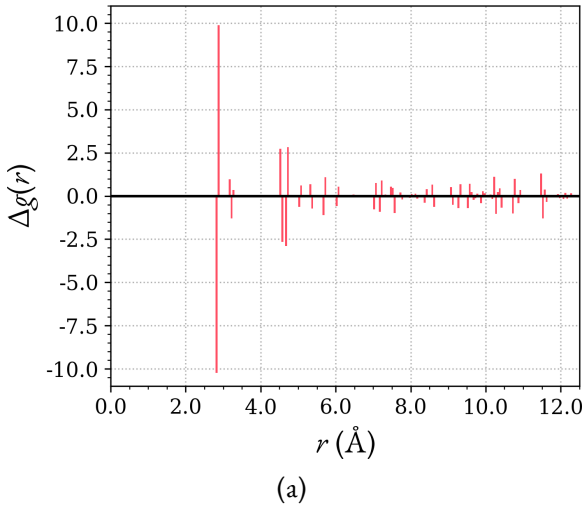

Figure 6.11: Change in the crystalline $g(r)$ produced by the undermelt-quench procedure.

In Fig. 6.11 we see spikes in $\Delta g(r)$ that appear to mostly come in pairs of opposite sign (*i.e.*, a positive spike followed by one of equal magnitude but negative, or *vice versa*), this suggests that the most important differ-

[2]The author wishes to thank his colleagues David Hinojosa-Romero and Gerardo A. Martínez for suggesting this procedure.

ence between the PDF before and after the undermelt-quench procedure is the splitting of some peaks into pairs of adjacent peaks. The existence of these differences may be partly attributed to the fact that Density-Functional approximations do not reproduce the experimental structures exactly, particularly PBEsol for transition metals has been observed to produce a mean absolute relative error of 0.9% in its predictions of crystal lattice constant, according to Zhang *et al.* [96].

Afterwards, we calculated the eDoS and vDoS for the resulting structure, as well as the variation of $\hbar\omega_D$ as a function of the smoothing. These are shown in Fig. 6.12.

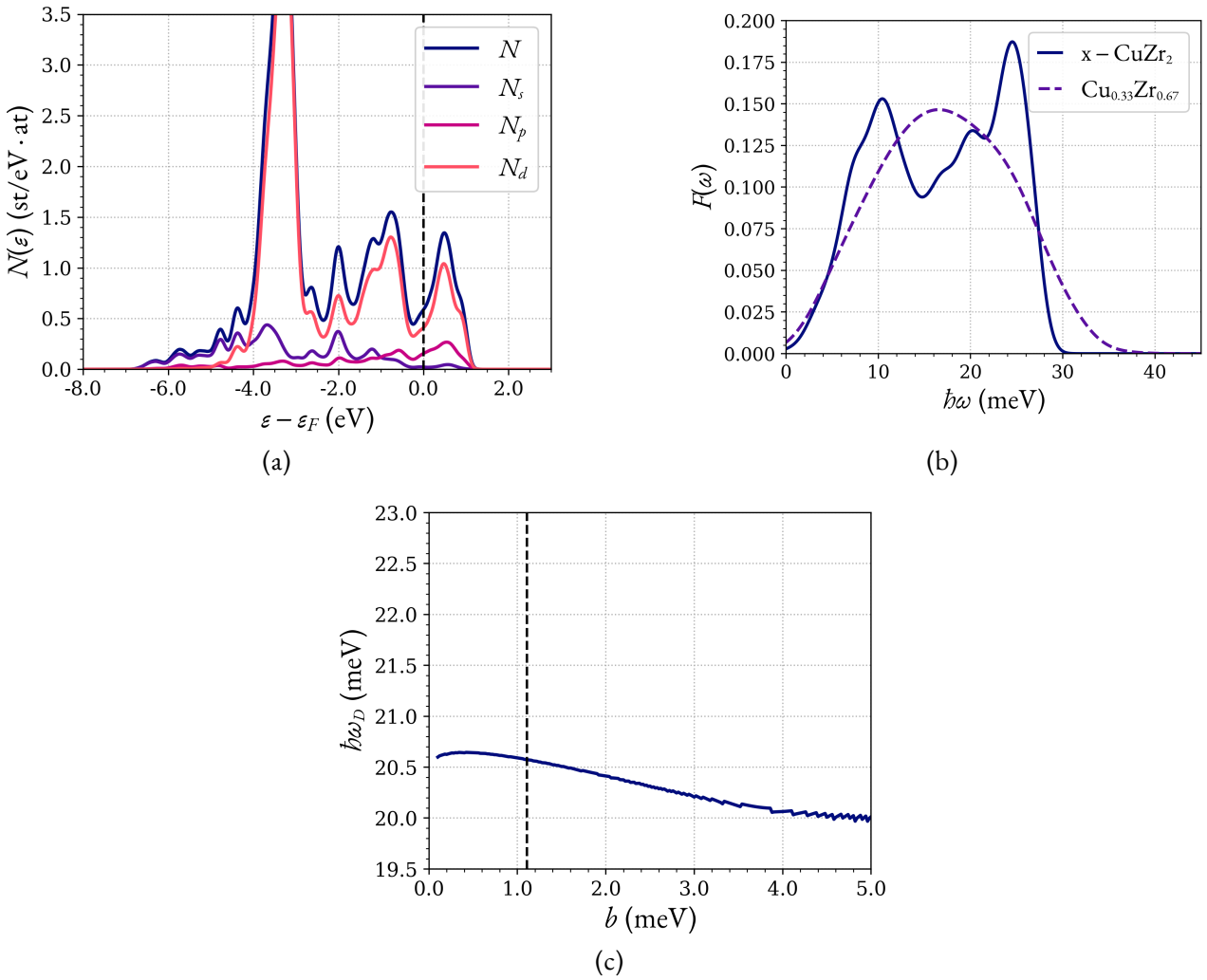

Figure 6.12: Electronic and vibrational spectra of the $CuZr_2$ crystalline intermetallic compound. (a) Partial and total eDoS with the Fermi level indicated by the dotted line, (b) the vDoS of the crystal (solid line) compared with the one of the amorphous sample (dotted line) obtained in Section 6.3, and (c) the variation of $\hbar\omega_D$ as a function of the smoothing bandwidth. The optimal bandwidth according the Sheather-Jones criterion is 1.107 meV and its indicated by the dotted line.

From the spectra in Fig. 6.12, we obtained a density at the Fermi level of $N_0 = 0.587$ st/eV · at, as well as a Debye frequency of $\hbar\omega_D = 20.55$ meV which corresponds to a Debye temperature $\Theta_D = 238.5$ K. Combining these values with the ones of the corresponding amorphous phase (*i.e.*, $x = 0.33$) into eq. (5.45), we predict a critical temperature for the crystalline phase given by:

$$T_c^{x\text{-CuZr}_2} \approx 0.0479 \text{ K} = 47.9 \text{ mK} \tag{6.2}$$

This value may be regarded, as was done in the work by Mata *et al.*, as an upper bound for the experimental value of T_c in the crystalline phase.

6.6 Comparison with Experimental Densities of State

In this section we present a comparison of our computational results of electronic and vibrational spectra with the corresponding data available in the literature.

We compare our eDoS with the experimental results obtained by Oelhafen, Hauser, and Güntherodt [64] through ultraviolet–photoemission spectroscopy (UPS), as well as the more recent result by Y. Takahara and N. Narita [87]. These comparisons are shown in Fig. 6.13, which we have split to make the comparison between the similar compositions easier and to avoid clutter.

In Fig. 6.13 we observe a relatively good match between our results and the experimental data, particularly two trends are clearly mirrored: firstly, the peak around −3 eV, which is associated with the d-shell of Cu broadens as x increases, whereas the plateau around the Fermi level which is associated with the d-shell of Zr decreases instead. Note that the experimental spectra drop off quickly above ε_F, this can be easily explained by the fact that the photoemission process underlying the UPS and XPS methods rely on the photoelectric effect, which requires the presence of electrons on the relevant states to be measured. An elementary computation shows that at room temperature $k_B T \sim 0.026$ eV, and therefore states with energies higher than ~ 0.1 eV remain unoccupied, and unmeasurable by either UPS or XPS. On the other hand, we observe that before the aforementioned drop-off, the eDoS close to the Fermi level in the experimental data is higher than our calculated value for comparable compositions. The explanation for this phenomenon is described by Bardeen in [7], where he notes that the electron-phonon interaction renormalises N_0 by a factor of $1 + \lambda$, where λ is a dimensionless coupling constant that measures the strength of this interaction. Our eDoS calculations were performed with static nuclei, and are therefore unable to account for this renormalisation of vibrational origin.

For the vDoS, there are unfortunately few experimental results available for comparison, they are close only to our $x = 0.5$ alloy. In Fig. 6.14, we compare our results with the inelastic neutron scattering data obtained

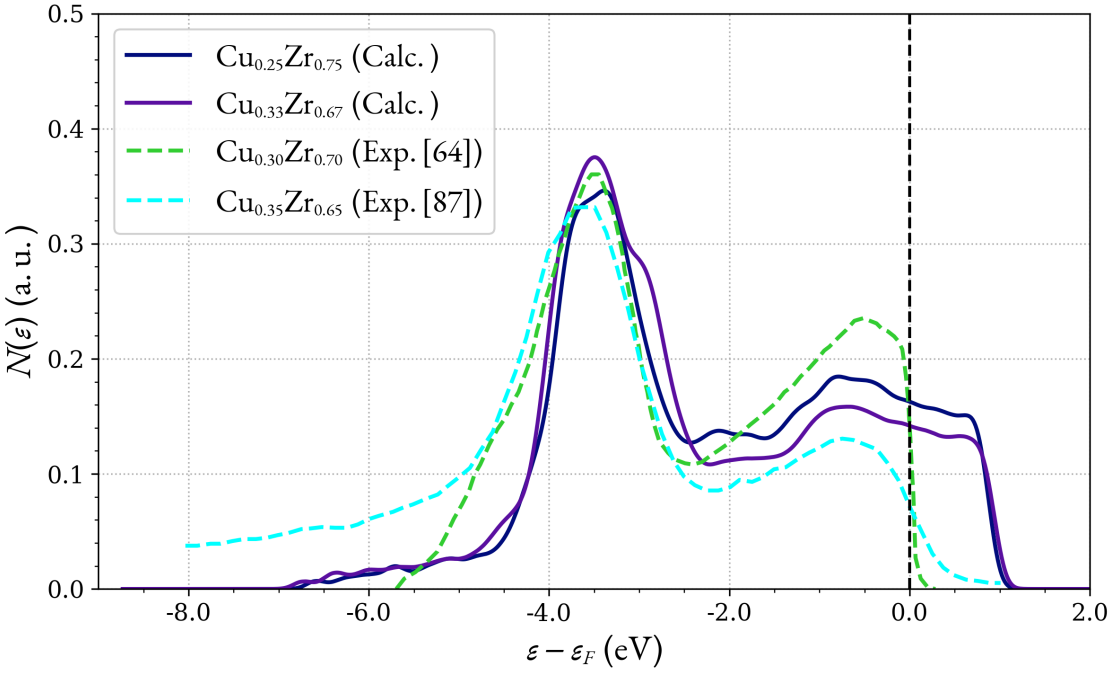

(a)

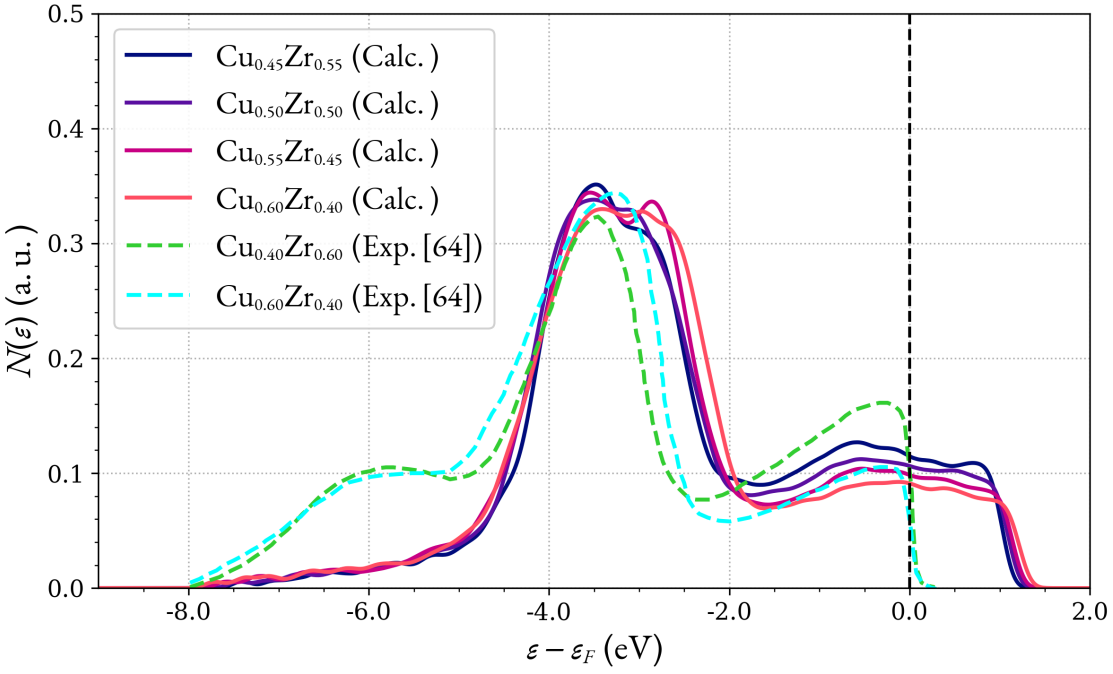

(b)

Figure 6.13: Comparisons between our calculations and experimental data [64, 87] for the eDoS of the Cu_xZr_{1-x} in the ranges: (a) $0.25 \leq x \leq 0.39$, and (b) $0.40 \leq x \leq 0.60$. All the spectra have been normalised to 1 for ease of comparison.

by Suck *et al.* [85], and the angular range chopper neutron spectrometer (ARCS) results of Smith *et al.* [83].

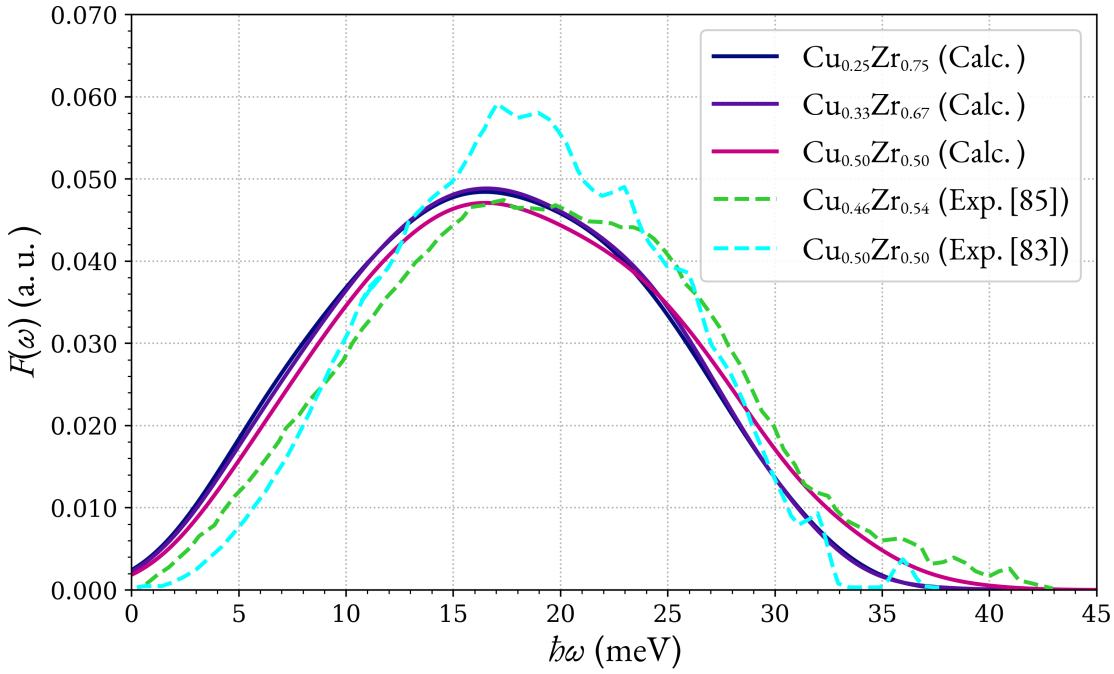

Figure 6.14: Comparisons between our calculations and experimental data [83, 85] for the vDoS. Note that the results of Smith *et al.* [83] (cyan dotted line) are not directly comparable to ours because they were obtained at a higher temperature (571 K), but they provide an interesting comparison. All the spectra have been normalised to 1 for ease of comparison.

We observe in Fig. 6.14 that our results compare reasonably well with those of Suck *et al.* [85], whereas the vDoS obtained by Smith *et al.* [83] is the one that differs the most from all the others. This might be because the latter experiment was performed at higher temperatures (between 571 and 700 K) to observe the variation of the vibrational spectrum through the cristallisation transition at 692 K. Here we have digitised only the lowest temperature result of Smith *et al.* [83] at 571 K, but it is reasonable to assume that the structure at that temperature will differ from the (metastable) equilibrium structure that we sought to obtain here.

6.7 Conclusions

We observe a systematic trend wherein the alloys with a higher critical temperature overestimate the corresponding value in alloys with a lower T_c, and conversely, the alloys with a lower T_c underestimate their higher counterparts. This points towards the fact that our approximation of constant Cooper pairing potential V

is not satisfied exactly, but it is instead a function of the concentration x and the material's structure. This is expected since we are dealing with a broad range of the Cu-Zr phase diagram, and it is seen in our results in Tab. 6.4, where V is seen to increase with the concentration. However, in this entire range, V varies only about 5.3%, which is remarkable given all of the complexities involved in the determination of the exact value of this coupling. Unfortunately, this error is amplified considerably in the estimation of T_c due to the high sensitivity of this quantity to variations in V in the weak coupling range ($N_0V < 1$) [8], which is where our samples reside.

Our estimation of T_c for the crystalline phase is in line with the experimental results of P. Garoche and J. J. Veyssie [30] who explored the superconductivity in both the amorphous and crystalline $CuZr_2$ down to 0.3 K, finding $T_c = 2.27$ K for the former, but not observing any transition in the latter. We suggest, based on our results, that future studies will indeed find superconductivity in the crystalline $CuZr_2$ compound if lower temperatures are achieved, with the value of 47.9 mK as an upper bound.

Our results seem to support the idea put forward by Mata *et al.* [59] that the density of states at the Fermi level is the most important factor in the determination of T_c, although the assumption of constant V has clear limitations. Nonetheless, we find that even between very distinct alloys, with $x = 0.25$ and 0.5, which are separated by a whole quarter of the phase diagram, the results are still predictive of the correct order of magnitude of the transition temperature. As Bardeen indicates [7], the fundamental reason for the pairing in superconductors is not actually the Bose-Einstein statistics of the pairs, but rather that pairing is the most efficient way for the electrons to use the accesible states in the vicinity of the Fermi surface to form a coherent low energy ground state. The number of accessible states is directly increased by raising the eDoS at the Fermi level, increasing in turn the ability of the electrons to pair up, increasing the stability of the superconducting phase at higher temeratures. This trend is observed systematically in our results.

In essence, our results in Section 6.4 have tested the limits of the assumption in the Mata-Valladares approach [59] of constant Cooper pairing potential V. Alternatively, this may be seen as a study of the variation of V as the composition and structure of the material is modified. Future research on this avenue might be to obtain systematic results for a more extensive section of the Cu_xZr_{1-x} phase diagram and generalisation to other alloys. A different direction for future work that has been contemplated is amorphous hydrogenated Cu-Zr alloys, the starting point of which could be the Python script presented in Section A.3.

A Appendix: Code

In this Appendix, we include the Python scripts used for plotting and smoothing the graphs presented in this document, as well as a simple program that randomly introduces interstitial atoms to any structure in a `.car` format, which we could use if we decide to extend our work to hydrogenated Cu-Zr alloys.

A custom Python script was made for every figure presented, making them redundant. Therefore, we do not include all of them but only the one used for plotting the DSPPs in Section 5.1.3, and the one for the vDoS and variation of $\hbar\omega$ with the smoothing in Section 6.3. All the other graphing programs are simpler than these two, and may be constructed by adapting blocks of code from them.

A.1 Code for plotting the DSPP

```
import numpy as np
import matplotlib.pyplot as plt

from matplotlib.ticker import FormatStrFormatter

Ha2eV = 27.2114e-3  # How many *keV* in 1 Ha
au2Ang = 0.529177249  # How many Angstroms per a. u. (i.e. Bohr radii)

lw = 2 # Linewidth
font = "EB Garamond"

line_colors = ["#000c7c", "#5a0fa0", "#c80083", "#ff4d62", "#ffac28",
    "#fff123"]
rc = {"font.family" : "serif",
      "mathtext.fontset" : "custom"}
plt.rcParams.update(rc)
plt.rcParams["font.sans-serif"] = [font] + plt.rcParams["font.serif"]
```

```
def nCk(n, k):
    return np.math.factorial(n)/(np.math.factorial(k)*np.math.factorial(n-k))

def LegPoly(x, l):
    return 2**(-l)*np.sum([nCk(l, k)**2*(x-1)**(l-k)*(x+1)**k
        for k in range(l+1)], axis=0)

def DSPP(x, r_c, a_i, z):
    return np.where(x < r_c, np.sum([a_i[i]*LegPoly(x/r_c, 2*i)
        for i in range(9)], axis=0), corePot(x, z))

def mth_deriv(f, x, m, *args):
    dx = 1e-4
    if m == 1:
        return (f(x+dx, *args)-f(x-dx, *args))/(2*dx)
    if m == 0:
        return f(x, *args)
    if m < 0:
        print("Error: There can't be negative derivatives")
        return None
    return (mth_deriv(f, x+dx, m-1, *args)
        -mth_deriv(f, x-dx, m-1, *args))/(2*dx)

def corePot(x, z):
    return -z/np.abs(x)

elem = 'Zr'
filen = f'{elem}-params.txt'
''' File formed from a snippet of the dspp_s_01d21 file, for example:

_  29 19  3  5   0.586  Cu   4.05E-04   0.00E+00   4.05E-04  0 0 0  0 1 1 0
    0.582287  -73.665516   59.608637  -21.283123    0.830049    3.558364
    0.585582   -3.579659  -59.476665   40.038219  -10.333632    1.522534
    0.511054  -12.683232  -46.813416   23.492868    0.542987   -0.635989
    0.573714  -70.395706   55.100762  -21.171123    1.076816    4.037596
  5   0.2820   -4.868563    8.639610    6.279978   -7.035533    2.511330
'''
```

```
header = np.genfromtxt(filen, max_rows=1, encoding=None)
z = header[2]

DSPP_params = np.genfromtxt(filen, skip_header=1, max_rows=4, encoding=None)

R_c = 0
for i in range(4):
    r_c_l = DSPP_params[i][0]
    R_c = max(R_c, r_c_l)

fig, ax = plt.subplots(figsize=(4.5, 5))

x = np.linspace(0, 0.9/au2Ang, 400)

V_loc = corePot(x, z)*Ha2eV
ax.plot(x*au2Ang, V_loc, linestyle='--', label=
    '$-\\dfrac{z_{\\mathrm{ion}}}{r}$', color=line_colors[0], linewidth=lw)

num = [3, 0, 1, 2] # Rearranging because the DSPP file starts with l=3, (the
# "local" part) then 0, 1, and 2.

for l in [1, 2, 3, 0]:
    r_c_l, a_i_l = DSPP_params[l][0], DSPP_params[l][1:]
    R_c = max(R_c, r_c_l)

    Mat = np.array([[mth_deriv(LegPoly, 1, m, 2*i)*(1/r_c_l)**m
        for i in range(5, 9)] for m in range(4)])
    vec = np.array([mth_deriv(corePot, r_c_l, m, z)-np.sum([a_i_l[i]
        *mth_deriv(LegPoly, 1, m, 2*i)*(1/r_c_l)**m for i in range(5)])
        for m in range(4)])
    a_i_l_ext = np.linalg.solve(Mat, vec)
    a_i_l = np.concatenate((a_i_l, a_i_l_ext))
    DSPP(x, r_c_l, a_i_l, z)*Ha2eV

    ax.plot(x*au2Ang, V_l, label=r'$v_{:d}$'.format(num[l]), color
        =line_colors[num[l]+1], linewidth=lw)
```

```
ax.vlines(R_c*au2Ang, ymin=-3.2, ymax=1.3, linestyle='--', color='k',
    linewidth=lw)

ax.set_ylim(ymin=-3.2, ymax=1.3)
ax.set_xlim(xmin=0, xmax=0.9)
plt.legend(loc="upper right", fontsize=16, framealpha=0.9)
plt.xlabel("$r~(\\mathrm{Å})$", fontsize=18)
plt.ylabel("$v~(\\mathrm{keV})$", fontsize=18)
ax.tick_params(axis='both', which='major', labelsize=12)
plt.text(R_c*au2Ang*0.98, -3, "$R_{\\mathrm{c}}$", fontsize=18, bbox=
    {"boxstyle": "Round, pad=0.05", "edgecolor": "w", "facecolor": "w"})
ax.set_xticks(np.arange(0, 0.9, 0.2))
ax.xaxis.set_major_formatter(FormatStrFormatter('%.2f'))
ax.yaxis.set_major_formatter(FormatStrFormatter('%.1f'))

# General plot setup
plt.grid(visible=True, which='major', linestyle=':')
ax.hlines(0, xmin=-1, xmax=2, linestyle='-', color='k', linewidth=0.75)
ax.minorticks_on()
plt.tight_layout()

plt.savefig(f"DSPP_{elem}.png", dpi=400)
```

A.2 Code for smoothing and plotting the vDoS

For the code in this section we used the Kernel Density Estimation technique (see section 10.2 of [31]). The method chosen for bandwidth selection was the Sheather–Jones (SJ) method because *"[it] generally performs extremely well. [...] Some [alternative plug-in] approaches give bandwidths that asymptotically converge more quickly to the optimal bandwidth than does the Sheather–Jones method [...]. However, none of these offer substantially easier practical implementation or broadly better performance than the Sheather–Jones approach."* [31]. In particular, we used the implementation of the SJ method from Steven Laan's `pythonABC` repository [49].

Our code is:

```
import numpy as np
import matplotlib.pyplot as plt

from matplotlib.ticker import FormatStrFormatter
import matplotlib._mathtext as mthtxt

from hselect import hsj  # SJ method from the pythonABC repository

font = "EB Garamond"

line_colors = ["#000c7c", "#5a0fa0", "#c80083", "#ff4d62", "#ffac28",
    "#fff123"]
rc = {"font.family" : "serif",
      "mathtext.fontset" : "custom"}
plt.rcParams.update(rc)
plt.rcParams["font.sans-serif"] = [font] + plt.rcParams["font.serif"]

mthtxt.SHRINK_FACTOR = 0.55
lw = 2 # Linewidth

def ker_g(z):  # Gaussian function kernel
    return np.exp(-z**2/2)/np.sqrt(2*np.pi)

def est(z, kernel, h, data): # Estimator
    return (1/(data.size*h))*sum(kernel((z-x_i)/h) for x_i in data)

def omega_D(X, kernel, h, data):
    vDoS = 3*est(X, kernel, h, data)

    ind = np.argwhere(X>0).flatten()  # Points x<0 are smoothing artefacts
    X, vDoS = X[ind], vDoS[ind]

    ln_F = np.nan_to_num(np.log(X)*vDoS)  # function replacing nan with zero
    denom = np.trapz(vDoS, X)  # Denominator of the faction
    numer = np.trapz(ln_F, X)  # Numerator of the fraction

    return np.exp(1/3+numer/denom)
```

```
fnames = ['Cu25Zr75-vDoS', 'Cu33Zr67-vDoS', 'Cu50Zr50-vDoS']

d_p = 1500  # Number of data points to graph
ker = ker_g
bandw = np.linspace(0.1, 5, 250)  # Array for bandwidths


b_set = [0, 0, 0]  # Set of optimal bandwidths
evals = []

for i in range(3):
    fname = fnames[i]
    dat = np.loadtxt(fname + '.txt')  # Loading data
    mx, mn = dat.max(), dat.min()

    Debye_freqs = np.zeros_like(bandw)

    for k in range(bandw.size) :  # Steps of 0.02
        b = bandw[k]

        x_c = 5*b # cutoff distance
        xx = np.linspace(mn-x_c, mx+x_c, d_p)

        Debye_freqs[k] = omega_D(xx, ker, b, dat)

    b_set[i] = hsj(dat)  # Optimal bandwidth according to SJ
    evals.append(Debye_freqs)

fig, ax = plt.subplots(figsize=(8.1, 5))
for i in range(3):
    fname = fnames[i]
    dat = np.loadtxt(fname + '.txt')
    mx, mn = dat.max(), dat.min()
    x_c = 5*b_set[i]  # cutoff distance for the Gaussian

    xx = np.linspace(mn-x_c, mx+x_c, d_p)
    vDoS = 3*est(xx, ker, b_set[i], dat)  # The estimated function
```

```
    Deb_freq = omega_D(xx, ker, b_set[i], dat)

    Cu_f = 0.25 if i == 0 else 0.33 if i == 1 else 0.5  # Cu fraction
    ax.plot(xx, vDoS, color=line_colors[i], label=
        '$\\mathrm{Cu}_{%.2f}\\mathrm{Zr}_{%.2f}$' % (Cu_f, 1-Cu_f),
        linewidth=lw)

ax.set_ylim(ymin=0, ymax=0.2)
ax.set_xlim(xmin=0, xmax=45)

plt.legend(loc="upper right", fontsize=16, framealpha=0.9)
plt.xlabel("$\\hbar\\omega~(\\mathrm{meV})$", fontsize=18)
plt.ylabel("$F(\\omega)$", fontsize=18)
ax.tick_params(axis='both', which='major', labelsize=12)
ax.xaxis.set_major_formatter(FormatStrFormatter('%d'))
ax.yaxis.set_major_formatter(FormatStrFormatter('%.3f'))

plt.grid(visible=True, which='major', linestyle=':')
ax.minorticks_on()
plt.tight_layout()

plt.savefig("vDoS.png", dpi=400)
plt.close()

for i in range(3):
    fig, ax = plt.subplots(figsize=(5, 4))

    plt.xlabel("$b~(\\mathrm{meV})$", fontsize=18)

    ax.set_ylabel("$\\hbar\\omega_D~(\\mathrm{meV})$", fontsize=18)
    ax.tick_params(axis='both', which='major', labelsize=12)
    ax.set_ylim(ymin=19.5, ymax=23)
    ax.xaxis.set_major_formatter(FormatStrFormatter('%.1f'))
    ax.yaxis.set_major_formatter(FormatStrFormatter('%.1f'))
    ax.minorticks_on()
```

```
        ax.plot(bandw, evals[i], color=line_colors[0], linewidth=lw)
        ax.axvline(b_set[i], linestyle='--', color='k')
        plt.grid(visible=True, which='major', linestyle=':')
        ax.set_xlim(xmin=0, xmax=5)

        plt.tight_layout()
        plt.savefig("Eval_{}.png".format(i+1), dpi=400)

        plt.close()
```

A.3 Random Interstitial Alloys

This script was created to assist other members of our group in the creation of amorphous alloys with interstitial hydrogenation, and has already been employed successfully to this end. As mentioned at the end of Chapter 6, a possible extension to the work in this document is amorphous hydrogenated Cu-Zr alloys. Those may be obtained by applying the code in this section to the unstable crystalline structure before the MD step of the undermelt-quench method.

```
import numpy as np

fname = 'Cu25Zr75' # The structure file's name, it should be in .CAR format.
dest_file = 'Alloyed.car'
N = 200 # Number of interstitial atoms to add
elem = 'H' # Element of the interstitial atoms
hard_core = True # If True there's no fitness function evaluation, the atom
# is immediately placed if its distance to others is beyond a threshold.
hc_thresh = 0.3  # Threshold distance for the "hard core" alloying mode

k_B = 8.617333262145e-5  # Boltzmann's constant (in eV/K)

ats = np.genfromtxt(fname=fname, skip_header=5, skip_footer=2, usecols=
    (1, 2, 3, 7), dtype=None, encoding=None)  # atoms
lat = np.genfromtxt(fname=fname, skip_header=4, max_rows=1, usecols=
    (1, 2, 3, 4, 5, 6))  # lattice
```

```
    ats = ats.tolist()  # Cast to list so we can append.

    for n in range(N):
        attempt = 1
        while True:
            nxt = True  # Generates trial positions while variable is False
            trial_pos = np.random.uniform(high=lat[0]), np.random.uniform(high=
            lat[1]), np.random.uniform(high=lat[2])
            if hard_core:
                for at in ats:
                    at_pos = np.mod(at[0], lat[0]), np.mod(at[1], lat[1]), \
                        np.mod(at[2], lat[2])
                    r = np.sqrt((trial_pos[0]-at_pos[0])**2+(trial_pos[1]-
                        at_pos[1])**2+(trial_pos[2]-at_pos[2])**2)
                    if r <= hc_thresh:
                        nxt = False
                        print(f"Failed to place interstitial atom {n} in attempt
{attempt}, retrying...")
                        attempt += 1
                        continue

            if nxt:
                interst = (trial_pos[0], trial_pos[1], trial_pos[2], elem)
                ats.append(interst)
                break

    with open(dest_file, 'w') as outfile, open(fname, 'r',
        encoding='utf-8') as infile:
        header = 1
        for line in infile:
            outfile.write(line)
            header += 1
            if header > 5:
                break

        count = 1
```

```
        for at in ats:
            tag = f'{at[3]}{count}'
            x = f'{at[0]:.9f}'
            y = f'{at[1]:.9f}'
            z = f'{at[2]:.9f}'
            el = f'{at[3]}'

            outfile.write(f'{tag:<5}{x:>15}{y:>15}{z:>15} XXXX 1'+
                f'      xx      {el:<2}  0.000\n')
            count += 1
        outfile.write('end\nend')
```

Bibliography

1. A. Altland and B. Simons. *Condensed Matter Field Theory*. 2nd ed. Cambridge University Press, Cambridge, UK, 2010.
2. Z. Altounian, T. Guo-hua, and J. O. Strom-Olsen. "Crystallization Characteristics of Cu-Zr Metallic Glasses from $Cu_{70}Zr_{30}$ to $Cu_{25}Zr_{75}$". *Journal of Applied Physics* 53:7, 1982, pp. 4755–4760. DOI: 10.1063/1.331304.
3. Z. Altounian and J. O. Strom-Olsen. "Superconductivity and Spin Fluctuations in M-Zr metallic glasses (M=Cu, Ni, Co,and Fe)". *Physical Review B* 27:7, 1983, pp. 4149–4156. DOI: 10.1103/physrevb.27.4149.
4. J. D. Anderson. "Governing Equations of Fluid Dynamics". In: *Computational Fluid Dynamics: An Introduction*. Ed. by J. F. Wendt. 3rd ed. Springer, Berlin, Germany, 2009, pp. 15–51.
5. N. W. Ashcroft and N. D. Mermin. *Solid State Physics*. Harcourt College Publishers, Fort Worth, USA, 1976.
6. P. W. Ayers and R. G. Parr. "Is it Impossible to Find the Universal Density Functional? Or is it Just Well-Hidden?" *Indian Journal of Chemistry* 53A:8–9, 2014, pp. 929–931. URL: http://nopr.niscpr.res.in/handle/123456789/29241.
7. J. Bardeen. "Electron-Phonon Interactions and Superconductivity". In: *Cooperative Phenomena*. Ed. by H. Haken and M. Wagner. Springer, Berlin, Germany, 1973, pp. 63–78. DOI: 10.1007/978-3-642-86003-4_6.
8. J. Bardeen, L. N. Cooper, and J. R. Schrieffer. "Theory of Superconductivity". *Physical Review* 108:5, 1957, pp. 1175–1204. DOI: 10.1103/PhysRev.108.1175.
9. C. A. Bertulani. *Nuclear Physics in a Nutshell*. Princeton University Press, Princeton, USA, 2007.
10. D. Bohm. "A Suggested Interpretation of the Quantum Theory in Terms of 'Hidden' Variables. I". *Physical Review* 85:2, 1952, pp. 166–179. DOI: 10.1103/physrev.85.166.
11. M. Born and K. Huang. *Dynamical Theory of Crystal Lattices*. Clarendon Press, Oxford, UK, 1954.
12. M. Born and J. R. Oppenheimer. "Zur Quantentheorie der Molekeln". *Annalen der Physik* 389:20, 1927, pp. 457–484. DOI: 10.1002/andp.19273892002.

13. V. N. Chebotnikov and V. V. Molokanov. "Structures and Properties of Amorphous and Crystalline Alloys in the Ti_2Cu-Zr_2Cu Section in the Ti-Zr-Cu System". *Izvestiya Akademii Nauk SSSR, Neorganicheskie Materialy* 26:5, 1990, pp. 960–964.

14. M. L. Cohen and V. Heine. "The Fitting of Pseudopotentials to Experimental Data and their Subsequent Application". In: *Solid State Physics: Advances in Research and Applications*. Ed. by H. Ehrenreich, F. Seitz, and D. Turnbull. Vol. 24. Academic Press, 1970, pp. 37–248.

15. L. N. Cooper. "Bound Electron Pairs in a Degenerate Fermi Gas". *Physical Review* 104:4, 1956, pp. 1189–1190. DOI: https://doi.org/10.1103/PhysRev.104.1189.

16. X.-Y. Cui, S. P. Ringer, G. Wang, and Z. H. Stachurski. "What Should the Density of Amorphous Solids be?" *The Journal of Chemical Physics* 151:19, 2019, p. 194506. DOI: 10.1063/1.5113733.

17. Dassault Systèmes Biovia Corp. *Biovia Discovery Studio Visualizer [Computer Software]*. Version 2021. San Diego, USA, 2020.

18. Dassault Systèmes Biovia Corp. *Biovia Materials Studio [Computer Software]*. Version 2016-1. San Diego, USA, 2015.

19. R. De Vogelaere. *Methods of Integration which Preserve the Contact Transformation Property of the Hamilton Equations*. Tech. rep. 4. Notre Dame, USA: Center of Numerical Analysis, University of Notre Dame, 1956, p. 16. URL: https://curate.nd.edu/show/6395w665s0q.

20. (a) B. Delley. "An All-Electron Numerical Method for Solving the Local Density Functional for Polyatomic Molecules". *The Journal of Chemical Physics* 92:1, 1990, pp. 508–517. DOI: 10.1063/1.458452; (b) B. Delley. "From Molecules to Solids with the $DMol^3$ Approach". *The Journal of Chemical Physics* 113:18, 2000, pp. 7756–7764. DOI: 10.1063/1.1316015.

21. B. Delley. "Hardness conserving semilocal pseudopotentials". *Physical Review B* 66:15, 2002, p. 155125. DOI: 10.1103/physrevb.66.155125.

22. D. Donnelly and E. Rogers. "Symplectic Integrators: An introduction". *American Journal of Physics* 73:10, 2005, pp. 938–945. DOI: 10.1119/1.2034523.

23. H. B. Dwight. *Tables of Integrals and Other Mathematical Data*. 3rd ed. Macmillan, New York, USA, 1957.

24. S. R. Elliott. *Physics of Amorphous Materials*. Longman, London, UK, 1984.

25. S. R. Elliott. "The Structure of Amorphous Materials". In: *Properties and Applications of Amorphous Materials*. Ed. by M. F. Thorpe and L. Tichý. Kluwer Academic Publishers, Dordrecht, Netherlands, 2001, pp. 1–11.

26. E. Engel and R. M. Dreizler. *Density Functional Theory: An Advanced Course*. Springer, Heidelberg , Germany, 2011.

27. R. Fletcher. *Practical Methods of Optimization*. 2nd ed. John Wiley & Sons, Chichester, UK, 1987.

28. H. Fröhlich. "Interaction of Electrons with Lattice Vibrations". *Proceedings of the Royal Society of London A* 215:1122, 1952, pp. 291–298. DOI: 10.1098/rspa.1952.0212.

29. H. Fröhlich. "Theory of the Superconducting State. I. The Ground State at the Absolute Zero of Temperature". *Physical Review* 79:5, 1950, pp. 845–856. DOI: 10.1103/physrev.79.845.

30. P. Garoche and J. J. Veyssie. "Superconductivity in Amorphous versus Crystalline $Cu_{0.33}Zr_{0.66}$ Alloys". *Journal de Physique Lettres* 42:15, 1981, pp. 365–368. DOI: 10.1051/jphyslet:019810042015036500.

31. G. H. Givens and J. A. Hoeting. *Computational Statistics*. 2nd ed. Wiley, 2013.

32. A. M. Glezer and N. A. Shurygina. *Amorphous-Nanocrystalline Alloys*. CRC Press, Boca Raton, USA, 2020.

33. S. Goedecker and G. E. Scuseria. "Linear Scaling Electronic Structure Methods in Chemistry and Physics". *Computing in Science & Engineering* 5:4, 2003, pp. 14–21. DOI: 10.1109/MCISE.2003.1208637.

34. H. Goldstein, J. L. Safko, and C. P. Poole. *Classical Mechanics*. 3rd ed. Pearson, Harlow, UK, 2013.

35. G. Grimvall. *Thermophysical Properties of Materials*. Elsevier, Amsterdam, Netherlands, 2008.

36. G. G. Hall. "The Molecular Orbital Theory of Chemical Valency VIII. A Method of Calculating Ionization Potentials". *Proceedings of the Royal Society of London A* 205:1083, 1951, pp. 541–552. DOI: 10.1098/rspa.1951.0048.

37. R. Heid. "Electron-Phonon Coupling". In: *The Physics of Correlated Insulators, Metals, and Superconductors: Lecture Notes of the Autumn School on Correlated Electrons 2017*. Ed. by E. Pavarini, E. Koch, R. Scalettar, and R. Martin. Forschungszentrum Jülich, Jülich, Germany, 2017, pp. 15.1–15.29.

38. V. Heine. "The Pseudopotential Concept". In: *Solid State Physics: Advances in Research and Applications*. Ed. by H. Ehrenreich, F. Seitz, and D. Turnbull. Vol. 24. Academic Press, 1970, pp. 1–36.

39. C. Herring. "A New Method for Calculating Wave Functions in Crystals". *Physical Review* 57:12, 1940, pp. 1169–1177. DOI: 10.1103/physrev.57.1169.

40. F. B. Hildebrand. *Introduction to Numerical Analysis*. 2nd ed. Dover Publications, New York, USA, 1987.

41. D. Hinojosa-Romero, I. Rodriguez, A. Valladares, R. M. Valladares, and A. A. Valladares. "Possible Superconductivity in Bismuth (111) Bilayers. Their Electronic and Vibrational Properties from First Principles". *MRS Advances* 3:6–7, 2018, pp. 313–319. DOI: 10.1557/adv.2018.119.

42. D. Hinojosa-Romero, I. Rodríguez, Z. Mata-Pinzón, A. Valladares, R. Valladares, and A. A. Valladares. "Compressed Crystalline Bismuth and Superconductivity — An *Ab Initio* Computational Simulation". *MRS Advances* 2:9, 2017, pp. 499–506. DOI: 10.1557/adv.2017.66.

43. P. Hohenberg and W. Kohn. "Inhomogeneous Electron Gas". *Physical Review* 136:3B, 1964, B864–B871. DOI: 10.1103/physrev.136.b864.

44. H. Ibach and H. Lüth. *Solid-State Physics: An Introduction to Principles of Materials Science*. Springer, Berlin, Germany, 2009.

45. J. D. Jackson. *Classical Electrodynamics*. 3rd ed. John Wiley & Sons, New York, USA, 1999.

46. M. Kardar. *Statistical Physics of Particles*. Cambridge University Press, Cambridge, UK, 2007.

47. W. Kohn and L. J. Sham. "Self-Consistent Equations Including Exchange and Correlation Effects". *Physical Review* 140:4A, 1965, A1133–A1138. DOI: 10.1103/PhysRev.140.A1133.

48. K. Konishi and G. Paffuti. *Quantum Mechanics: A new introduction*. Oxford University Press, Oxford, UK, 2009.

49. S. Laan. *pythonABC*. 2015. URL: https://github.com/Neojume/pythonABC.

50. T. Lancaster and S. J. Blundell. *Quantum Field Theory for the Gifted Amateur*. Oxford University Press, Oxford, UK, 2014.

51. L. D. Landau. "On the Theory of Phase Transitions". *Zhurnal Eksperimentalnoi i Teoreticheskoi Fiziki* 11, 1937, p. 19.

52. R. H. Landau, M. J. Páez, and C. C. Bordeianu. *Computational Physics: Problem Solving with Python*. 3rd ed. Wiley-VCH, Weinheim, Germany, 2015.

53. Y. Li, Q. Guo, J. A. Kalb, and C. V. Thompson. "Matching Glass-Forming Ability with the Density of the Amorphous Phase". *Science* 322:5909, 2008, pp. 1816–1819. DOI: 10.1126/science.1163062.

54. F. A. Lindemann. "Über die Berechnung Molekularer Eigenfrequenzen". *Physikalische Zeitschrift* 11, 1910, pp. 609–612.

55. S. G. Louie, S. Froyen, and M. L. Cohen. "Nonlinear Ionic Pseudopotentials in Spin-Density-Functional Calculations". *Physical Review B* 26:4, 1982, pp. 1738–1742. DOI: 10.1103/physrevb.26.1738.

56. G. D. Mahan. *Many-Particle Physics*. 3rd ed. Kluwer Academic Press, New York, USA, 2000.

57. R. M. Martin. *Electronic structure: basic theory and practical methods*. 2nd ed. Cambridge University Press, Cambridge, UK, 2020.

58. D. Marx and J. Hutter. *Ab Initio Molecular Dynamics: Basic Theory and Advanced Methods*. Cambridge University Press, Cambridge, UK, 2009.

59. Z. Mata-Pinzón, A. A. Valladares, R. M. Valladares, and A. Valladares. "Superconductivity in Bismuth. A New Look at an Old Problem". *PLOS ONE* 11:1, 2016. DOI: 10.1371/journal.pone.0147645.

60. E. Maxwell. "Isotope Effect in the Superconductivity of Mercury". *Physical Review* 78, 4 1950, pp. 477–477. DOI: 10.1103/PhysRev.78.477.

61. W. L. McMillan. "Transition Temperature of Strong-Coupled Superconductors". *Physical Review* 167:2, 1968, pp. 331–344. DOI: 10.1103/physrev.167.331.

62. B. Monserrat. "Electron–Phonon Coupling from Finite Differences". *Journal of Physics: Condensed Matter* 30:8, 2018, p. 083001. DOI: 10.1088/1361-648x/aaa737.

63. M. V. Nevitt and J. W. Downey. "Family of Intermediate Phases having Si_2Mo-Type Structure". *Transactions of the Metallurgical Society of AIME* 224:1, 1962, pp. 195–196.

64. P. Oelhafen, E. Hauser, H. .-. Güntherodt, and K. H. Bennemann. "New Type of d-Band-Metal Alloys: The Valence–Band Structure of the Metallic Glasses Pd–Zr and Cu–Zr". *Physical Review Letters* 43:15, 1979, pp. 1134–1137. DOI: 10.1103/physrevlett.43.1134.

65. H. Okamoto. "Cu-Zr (Copper-Zirconium)". *Journal of Phase Equilibria and Diffusion* 33:5, 2012, pp. 417–418. DOI: 10.1007/s11669-012-0077-1.

66. S. R. Ovshinsky. "Fundamentals of Amorphous Materials". In: *Physical Properties of Amorphous Materials*. Ed. by D. Adler, B. B. Schwartz, and M. C. Steele. Springer, New York, USA, 1985, pp. 105–155.

67. R. G. Parr and W. Yang. *Density-Functional Theory of Atoms and Molecules*. Oxford University Press, New York, USA, 1989.

68. J. P. Perdew, K. Burke, and M. Ernzerhof. "Generalized Gradient Approximation Made Simple". *Physical Review Letters* 77:18, 1996, pp. 3865–3868. DOI: 10.1103/PhysRevLett.77.3865.

69. J. P. Perdew, A. Ruzsinszky, G. I. Csonka, O. A. Vydrov, G. E. Scuseria, L. A. Constantin, X. Zhou, and K. Burke. "Restoring the Density-Gradient Expansion for Exchange in Solids and Surfaces". *Physical Review Letters* 100:13, 2008, p. 136406. DOI: 10.1103/PhysRevLett.100.136406.

70. J. P. Perdew and Y. Wang. "Accurate and Simple Analytic Representation of the Electron-Gas Correlation Energy". *Physical Review B* 45:23, 1992, pp. 13244–13249. DOI: 10.1103/PhysRevB.45.13244.

71. P. Phillips. *Advanced Solid State Physics*. Westview Press, Boulder, USA, 2003.

72. D. Pines and D. Bohm. "A Collective Description of Electron Interactions: II. Collective vs Individual Particle Aspects of the Interactions". *Physical Review* 85:2, 1952, pp. 338–353. DOI: 10.1103/physrev.85.338.

73. D. Reinsel, J. Gantz, and J. Rydning. *The Digitization of the World, From Edge to Core*. White Paper #US444133. Framingham, USA: IDC, sponsored by Seagate, 2018, p. 28. URL: https://www.seagate.com/files/www-content/our-story/trends/files/idc-seagate-dataage-whitepaper.pdf.

74. C. A. Reynolds, B. Serin, W. H. Wright, and L. B. Nesbitt. "Superconductivity of Isotopes of Mercury". *Physical Review* 78, 4 1950, pp. 487–487. DOI: 10.1103/PhysRev.78.487.

75. I. Rodriguez, R. M. Valladares, A. Valladares, D. Hinojosa-Romero, U. Santiago, and A. A. Valladares. "Correlation: An Analyzing Tool for Liquids and for Amorphous Solids [Computer Software]". Version 1.0.4. *Journal of Open Source Software* 6:65, 2021, p. 2976. DOI: 10.21105/joss.02976. URL: https://github.com/Isurwars/Correlation.

76. I. Rodríguez, D. Hinojosa-Romero, A. Valladares, R. M. Valladares, and A. A. Valladares. "A Facile Approach to Calculating Superconducting Transition Temperatures in the Bismuth Solid Phases". *Scientific Reports* 9:1, 2019. DOI: 10.1038/s41598-019-41401-z.

77. C. C. J. Roothaan. "New Developments in Molecular Orbital Theory". *Reviews of Modern Physics* 23:2, 1951, pp. 69–89. DOI: 10.1103/revmodphys.23.69.

78. M. Ross. "Generalized Lindemann Melting Law". *Physical Review* 184:1, 1969, pp. 233–242. DOI: 10.1103/physrev.184.233.

79. U. Rössler. *Solid State Theory: An Introduction*. 2nd ed. Springer, Berlin, Germany, 2009.

80. R. D. Ruth. "A Canonical Integration Technique". *IEEE Transactions on Nuclear Science* 30:4, 1983, pp. 2669–2671. DOI: 10.1109/tns.1983.4332919.

81. J. R. Schrieffer. *Theory of Superconductivity*. Perseus Books, USA, 1999.

82. J. C. Slater. "Wave Functions in a Periodic Potential". *Physical Review* 51:10, 1937, pp. 846–851. DOI: 10.1103/physrev.51.846.

83. H. L. Smith, C. W. Li, A. Hoff, G. R. Garrett, D. S. Kim, F. C. Yang, M. S. Lucas, T. Swan-Wood, J. Y. Lin, M. B. Stone, and et al. "Separating the Configurational and Vibrational Entropy Contributions in Metallic Glasses". *Nature Physics* 13:9, 2017, pp. 900–905. DOI: 10.1038/nphys4142.

84. Z. H. Stachurski. *Fundamentals of Amorphous Solids: Structure and Properties*. Wiley-VCH, Weinheim, Germany, 2015.

85. J. B. Suck, H. Rudin, H. J. Guntherodt, H. Beck, J. Daubert, and W. Glaser. "Dynamical Structure Factor and Frequency Distribution of the Metallic Glass $Cu_{46}Zr_{54}$ at room temperature". *Journal of Physics C: Solid State Physics* 13:8, 1980, pp. L167–L172. DOI: 10.1088/0022-3719/13/8/006.

86. A. P. Sutton. *Electronic Structure of Materials*. Oxford University Press, Oxford, UK, 1993.

87. Y. Takahara and N. Narita. "Local Electronic Structures and Chemical Bonds in Zr–Based Metallic Glasses". *Materials Transactions* 45:4, 2004, pp. 1172–1176. DOI: 10.2320/matertrans.45.1172.

88. T. Tohei, A. Kuwabara, F. Oba, and I. Tanaka. "Debye Temperature and Stiffness of Carbon and Boron Nitride Polymorphs from First Principles Calculations". *Physical Review B* 73:6, 2006, p. 064304. DOI: 10.1103/physrevb.73.064304.

89. A. A. Valladares, I. Rodríguez, D. Hinojosa-Romero, A. Valladares, and R. M. Valladares. "Possible Superconductivity in the Bismuth IV Solid Phase under Pressure". *Scientific Reports* 8:1, 2018. DOI: 10.1038/s41598-018-24150-3.

90. A. A. Valladares. "A New Approach to the Ab Initio Generation of Amorphous Semiconducting Structures". In: *Glass Materials Research Progress*. Ed. by J. C. Wolf and L. Lange. Nova Science Publishers, 2008, pp. 61–123.

91. J. I. Verdeja González, D. Fernández-González, and L. F. Verdeja González. *Physical Metallurgy and Heat Treatment of Steel*. Springer, Cham, Switzerland, 2022.

92. S. H. Vosko, L. Wilk, and M. Nusair. "Accurate spin-dependent electron liquid correlation energies for local spin density calculations: a critical analysis". *Canadian Journal of Physics* 58:8, 1980, pp. 1200–1211. DOI: 10.1139/p80-159.

93. Y. Waseda. *The Structure of Non-Crystalline Materials*. McGraw-Hill, New York, USA, 1980.

94. S. Weinberg. *Lectures on Quantum Mechanics*. 2nd ed. Cambridge University Press, Cambridge, UK, 2015.

95. R. Windiks and B. Delley. "Massive Thermostatting in Isothermal Density Functional Molecular Dynamics Simulations". *The Journal of Chemical Physics* 119:5, 2003, pp. 2481–2487. DOI: 10.1063/1.1586913.

96. G.-X. Zhang, A. M. Reilly, A. Tkatchenko, and M. Scheffler. "Performance of Various Density-Functional Approximations for Cohesive Properties of 64 Bulk Solids". *New Journal of Physics* 20:6, 2018, p. 063020. DOI: 10.1088/1367-2630/aac7f0.